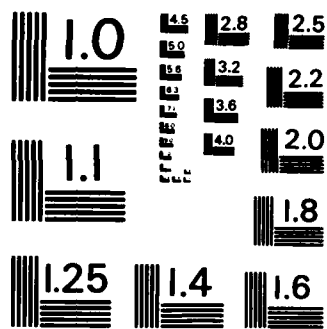END
FILMED
DTIC

MICROCOPY RESOLUTION TEST CHART

NATIONAL BUREAU OF STANDARDS-1963-A

(12)

CENTER FOR DIELECTRIC STUDIES

Contract No. N00014-82-K-0339

Sponsored by

The Office of Naval Research

L.E. Cross

R.E. Newnham

J.V. Biggers

May, 1983

DTIC
ELECTE
SEP 2 6 1984
S D
B

THE MATERIALS RESEARCH LABORATORY

THE PENNSYLVANIA STATE UNIVERSITY

UNIVERSITY PARK, PENNSYLVANIA

84 08 28 007

Table of Contents

Abstract

This report documents the first year of the Dielectric studies under ONR contract N00014-82-K0339 which initiated the formation of a National Center for Dielectric Studies at Penn State. Over the first year, a major effort has been made to establish a sound base of Industrial support, a process much aided by a planning grant from the National Science Foundation and a special grant award from IBM. Organizationally, the Penn State Center is coordinated with efforts at a number of other schools who have ONR-supported programs related to dielectric studies.

Topics which have been of special interest over the first year include: relaxor ferroelectrics based on lead magnesium niobate, where the interest has been in the influence of modifier cations on both the sintering and electrical properties; relaxors in the $PbFe_{1/2}Nb_{1/2}O_3:Pb(Ni_{1/3}Nb_{2/3})O_3$ system; non-relaxor perovskites including materials with $Li^{(+1)}$ and $Na^{(+1)}$ forced onto the B site in the ABO_3 structure. Low temperature studies in the $KTaO_3$ system. A new look is being taken at the grain size effects in $BaTiO_3$ on a joint program with Leeds University in England, and new measuring equipment has been added to the Laboratory both for ultra low $(f < 10^{-3}$ Hz) and ultra high $(f > 3.10^{11}$ Hz) frequencies.

Papers which have been published from work on the program are included as technical appendices.

1

1. INTRODUCTION

On March 1, 1982, the Office of Naval Research (ONR), in response to a major proposal for Dielectric Studies at Penn State, initiated the formation of a Center for Dielectric Studies in the Materials Research Laboratory.

The proposal for this work had stemmed from a series of meetings with representatives from the ceramic capacitor manufacturers, with companies which supplied materials to the capacitor companies, and with major electronics companies who are users of ceramic capacitors. The proposal sought to establish a critical size effort which would be able to make a significant impact upon the basic materials problems relevant to the multilayer ceramic capacitor (MLC). The ultimate aim was to establish at Penn State a National Center recognized by the National Science Foundation in its Centers Program. Unlike other NSF centers however, we proposed to coordinate work at Penn State with parallel efforts at other electroceramic schools which have special areas of competance in the field.

We believe that the Penn State Center is the first attempt in this country to 'network' an approach to applied research, and to draw upon the special skills of the most productive faculty in a number of schools, on a scale and with a breadth reminiscent of the major applied research efforts in Japan.

Over the first year of the contract, a major effort has been made to establish a sound basis for industrial participation in the Center program. Planning for this function was much aided by a planning grant from the NSF Centers Program. We were also further helped by a very early grant award from IBM, which was keyed to the development of the Center.

Contact with industry, and between the major industrial companies was much aided by a timely study on 'The Reliability of Multilayer Ceramic Capacitors' by the National Materials Advisory Board in March, 1981, under the

chairmanship of Professor L.E. Cross (NMAB-400). This study was instrumental in underscoring the common features of many of the reliability problems experienced by different suppliers and capacitor users.

The major scope of electronic ceramic research in Japan was also made evident to a number of senior scientists from industry and academe by a US:Japan Workshop on Electroceramic Materials in Tokyo, Japan in May, 1982, sponsored by ONR and co-chaired by K. Okazaki and L.E. Cross.

This report delineates work which has been initiated over the first year of the contract. It is perhaps not surprising that only a few have matured yet to the point of generating publishable results, however, faculty upon the program have been involved also in several major invited papers summarizing problems and opportunities in the dielectrics field, and the papers are briefly discussed in the text and included in this report as technical appendices.

2.0 FERROELECTRIC RELAXOR DIELECTRICS

2.1 Lead Magnesium Niobate Based Compositions

It was evident from earlier studies upon our piezoelectric materials programs that the perovskite solid solutions sequence $PbMg_{1/3}Nb_{2/3}O_3:PbTiO_3$ which was developed initially for its electrostrictive properties had most interesting high permittivity dielectric properties.

A major problem in the past with these ceramics has been the tendency to form a defect pyrochlore structure rather than the disordered perovskite. In a study during the current year which was reported at the fall meeting of the Ceramic Society (S.L. Swartz and T.R. Shrout, 'Fabrication of Perovskite Lead Magnesium Niobate,' Materials Research Bulletin 17:1245-50 [1982]). A new technique has been devised for processing a pyrochlore-free lead magnesium

3

niobate. The method consists of pre-reacting magnesium and niobium oxides (without lead) to form the columbite $MgNb_2O_6$ prior to reaction with PbO. The perovskite PMN then forms by the reaction

$$3PbO + MgNb_2O_6 \rightarrow 3PbMg_{1/3}Nb_{2/3}O_3.$$
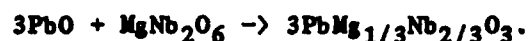
By this method, the amount of the pyrochlore phase is reduced to less than 2% as compared to almost 30% in some batches fabricated by simple mixed oxide techniques. Even the low 2% level afforded by this method can be further reduced and the pyrochlore completely eliminated by the addition of excess MgO (~2 mole%).

The purpose of the current investigation is to study the microstructure and dielectric properties of sintered PMN ceramics fabricated by the above processing so as to eliminate perturbation from the low permittivity pyrochlore phase. Variables which are under study include deviations from the PMN stoichiometry, calcining temperature, and sintering temperatures. The compositions under study range from pure PMN to PMN with 10% $PbTiO_3$ a material in which the transition range is moved closer to room temperature.

Trends in the data which are already observable include:

(1) Increasing sintering temperature increases grain size with a minor decrease in density.

(2) Excess MgO also increases grain size but without corresponding loss in density.

(3) $PbTiO_3$ addition increases the average Curie temperature from —15°C in pure PMN to ~40°C in PMN:10% PT.

(4) Absence of pyrochlore phase permits maximum permittivities up to 30,000 in PMN:10% PT.

(5) Dispersion range is decreases with the addition of PT.

2.2 Lead Magnesium Niobate Pyrochlore Structure

Parallel work on the piezoelectric program has identified the pyrochlore composition in the lead magnesium niobate as

$$Pb_{1.83}Nb_{1.71}Mg_{0.29}O_{6.39}$$
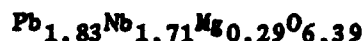
To study the dielectric properties of the pure pyrochlore phase we are fabricating ceramics by mixed oxide techniques at this stoichiometry. Initial x-ray measurements using a Philips ADP 3600 automatic diffractometer. Indications are that the pattern is that of a defect pyrochlore structure (space group Fd3m) with lattice parameter a = 10.5988 $\overset{\circ}{A}$.

The dielectric permittivity as expected is low ~130 at 25°C, with tan δ < 0.002 on cooling to 4.2 K the permittivity climbs to 200 near 30°K with evidence of a weak dielectric maximum with relaxation character.

2.3 Modification to the Lead Magnesium Niobate

A wide ranging study has been initiated to explore the influence of composition modification upon the properties of lead magnesium niobate. To maintain the perovskite PMN structure the level of solid substitution is being kept low, and a wide range of cations substituted with not more than 10 mole% B cation modification.

Substituents being tested include: Ni^{+2}, Mg^{+2}, Co^{+2}, Zn^{+2}, Mn^{+2}, Cd^{+2}, Fe^{+3}, Sc^{+3}, Ti^{+4}, Sn^{+4}, Hf^{+4}, Zr^{+4}, Ta^{+5}, W^{+6}. In each case, the added cations are being pre-reacted to form a suitable precursor, as with the columbite phase in PMN so as to avoid problems with the defect pyrochlore formation.

2.4 Dielectric Properties in the $Pb(Fe_{1/2}Nb_{1/2})O_3:Pb(Ni_{1/3}Nb_{2/3})O_3$ System

Dielectric studies have been initiated across the solid solution system $PbFe_{1/2}Nb_{1/2}O_3:PbNi_{1/3}Nb_{2/3}O_3$ (PFN:PNN). The objective is to test out a low

firing relaxor material which could be compatible with Pd:Ag electrodes. To explore the effects of fabrication from the pre-cursor columbite ($NiNb_2O_6$) and wolframite $FeNbO_4$ phases. The role of firing temperature upon densification, grain size and permittivity level and the possible influences of MnO_2 additions upon the resistivity and dielectric properties in the Fe based relaxor system.

Early results suggest that high resistivity ($\rho > 10^{12}$ ohm cm) ceramics can be fabricated with peak permittivities greater than 15,000 close to room temperature and a relaxation character which shows increasing dispersion with increasing level of $PbNi_{1/3}Nb_{2/3}O_3$ in the solid solution.

3.0 NON-RELAXOR PEROVSKITE MATERIALS

3.1 $A(B_{1/4}Nb_{3/4})O_3$ Compositions

It has been reported that the monovalent cations Li^{+1} and Na^{+1} can be forced over into the B octahedral site in ABO_3 structures with compositions of the type $A(B_{1/4}Nb_{3/4})O_3$ in which the A cation is barium or strontium, and B is Li or Na.

Cubic perovskites were in fact prepared by solid state reaction with the oxides or carbonates at 1000°C in 3 hours, although the cubic structure appears to be unstable at higher temperatures and transforms or decomposes to a hexagonal form.

Dielectric constants of the lithium and sodium compounds were not large, being in the range 38-50, but were independent of temperature over the range - 80°C to +200°C in the frequency range 10^3-10^7 Hz. Dielectric loss tan ρ is also low in the range 10^{-3}.

A more complete description of these studies is given in appendices 1 and 2.

3.2 Low Temperature Studies of $KTaO_3$

Potassium tantalate has been extensively studied in single crystal form in both normal paraelectric, and quantum ferroelectric temperature regimes. In the ceramic, the picture is much less clear and the work described in detail in Appendix 3 was carried out to clear up some of the inconsistencies in earlier work.

It would appear that much of the confusion in earlier studies stems from the difficulty of fabricating dense, crack free samples for dielectric study. For this work it was found to be essential to Hot Isostatically Press (HIP) the sintered compacts before reproducible results could be obtained.

In brief summary, over the range from 4.2 to 300 K, the weak field dielectric response was well described by the Barrett function. A small additional polarizability which had relaxation character was also evidenced at higher temperature, but may be an artifact of the microstructure. The permittivity shows a weak peak near 10°K which also has clear relaxation character and closely duplicates the behavior of high purity single crystal material. No dielectric hysteresis could be induced at high fields for cycling fields down to 0.04 Hz at any temperature in the measuring range.

3.3 Grain Size Effects in $BaTiO_3$

3.3.1 Introduction

In 1966, Buessem, Cross and Goswami published an internal stress model to explain the enhancement of the dielectric permittivity in fine grain $BaTiO_3$ which used the Devonshire phenomenological theory to analyse the consequences of mechanical stress fields which must occur due to the absence of 90° twins in the fine grain ceramic.

The proposed model was very simple, but did permit the derivation of the order of magnitude of the internal stress required for the observed

7

enhancement. Some years later in careful studies of the mechanical properties of $BaTiO_3$ ceramics, Pohanka and co-workers verified the existence of internal stresses below the Curie point Tc and derived magnitudes for the stress levels which were not inconsistent with the earlier dielectric calculations.

More recently, a number of workers in Japan have extended measurements to a wider range of grain sizes in hot pressed $BaTiO_3$, where extreme care has been taken to maintain 'clean' grain boundaries. These samples show, as expected from the model, almost no effect of grain size on weak field permittivity for T > Tc (verifying the clean boundary structure) and give excellent data over a very wide temperature range in the ferroelectric phase.

With the availability of this excellent data, and the emerging developments in MLC fabrication which all push towards thinner dielectric layers and thus necessitate finer grain ceramics, it appears well worthwhile to extend and refine the phenomenological calculations to cover the full temperature range from -190°C to +135°C.

3.3.2 Phenomenological Studies

During the year we were in close contact with Andrew Bell, a graduate student at Leeds University, England, who has taken up the problem of the phenomenological derivation. Rather than initiate a separate program here at Penn State, it seemed desirable to cooperate with Leeds and under the invitation from R. Brooks to act as co-advisor for Mr. Bell.

In developing the elastic gibbs function which will be required, the Buessem, Goswami, Cross (BGC) coefficients are a good starting point. For these constants, however, the function was refined using zero stress single crystal dielectric data so that it described most precisely the temperature region around 0°C. To extend the function for the whole ferroelectric range in $BaTiO_3$, it is necessary to add a term of the form

8

$$\frac{1}{2} \text{ H } P_1^2 P_2^2 P_3^2$$

to move the stability of the rhombohedral phase into the correct temperature range. However, below 0°C, the dielectric data on single crystals is not trustworthy, due to twinning in the orthorhombic and rhombohedral phases.

Clearly, H can be chosen so as to place the orthorhombic:rhombohedral phase change at the observed temperature, but now as a check upon the validity of the function, we propose to model the electric field dependence of the lower temperature phase boundaries. Measurements of the E field dependence of both low temperature phase boundaries up to incredibly high fields (650 kV/cm) have recently been performed by Fesenko et al. on single domain Remeika grow flakes of $BaTiO_3$ and provides the basic data required for this validation.

The proposed plan of attack is as follows.

(1) To add a temperature independent H coefficient to the BGC function.

(2) To calculate the value of H required to bring the orthorhombic:rhombohedral phase change to the correct position.

(3) To validate the function by calculating E field dependence for all three phase transitions and compare to measured values.

To derive the average stress field acting upon the grain, and its temperature dependence, it is proposed to use the precise lattice measurement capability at Oxford, with the automatic temperature control devised by M. Glazer. Measuring the lattice strain in the fine grain ceramic, and comparing to the powder at the same grain size, the internal stress can be derived as a function of temperature from the known elastic compliances.

With these averaged stress values, we may then use the modified BGC function to calculate the intrinsic average permittivity as a function of temperature to compare to the data from Japan.

4. DIELECTRIC MEASURING TECHNIQUES

4.1 Introduction

The ferroelectrics group at MRL has, during the course of many years of work in electronic ceramics, built up excellent computer controlled dielectric measuring equipments covering the frequency range from 100 Hz to 1 GHz (10^9 Hz). For frequencies below 100 Hz, we have a specialized balanced Sawyer:Tower circuit which is used primarily to measure nonlinearity and slow ferroelectric switching, displaying hysteresis loops down into the frequency range to 0.01 Hz. It is our intention now to extend this frequency range so as to be able to measure quasi-static capacitance to .001 Hz and below, so as to be able to explore the range of frequencies between 'normal' dielectric relaxation and what is conventionally regarded as 'aging' in ferroelectric and relaxor ferroelectric compositions.

4.2 Proposed Linear Voltage Ramp (LVR) Method

4.2.1 Theory of Operation

If a dielectric is formed into a simple parallel plate capacitor, and the capacitor is subjected to an electric potential difference between plates of the form

$$V = V_o - \alpha t \tag{1}$$

where V is the instantaneous applied voltage, V_o is some positive starting voltage, α a constant ramp rate (dV/dt) of reduction of the voltage and t the time.

10

At any instant of time, the total current I_T is made up of two components, a conduction term I_c given by

$$I_c = V/R_i \qquad (2)$$

where R_i is the effective instantaneous resistance and a displacement current I_D in the form

$$I_D = dQ/dt \qquad (3)$$

where Q is the instantaneous value of the charge stored on the capacitor. Clearly for a linear dielectric

$$Q = CV \qquad (4)$$

but in the cases of interest here with C and V are functions of time so that

$$dQ/dt = C \ dV/dt \div V \ dC/dt. \qquad (5)$$

Thus I_T is given by

$$I_T = I_c + I_D = V/R_i + V \ dC/dt + C \ dV/dt \qquad (6)$$

and C now defines the quasi-static capacitance.

For capacitors with finite leakage currents and significant time dependence of the quasi-static capacitance, the terms in equation (6) may be separated by a zero crossing method. Clearly from equation (1) when $V_o - at$, the instantaneous $V = 0$ and from (6) the total current now becomes

$$I_T = C \ dV/dt = C\alpha$$

thus for a given ramp rate α, the quasi-static capacitance C can be measured.

It is interesting to note from equation (1) that unlike dielectric bridge methods which subject the sample to an alternating field, in the LVR method

11

the sample sees only a unidirected field. For samples in which a part of the dielectric response is irreversible, as for example some types of domain motion in ferroelectrics, it may be expected that the LVR method will give different values for positive and negative ramp functions. By analysing these differences, and comparing quasi-static to weak field AC dielectric data, it may then be possible to separate reversible and irreversible components of the response.

4.3 Experimental Studies by the LVR Method

The experimental setup is relatively simple (Fig. 1). The dielectric under test is fabricated as a capacitor of simple geometry, with capacitance in the range 100 to 1,000 pf. A linear voltage ramp is generated under HP9816 computer control using the internal supply of the HP4140B pico ammeter/DC voltage supply. Current through the capacitor is monitored on the pico ammeter and recorded on 9121 floppy disk for later processing.

Variables under control are the starting voltage for the experiment (V_s), the soak time over which the sample is subjected to this DC bias (t_s) and the ramp rate a (dV/dt). Clearly, zero voltage crossing can be achieved either with a positive start voltage and a negative ramp, as in equation (1), or by a negative start voltage and a positive ramp. The time after initiating voltage change at which I_D can be measured, that is the time to zero crossing can be varied either by fixing V_s and varying a, or by fixing a and varying the start voltages V_s (Fig. 2).

To test the experimental system, we first measured a very high quality polystyrene integrating capacitor (225 pf) which should have no time dependence in its low frequency dielectric properties. The constancy of the capacitance over a range of times from 20 to 2,000 seconds is shown in Figure 3.
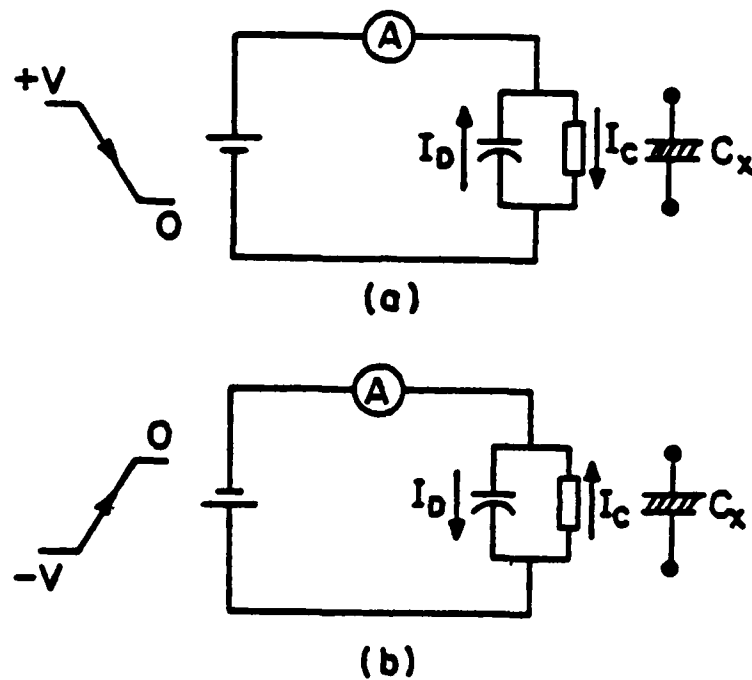
12

Figure 1. Schematic diagram of the constant voltage ramp method.

(a) Ramping down from positive voltage.

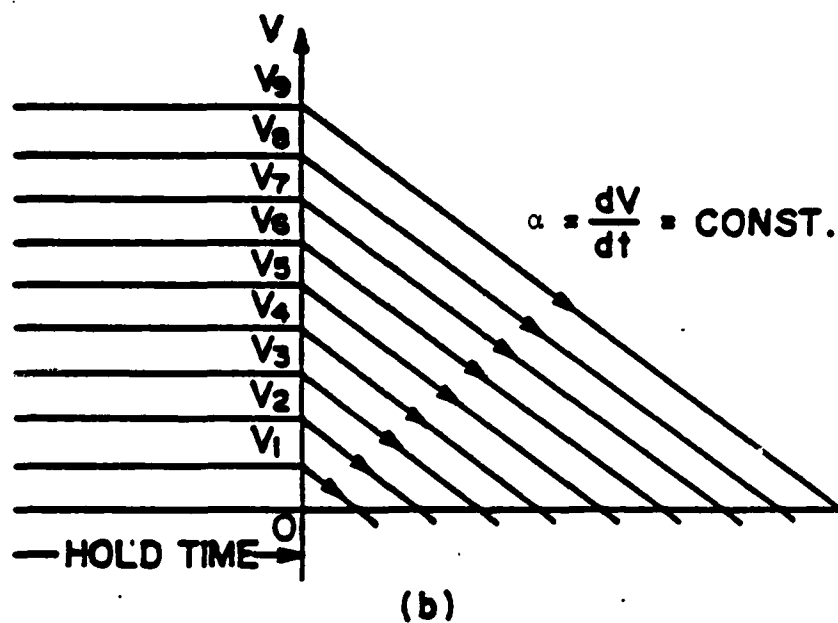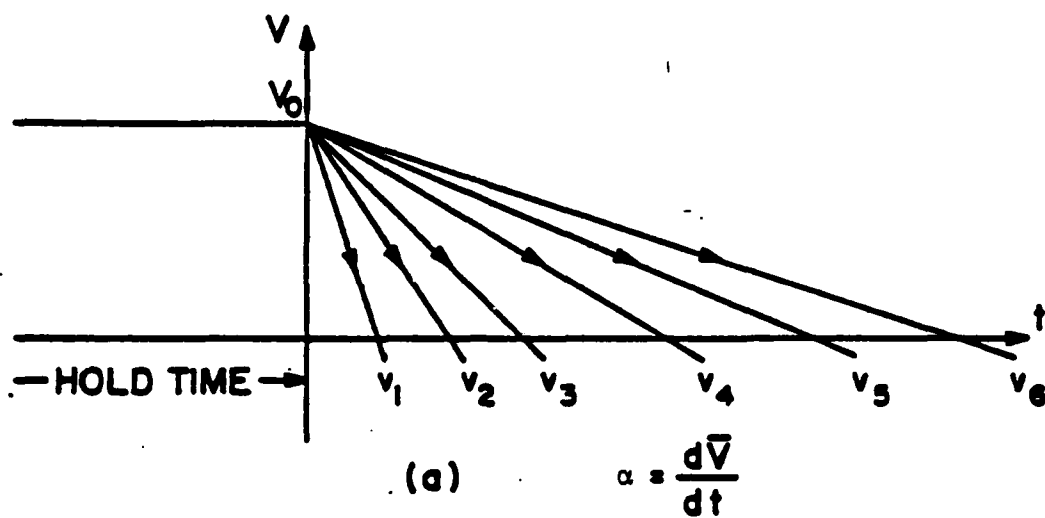(b) Ramping up from negative voltage.

13

Figure 2. Voltage vs time sequences used in the zero-crossing method.

    (a) Constant soak V_0 variable ramp α.

    (b) Constant ramp α variable soak voltage.
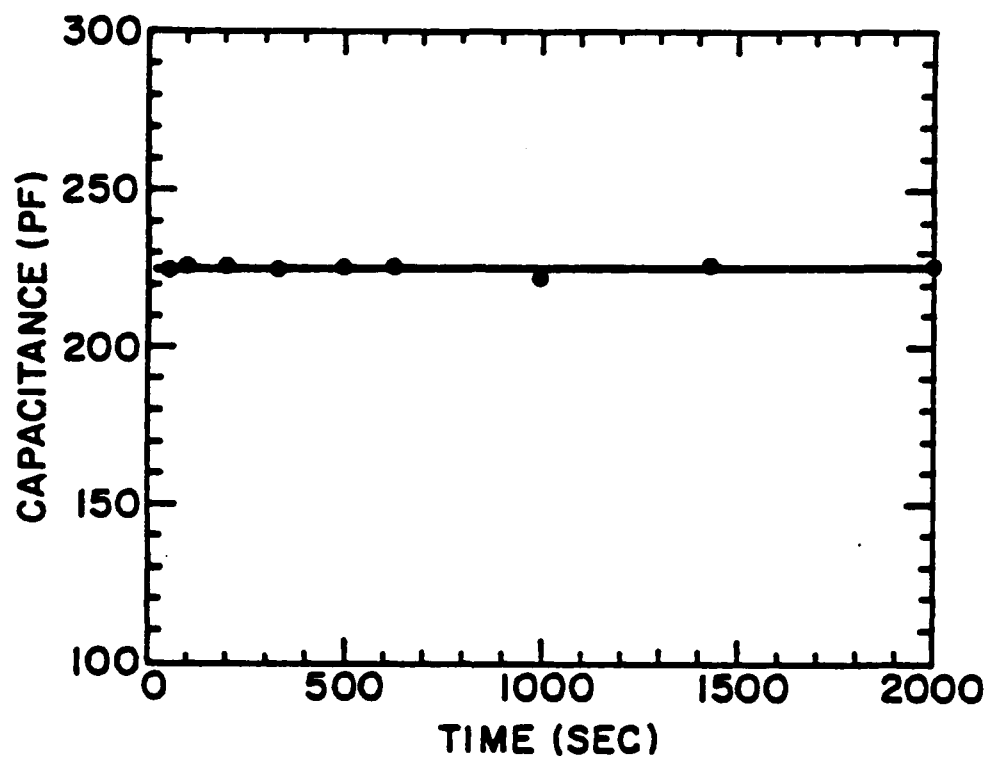
14

Figure 3. Time dependence of quasi-static capacitance of a polystyrene
capacitor measured with constant starting voltage.

15

Time dependence of C for a mica capacitor over a similar time range shows marked dispersion. Data for both constant ramp rate a (variable V_s) and constant V_s (variable ramp rate a) is shown in Figure 4. Computer fitting suggests that for this capacitor, $C_\infty = 111.4$ pf, $C_s = 181.6$ pf and the time constant $\tau \sim 520$ sec. By AC bridge method, the capacitor read 111 pf at 1 kHz.

Preliminary data showing the irreversibility of the quasi-static capacitance in a poled soft PZT (501A) is shown in Figure 5. Starting from a positive bias of 100 V with a negative $C \sim 350$ pf, however, starting from a negative bias of −20 V with an equivalent positive a $C \sim 220$ pf and clearly decreases further as $|-V|$ is decreased.

It would appear that the negative voltage 'unpicks' some of the easily reversed domains, giving a negative contribution for this irreversible component. A question of interest is whether in a softer material, or with slower ramp, this negative contribution could over-ride the reversible permittivity giving an overall negative permittivity.

5.0 GENERAL PAPERS

During 1982, senior personnel from the Dielectrics Center were invited participants in the US:Japan Workshop on Electronic ceramics. Professor L.E. Cross presented an invited paper on 'Polarization Mechanisms in High K Dielectrics' which is included here as Appendix 4. Dr. W.A. Schulze presented a poster on 'Possible Space Charge Effects in Multilayer Capacitors' included as Appendix 5.

Over the year, two papers presented at the NAS workshop on reliability of MLCs appeared in print. The paper by R.E. Newnham which was an in-depth review on 'Structure:Property Relations in Multilayer Ceramics,' Appendix 6, and a review on 'New Dielectrics' by L.E. Cross which is Appendix 7.
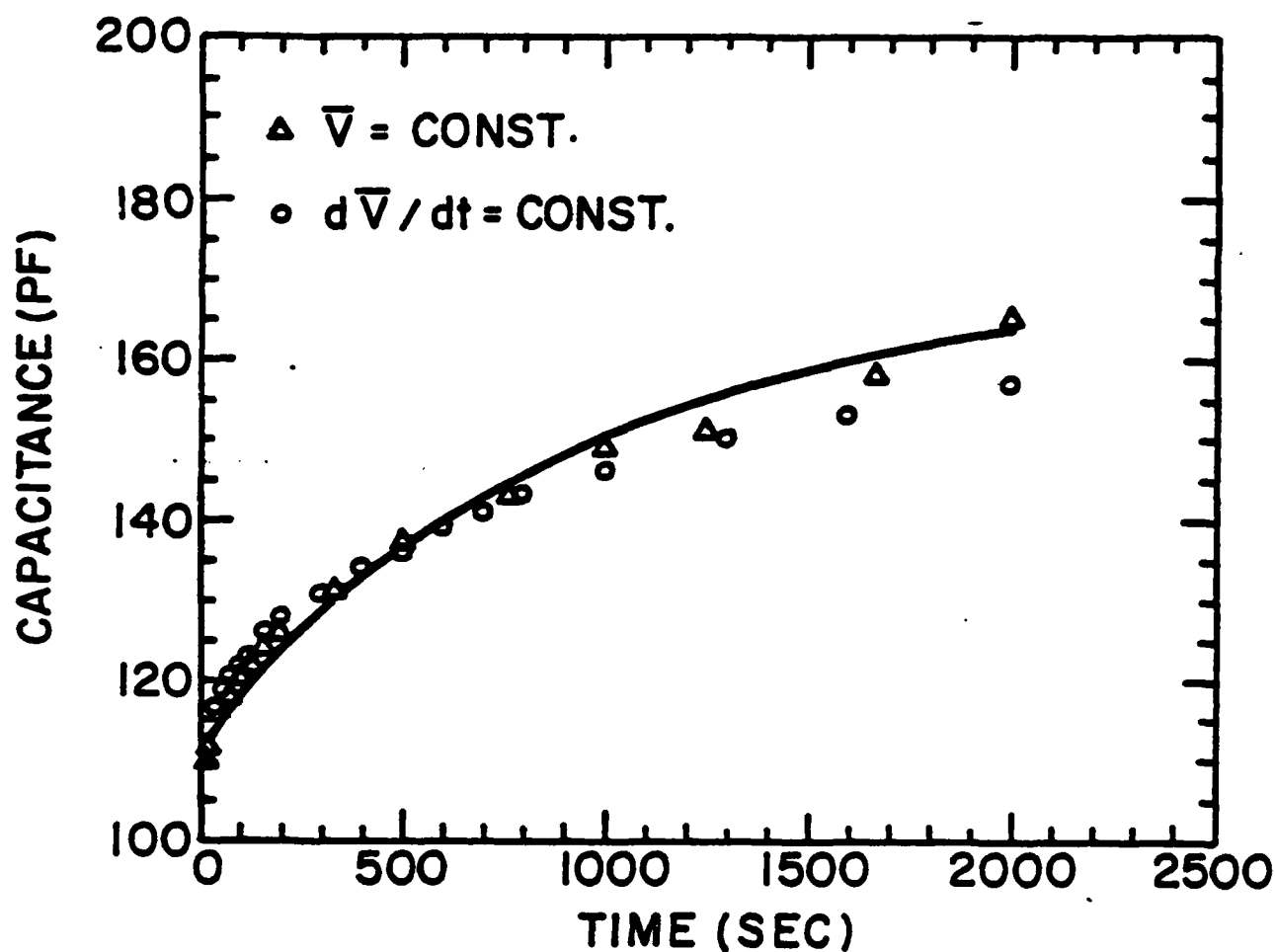
Figure 4. Time dependence of the quasi-static capacitance of a mica capacitor measured both for fixed starting voltage variable α and for fixed α variable V_0.

Full line fitted exponential with $C_\infty = 111.4$ pf, $C^s = 181.6$ pf and $\tau = 520$ sec.
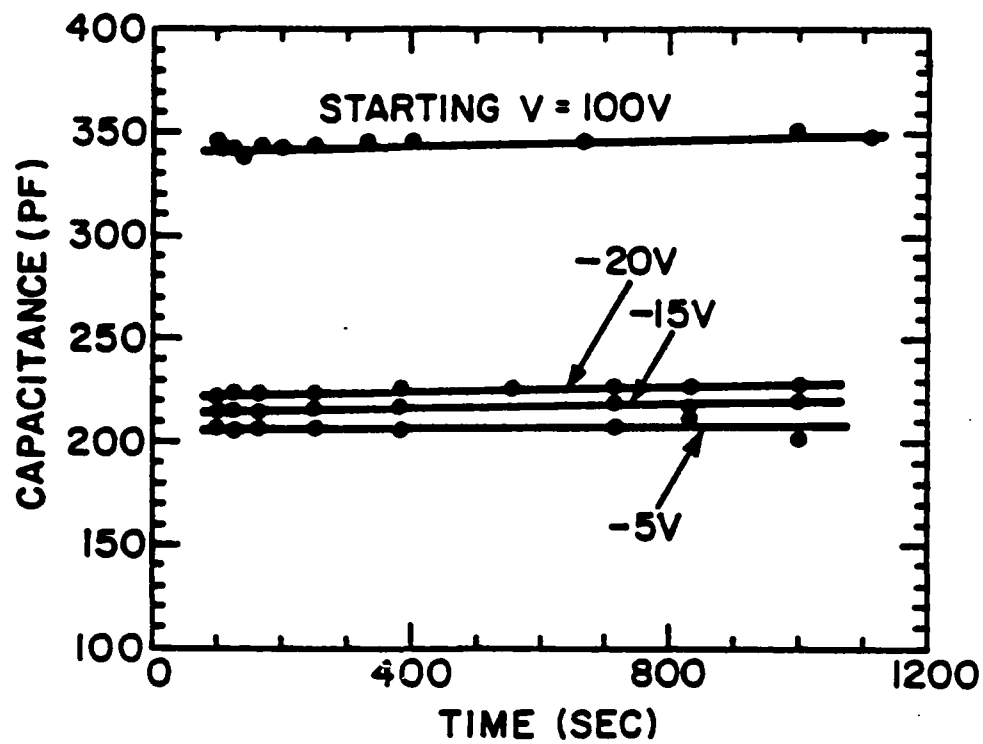
17

Figure 5. Capacitance of a PZT 501A disk in poled condition showing capacitance change between negative and positive ramp voltages. Irreversible component is negative for negative voltage.

18

6.0 EQUIPMENT

During 1982, the group shared in the acquisition of an IBM Model IR/90 series fast fourier transform (FFT) optical spectrometer. This excellent spectrometer covers the longer wavelength IR spectrum down to 10 cm^{-1}, i.e. 300 GHz, using a mercury arc source and a deuterated triglycine sulphate (DTGS) pyroelectric bolometer detector.

In 1983, under Dielectric Center Industry funding, we shall be extending our frequency range up to 20 GHz with the installation of an HP 8755S scalar network analyser and 816A slotted line. This equipment together with appropriate sample holder cavities will extend our present measuring range from 1 GHz to 20 GHz.

We have excellent cooperation with Dr. W. Ho and W. Hall at Rockwell Science Center in Thousand Oaks who have equipment covering the 30, 90 and 120 GHz frequency bands, so that it is now possible to measure over virtually the whole EM spectrum from 10^{-4} Hz to optical frequencies.

We anticipate first usage of the FFT.IR system on SbSI evaporated films which are being generated for dielectric and piezoelectric studies.

APPENDIX 1

PREPARATION, THERMAL CHANGE AND DIELECTRIC PROPERTIES OF CUBIC
PEROVSKITES $A(B_{1/4}Nb_{3/4})O_3$ (A = Ba or Sr, B = Na or Li)

Y. Hikichi, Zhili Chen, R.E. Newnham and L.E. Cross
Materials Research Laboratory
The Pennsylvania State University
University Park, PA 16802

ABSTRACT

Cubic Perovskites $A(B_{1/4}Nb_{3/4})O_3$ (A = Ba or Sr, B = Na or Li) were
prepared by solid state reaction at 1000°C for 3 hours, starting
with oxides or carbonates of the various elements. $Ba(Li_{1/4}Nb_{3/4})O_3$
transformed sluggishly from a cubic into a hexagonal form above
900°C. Cubic $Ba(Na_{1/4}Nb_{3/4})O_3$, $Sr(Na_{1/4}Nb_{3/4})O_3$ and $Sr(Li_{1/4}$
$Nb_{3/4})O_3$ decomposed at high temperature without transformation
into a hexagonal form to give $Ba_5Nb_4O_{15}$ or $Sr_5Nb_4O_{15}$. When K_2CO_3
was used as a source of B^+ ion, only $Sr_6Nb_2O_{11}$, $Sr_5Nb_4O_{15}$ and
$Ba_5Nb_4O_{15}$ appeared at 1000°C. It is difficult for potassium to
enter into the octahedral sites of the perovskite structure
because of its large ionic size. Dielectric constants of the
cubic $A(B_{1/4}Nb_{3/4})O_3$ ceramics sintered at 1450°C for 1 hour were
not large (38-53), but were independent of temperature (-80 to
+200°C) and frequency (10^3-10^7 Hz).

Introduction

Perovskite ABO_3 is described by a cubic unit cell with a large A cation at
the center, smaller B cations at the corners, and oxygen ions at the centers of
the edges.

Kapyshev et al. (1) first prepared the cubic perovskites $Ba(Na_{1/4}Nb_{3/4})O_3$
(BNN) and $Ba(Li_{1/4}Nb_{3/4})O_3$ (BLN) from $BaCO_3$, Na_2CO_3, Li_2CO_3 and Nb_2O_5. Matsuo
et al. (2) prepared the cubic perovskites $Sr(Na_{1/4}Nb_{3/4})O_3$ (SNN) and $Sr(Li_{1/4}$
$Nb_{3/4})O_3$ (SLN) from $SrCO_3$, Na_2CO_3, Li_2CO_3 and Nb_2O_5. Negas et al. (3)
reported a phase transformation in BLN to hexagonal by heating the cubic form
at 900°C for 1 week.

However, there are several uncertainties regarding these perovskites
$A(B_{1/4}Nb_{3/4})O_3$ (A = Ba or Sr, B = Na or Li, abbreviated as ABN) including the
question of order or disorder among the octahedral ions, as well as the
dielectric coefficients and loss. Several of these points are discussed in
this paper.

Experimental Procedures

The starting materials, reagent grade $BaCO_3$, $SrCO_3$, K_2CO_3, Na_2CO_3, Li_2CO_3 and Nb_2O_5 were obtained from Alfa Division, Ventron Co. Stoichiometric mixtures of the starting materials ($BKN(Ba(K_{1/4}Nb_{3/4})O_3)$, BNN, BLN, SKN ($Sr(K_{1/4}Nb_{3/4})O_3$), SNN and SLN) were ball-milled under alcohol for 20 hours. After drying at 105°C, the milled powders were heated for 3 hours at temperatures ranging from 1000°C to 1400°C in a sintered alumina crucible. There was no reaction with the crucible.

Pure cubic BNN, BLN, SNN and SLN were obtained at 1000°C. To test their stability, these cubic forms were heated in air at 900-1500°C for time periods of 1.5 to 240 hours.

A powder x-ray diffractometer using CuKα radiation and an x-ray fluorescence spectrometer were used for phase identification and for chemical analysis.

The cubic perovskites obtained were ground again to pass through a 200 mesh sieve, and then pressed into pellets (1x10φmm) using a small amount of polyvinyl alcohol as a binder. The pellets were sintered at 1450°C for 1 hour on Pt foil to give ceramics suitable for property measurement. Bulk densities exceeded 92% of theoretical, and the sintered pellets were identified as cubic perovskite, as verified by x-ray diffraction.

Dielectric constants of the sintered pellets were measured from -80 to +200°C at frequencies ranging from 10^3 to 10^7 Hz under weak ac fields using a Hewlett Packard automatic capacitance bridge.
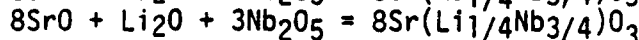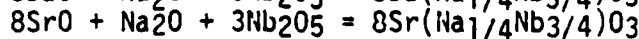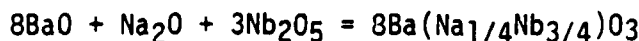
Results and Discussion

Pure cubic BLN (a = 4.095Å) was obtained at 1000°C when fired for 3 hours, but was accompanied by a small amount of hexagonal BLN (a = 5.804Å, c = 19.076 Å) after 3 hours at 1150°C. The amount of cubic BLN continued decreasing at higher temperatures. When fired for 3 hours at temperatures ranging from 1300 to 1500°C, pure hexagonal BLN was formed without other phases. There was no weight loss during the reactions at 1000-1500°C. Therefore, BLN seems to be produced by the following reaction:

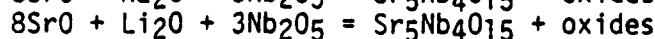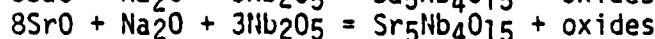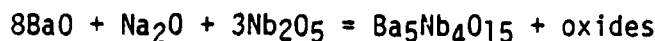$$8BaO + Li_2O + 3Nb_2O_5 = 8\ Ba(Li_{1/4}Nb_{3/4})O_3$$
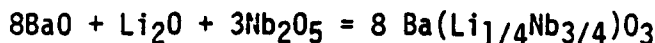
Negas et al. (3) reported that hexagonal BLN melts at 1600°C.

Pure cubic BNN (a = 4.149Å), SNN (a = 4.059Å) and SLN (a = 4.012Å) were obtained without weight loss after 3 hour firings at 1000-1300°C. When heated for 3 hours at 1350°C, the cubic phases were accompanied by a small amount of hexagonal $Ba_5Nb_4O_{15}$ or $Sr_5Nb_4O_{15}$. At 1400°C for 5 hours, pure $Ba_5Nb_4O_{15}$ or $Sr_5Nb_4O_{15}$ were observed without other phases. When $Ba_5Nb_4O_{15}$ or $Sr_5Nb_4O_{15}$ were observed, a weight loss occurred corresponding to the evaporation of Na_2O or Li_2O. Therefore, BNN, SNN, SLN, $Ba_5Nb_4O_{15}$ or $Sr_5Nb_4O_{15}$ seem to be produced by the following reactions:

At low temperature,

$$8BaO + Na_2O + 3Nb_2O_5 = 8Ba(Na_{1/4}Nb_{3/4})O_3$$
$$8SrO + Na_2O + 3Nb_2O_5 = 8Sr(Na_{1/4}Nb_{3/4})O_3$$
$$8SrO + Li_2O + 3Nb_2O_5 = 8Sr(Li_{1/4}Nb_{3/4})O_3$$

At 1400°C for 5 hours,

$$8BaO + Na_2O + 3Nb_2O_5 = Ba_5Nb_4O_{15} + oxides$$
$$8SrO + Na_2O + 3Nb_2O_5 = Sr_5Nb_4O_{15} + oxides$$
$$8SrO + Li_2O + 3Nb_2O_5 = Sr_5Nb_4O_{15} + oxides$$

x-ray peak intensities of the secondary oxide phases were too weak to be con-
clusively identified.

When K_2CO_3 was used as a source for B ions, only $Sr_6Nb_2O_{11}$ (cubic a =
4.130Å) (9), $Sr_5Nb_4O_{15}$ and $Ba_5Nb_4O_{15}$ were formed during a 3 hour firing at
1000°C without other perovskites. For longer firings, the amount of $Sr_6Nb_2O_{11}$
continued to decrease with increasing $Sr_5Nb_4O_{15}$ at 1000°C when the time was
extended from 3 to 240 hours. When heated for 3 hours at 1300°C, pure
$Sr_5Nb_4O_{15}$ was formed without other phases. $Ba_6Nb_2O_{11}$ was not observed in the
samples heated at 1000-1500°C, because it is less stable than $Sr_6Nb_2O_{11}$.
During these reactions at 1000-1500°C, a weight loss occurred corresponding to
evaporation of potassium. Since the ionic size of K is larger than that of Na
or Li. It appears to be more difficult for potassium to enter into perovskite
structure in the presence of Sr or Ba.

Powder x-ray diffraction patterns of the samples heated at 1000-1400°C
for 3 hours are given in Figure 1.
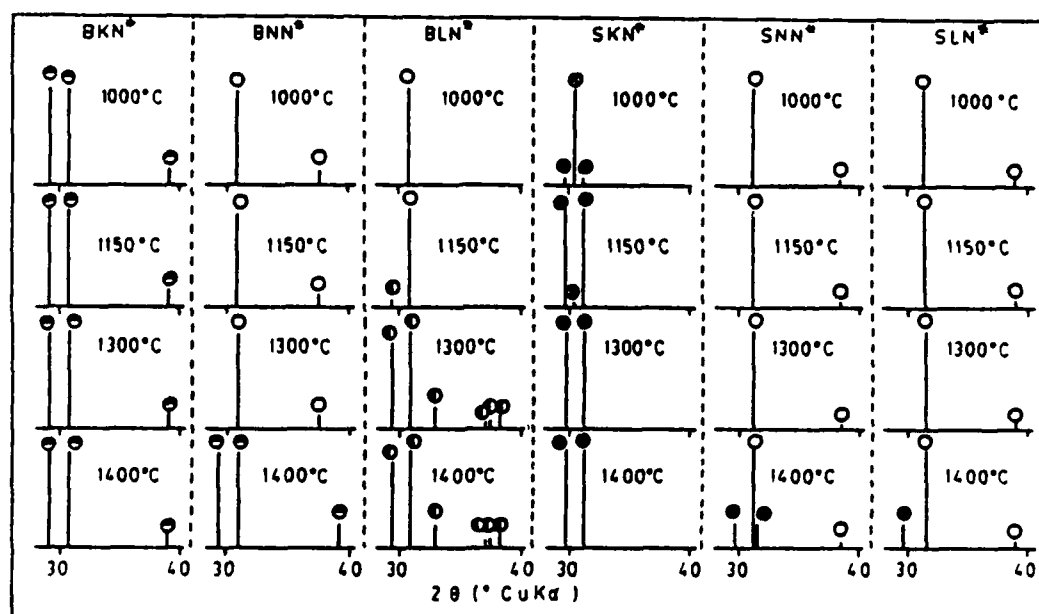
FIG. 1

The powder x-ray diffraction patterns of samples heated
at 1000-1400°C for 3 hours. * : mixtures, 0:cubic
perovskite, ◑:$Ba_5Nb_4O_{15}$, ◐:hexagonal BLN, ◓:$Sr_6Nb_2O_{11}$,
●:$Sr_5Nb_4O_{15}$.

Negas et al. (3) synthesized hexagonal BLN by heating the cubic form, but
up to the present, no other hexagonal ABN phases have been reported. In this
investigation, we tried to obtain analogous phases by heating cubic BNN, SNN
and SLN at 900-1500°C for periods of 1.5 to 240 hours. The cubic perovskite
phases used had previously been prepared by reacting the carbonates and oxides
at 1000°C for 3 hours.

Figure 2 shows the phases obtained by heating cubic perovskites at 900 - 1400°C, and Figure 3 shows the powder x-ray diffraction patterns of the samples heated at 1350°C for 20 hours.

FIG. 2

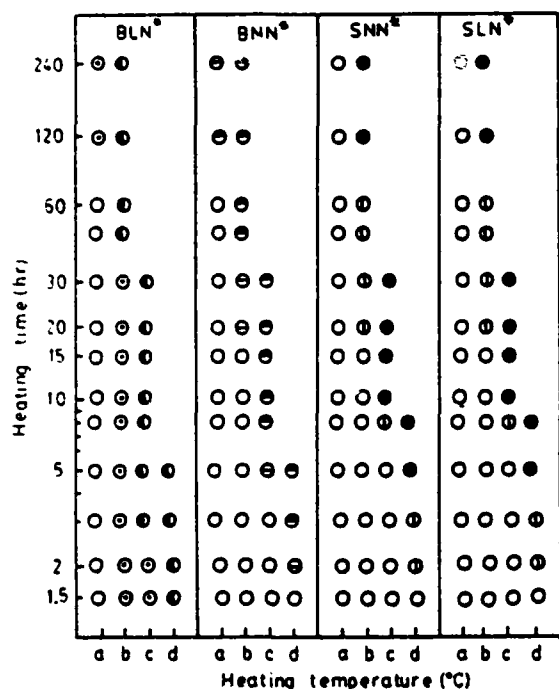The phases obtained by heating cubic ABN at (a) 900°C, (b) 1150°C, (c) 1300°C and (d) 1400°C for 1.5-240 hours. *:mixtures, O:cubic ABN, $\ominus$:cubic BLN+hexagonal BLN, $\mathbf{0}$:hexagonal BLN, θ:cubic BNN+$Ba_5Nb_4O_{15}$, $\bullet$:$Ba_5Nb_4O_{15}$, $\mathbb{O}$:cubic ABN+ $Sr_5Nb_4O_{15}$, $\bullet$:$Sr_5Nb_4O_{15}$

FIG. 3

The powder x-ray diffraction patterns of the samples obtained by heating (A) cubic BNN, (B) cubic BLN, (C) cubic SNN and (D) cubic SLN at 1350°C for 20 hours. θ:$Ba_5Nb_4O_{15}$, 0:hexagonal BLN, $\bullet$:$Sr_5Nb_4O_{15}$

According to the spectrographic chemical analyses of the samples obtained by heating cubic ABN at 900-1400°C, the percentage Na_2O or Li_2O decreased with increasing $Ba_5Nb_4O_{15}$ or $Sr_5Nb_4O_{15}$. Table 1 compares the chemical compositions (wt%) of the cubic perovskites obtained at 1000°C for 3 hours with the samples obtained by heating cubic ABN at 1350°C for 20 hours.

Weight loss percentages of the samples heated at high temperatures were directly proportional to the decrease in Na_2O or Li_2O.

Cubic BNN, SNN and SLN were not stable at high temperature. Their structures were destroyed gradually by heating as Na or Li evaporated, leading to the formation of $Ba_5Nb_4O_{15}$ or $Sr_5Nb_4O_{15}$. No hexagonal BNN, SNN and SLN were observed in the heated samples. Only BLN transformed from a cubic into a hexagonal form above 900°C. The hexagonal BLN did not transform into a cubic phase on cooling. Therefore, this transformation could be characterized as monotropic and sluggish.

As cubic perovskite decomposes at high temperatures, accompanied by the evaporation of Na or Li, the amount of BaO or SrO was in excess of the amount needed for the formation of $Ba_5Nb_4O_{15}$ or $Sr_5Nb_4O_{15}$.
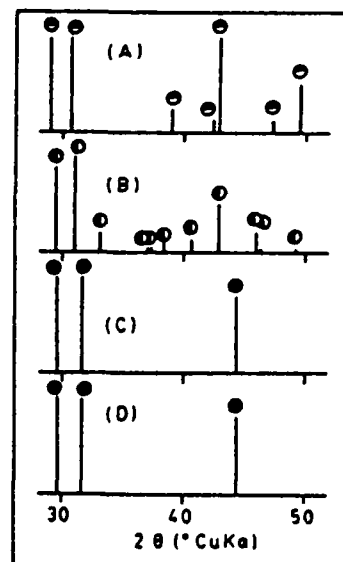
TABLE 1

Chemical compositions (wt%) of (1) cubic BNN, (3) BLN, (5) SNN
and (7) SLN, and products obtained by heating (2) cubic BNN,
(4) BLN, (6) SNN and (8) SLN at 1350°C for 20 hours.

	(1)	(2)	(3)	(4)	(5)	(6)	(7)	(8)
BaO	58.30	61.11	59.25	59.32	-	-	-	-
SrO	-	-	-	-	48.12	50.86	50.37	50.76
Na_2O	3.05	tr	-	-	3.57	tr	-	-
Li_2O	-	-	1.53	1.48	-	-	1.81	tr
Nb_2O_5	38.18	38.70	39.09	39.11	48.34	48.92	48.23	48.79
total	99.53	99.81	99.87	99.91	100.03	99.78	100.41	99.55

Galasso et al. (4,5) found that $Ba_5Ta_4O_{15}$ or $Sr_5Ta_4O_{15}$ was obtained by
mixing BaO or SrO in about 2% excess of the stoichiometric percentage when
heated in air at 1150°C. They also reported that cubic perovskites $Sr(Na_{1/4}$
$Ta_{3/4})O_3$ (SNT) and $Sr(Li_{1/4}Ta_{3/4})O_3$ (SLT) decomposed on heating at high
temperatures to give $Sr_5Ta_4O_{15}$. No hexagonal SNT or SLT was observed.

Since the ionic radius and valence of niobium are similar to those of
tantalum, it is not surprising that $Ba_5Nb_4O_{15}$ and $Sr_5Nb_4O_{15}$ form at high
temperature when the cubic phase decomposes. Powder x-ray diffraction
patterns showed only $Ba_5Nb_4O_{15}$ or $Sr_5Nb_4O_{15}$ at high temperatures.

The structural chemistry of the ABO_3 perovskite type can be described in
terms of close packed AO_3 layers with B cations in octahedral interstices. If
the layers are cubic close-packed, the octahedra form a three-dimensional
array with corner sharing to give the ideal perovskite structure. Deviations
from the ideal structure may be understood in terms of a tolerance factor
defined as

$$t = (r_A + r_0)/\sqrt{2}(r_B + r_0)$$

where r is the ionic radius. For perfect close packing, t has a value of 1.0.
When t > 1.0, structures involving either mixed cubic and hexagonal or pure
hexagonal close packing of the AO_3 layers are observed.

Tolerance factors of our samples are as follows: BLN 0.94, BNN 0.90,
SLN 0.85, and .N 0.82. Therefore, BLN has a higher probability of adopting
the hexagonal form than do the others. The failure to form hexagonal BNN and
SNN is due to the fact that Na is much larger than Li and the absence of hexa-
gonal SLN can be attributed to the smaller size of Sr compared to Ba. Conse-
quently, only BLN transforms from a cubic to a hexagonal form without evapora-
tion of Li at high temperature, and there are no other hexagonal ABN structures.

There has been conjecture concerning the ordered or disordered distribu-
tion of B and C cations in complex perovskite $A(B_{1/2}C_{1/2})O_3$. Ordered distri-
bution of B and C ions in the B-sites are most probable when large differences
exist in either charge or ionic radius (4,7,8). $Ba(Mg_{1/2}W_{1/2})O_3$ and
$Ba(La_{1/2}Ta_{1/2})O_3$, for example, are ordered distributions. Therefore, it was
expected that cubic BNN, BLN, SNN and SLN might be ordered because of large
differences between Na (or Li) and Nb.

However, no superstructure lines were observed in powder x-ray diffraction patterns of the cubic perovskites annealed at 400-1500°C for times ranging from 1.5 to 240 hours. Perhaps more prolonged heating times at high temperature may be required.

It is difficult to compare the relative distributions of Na (or Li) and Nb atoms in the B-sites because no other detailed investigation of cubic $A(B_{1/4}Nb_{3/4})O_3$ (A = Ca, Ba, Sr, Pb; B = Na or Li) have been reported.

$BaTiO_3$ has the same structure as cubic ABN and is an important ferroelectric. In the perovskites, the Curie-Weiss constant (appearing in the Curie-Weiss equation $K - K_0 = C/(T-T_0)$) is about 10^5 in the presence of active ions such as Ti^{4+}, Nb^{5+} and W^{6+}, which tend to promote distortions. It is expected that dielectric properties of cubic ABN would be relatively independent of the temperature and frequencies because a quarter of the octahedral sites are occupied by Na or Li ions which tend to prop open the structure.

Dielectric constants and dielectric loss of sintered cubic ABN were shown in Figure 4 (at -80 to +200°C under 10^5 Hz) and Figure 5 (at 20°C under 10^3 to 10^7 Hz).
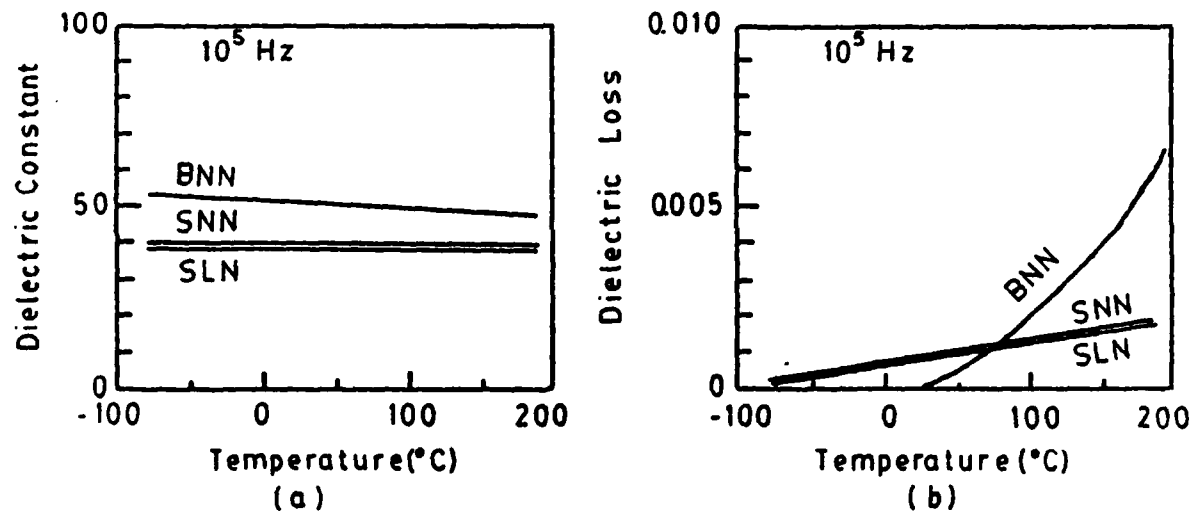

FIG. 4

Dielectric constant (a) and dielectric loss (b) of sintered cubic ABN at -80 to +200°C under 10^5 Hz.

Dielectric constants of cubic ABN (38-53) were not large, but were relatively independent of temperature and frequency. T. Mizutani et al. (10) sintered the mixtures of SLN 90 and $SrTiO_3$ 10 mole% to form ceramics at high temperatures, and reported that the dielectric constant, mechanical quality factor (Q) and temperature coefficient of the ceramics were 34, 3600 and +1 ppm/degree, respectively. These properties may make the ABN ceramics attractive new materials for high frequency applications.
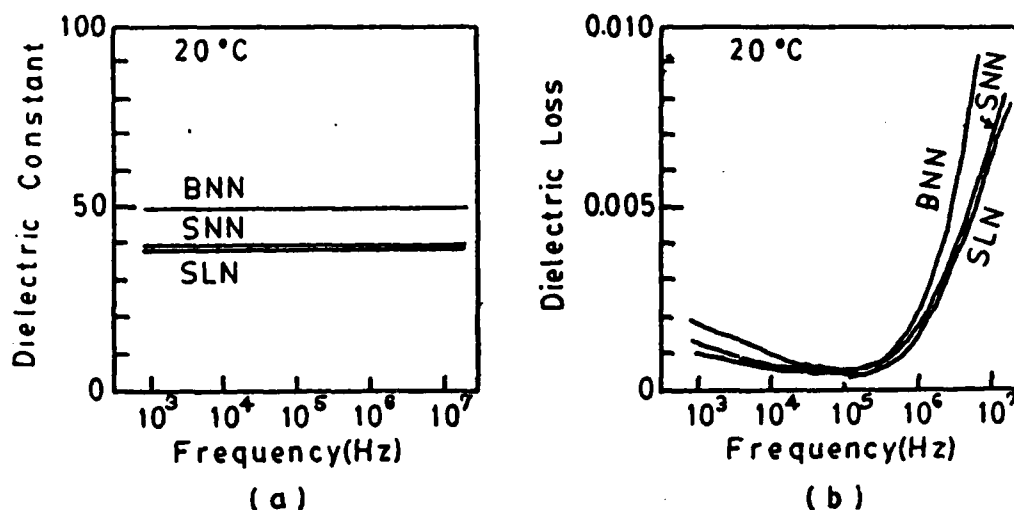
FIG. 5

Dielectric constant (a) and dielectric loss (b) of
sintered ABN at 20°C under 10^3-10^7 Hz.

Acknowledgement

References

1. A.G. Kapyshev, V.V. Ivanova, and Yu. N. Venevtsev, Dokl. Akad. Nauk SSSR
   167, 564 (1966).
2. Y. Matsuo, H. Sasaki and S. Hayakawa, Patent, Ser. No. 45869 (1970).
3. T. Negas, R.S. Roth, H.S. Parker and W.S. Brower, J. Solid State Chem.,
   8, 1 (1973).
4. F. Galasso and J. Pinto, Inorg. Chem., 4, 255 (1965).
5. F. Galasso and L. Katz, Acta Cryst., 14, 1647 (1961).
6. B.M. Collins, A.J. Jacobson and B.E.F. Fender, J. Solid State Chem., 10,
   29 (1974).
7. N. Setter and L.E. Cross, J. Mat. Sci., 15, 2478 (1980).
8. F. Galasso and W. Darby, S. Phys. Chem., 66, 131 (1962).
9. L.H. Brixner, J. Am. Chem. Soc., 80, 3214 (1958).
10. T. Mizutani, H. Iwasaki, H. Egami, Japan Kokai Patent, 76, 84099, 23 July
   1976, Appl. 75/8361, 21 Jan. 1975.

APPENDIX 2

PREPARATION AND DIELECTRIC PROPERTIES OF CUBIC PEROVSKITE
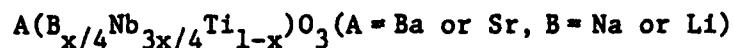
$$A(B_{x/4}Nb_{3x/4}Ti_{1-x})O_3 \text{ (A = Ba or Sr, B = Na or Li)}$$

Y. Hikichi, Zhili Chen, R.E. Newnham and L.E. Cross
Materials Research Laboratory
The Pennsylvania State University
University Park, Pennsylvania 16802

ABSTRACT

Cubic perovskite solid solutions $A(B_{x/4}Nb_{3x/4}Ti_{1-x})O_3$ (A = Ba or Sr, B = Na or Li, and x = 0.2-1) were prepared by solid state reaction at 1450°C, starting with oxides or carbonates of the elements. X-ray diffraction lines were indexed on the basis of a cubic unit cell with a lattice parameter near 4Å, and with no other detectable phases or superstructure lines arising from ordering of the octahedral ions. Dielectric constants of ceramics sintered at 1450°C for one hour ranged from 38 to 300 at 10^5 Hz, and were relatively independent of temperature (-80 to 200°C) and frequency (10^3 to 10^7 Hz). These dielectric properties make these complex cubic perovskites attractive candidates for high frequency dielectric applications.

Introduction

Most of the ABO_3 compounds have the perovskite structure. The unit cell contains A ions at the corners of a cube, B ions at the body center, and oxygen ions at the centers of the faces.

Matsuo et al. (1) first prepared the complex cubic perovskites $Ba(Na_{x/4}Nb_{3x/4}Ti_{1-x})O_3$ for the range x = 0.01-0.30. Mizutani et al. (2) prepared another family of complex cubic perovskites $A(Li_{x/4}Nb_{3x/4}Ti_{1-x})O_3$ (A = Ba or Sr, and x = 0.5-1). These structures may be regarded as solid solutions between the perovskites $A(B_{1/4}Nb_{3/4})O_3$ (A = Ba or Sr, B = Na or Li, abbreviated as ABN) (3) and the perovskite $BaTiO_3$ (or $SrTiO_3$).

However, there are several uncertainties regarding these materials including the question of order or disorder among the octahedral ions, as well as the size of the dielectric coefficients and loss. Several of these points are discussed in this paper.

Experimental Procedures

The starting materials, reagent grade $BaCO_3$, $SrCO_3$, Na_2CO_3, Li_2CO_3, TiO_2

and Nb_2O_5, were obtained from Alfa Division, Ventron Co. The following mixtures of the starting materials were ball-milled under alcohol for 20 hours: $xBa(Na_{1/4}Nb_{3/4})O_3 - (1-x) BaTiO_3$ (BNNT series), $xSr(Na_{1/4}Nb_{3/4})O_3 - (1-x) SrTiO_3$ (SNNT series) and $xSr(Li_{1/4}Nb_{3/4})O_3 - (1-x) SrTiO_3$ (SLNT series), $x = 0.2, 0.4, 0.6, 0.8$ and 1.0.

After drying at 105°C, the milled powders were heated for one hour in a sintered alumina crucible at temperatures ranging from 1000°C to 1450°C. There was no reaction with the crucible.

Single-phase cubic perovskites were obtained when fired for one hour at 1450°C. To study the degree of ordering among the octahedral ions, the cubic phases were heated in air at various temperatures in the range 1000-1450°C for time periods of 1 to 10 hours.

A powder X-ray diffractometer using CuKα radiation and an X-ray fluorescence spectrometer were used for phase identification, measurement of lattice parameter, and for chemical analysis.

The cubic perovskites ($x = 0.2-1$) obtained at 1450°C were ground again to pass through a 200 mesh sieve, and then pressed into pellets (1x10 mm) using a small amount of polyvinyl alcohol as a binder. The pellets were sintered for one hour at 1450°C in a sintered alumina crucible to give ceramics suitable for property measurement. Bulk densities of these ceramics exceeded 96% of theoretical.

Dielectric constants of the sintered pellets were measured from -80 to +200°C at frequencies ranging from 10^3 to 10^7 Hz under weak ac fields using a Hewlett Packard automatic capacitance bridge.

Results and Discussion

The chemical compositions of the samples heated for one hour at 1000-1450°C were almost identical to the theoretical values. Table 1 shows the chemical analyses (wt%) of the complex cubic perovskites.

For the mixing mole ratio $x = 1.0$, single phase cubic perovskites $Ba(Na_{1/4}Nb_{3/4})O_3$ (a = 4.149Å, BNN), $Sr(Na_{1/4}Nb_{3/4})O_3$ (a = 4.059Å, SNN) and $Sr(Li_{1/4}Nb_{3/4})O_3$ (a = 4.012Å, SLN) were obtained at 1050°C for one hour. When $x>0$, single cubic form compounds were obtained at 1000-1450°C for one hour. Their X-ray diffraction lines were indexed on the basis of a cubic cell with a lattice parameter near 4Å, and no other phases were observed.

TABLE 1

Chemical compositions (wt%) of (1) cubic BNNT (x = 0.2), (2) BNNT (x = 0.5), (3) SNNT (x = 0.2), (4) SNNT (x = 0.5), (5) SLNT (x = 0.2) and (6) SLNT (x = 0.5) obtained at 1450°C for 1 hour.

	(1)	(2)	(3)	(4)	(5)	(6)
BaO	63.79	62.05	–	–	–	–
SrO	–	–	54.60	52.68	54.89	53.47
Na_2O	0.64	1.53	0.81	1.96	–	–
Li_2O	–	–	–	–	0.40	0.96
TiO_2	26.65	16.03	33.69	20.21	33.89	20.24
Nb_2O_5	8.45	20.29	10.58	25.36	10.56	25.41
Total	99.53	99.90	99.68	100.21	99.74	100.08

Lattice parameters of samples were determined with the X-ray diffractometer. Lattice parameters of the tetragonal $BaTiO_3$ (a = 3.994Å), c = 4.038Å, $\sqrt[3]{a^2c}$ = 4.009Å) and cubic $SrTiO_3$ (a = 3.905Å) are cited from a reference (4). Fig. 1 shows the relations between lattice parameter of cubic form compounds and x value. According to Fig. 1, nearly linear relationships between lattice parameter and x were obtained.
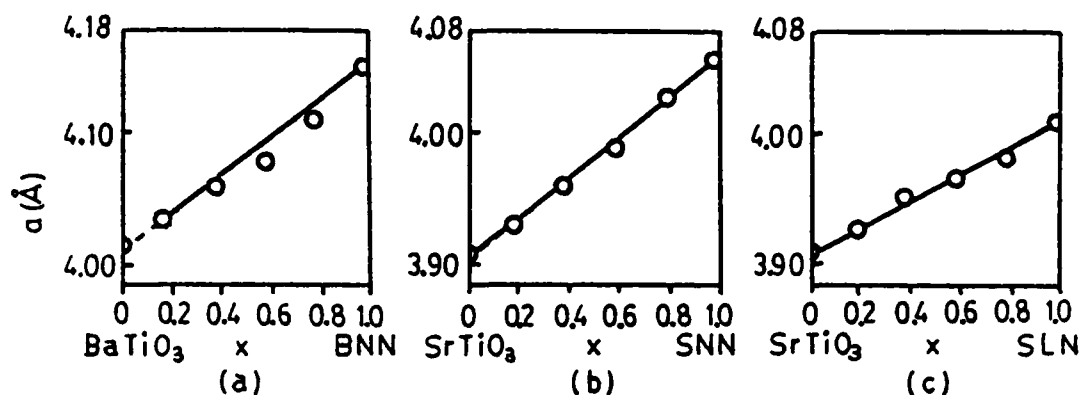

FIG. 1

Lattice parameter a(Å) of cubic compounds vs. x in the system of (a)$BaTiO_3$-BNN, (b)$SrTiO_3$-SNN and (c)$SrTiO_3$-SLN
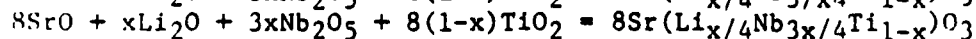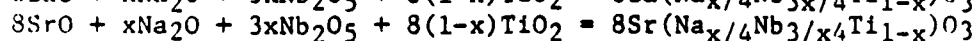
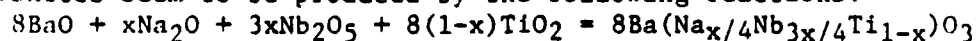It is apparent that cubic solid solutions were made up at 1450°C for one hour in air in the system of xBNN-(1-x)$BaTiO_3$, xSNN-(1-x)$SrTiO_3$ and xSLN-(1-x)$SrTiO_3$ with x = 0.2-1.

In the ABO_3 perovskite structure, the A cation is coordinated with twelve oxygens and the B cation with six. Thus, the A cation is normally somewhat larger than the B cation. Ionic radii of the ion (5) are Ba(1.34Å) > Sr(1.12Å) > Na(0.94Å) > Nb(0.74Å) > Li(0.68Å) = Ti(0.68Å).

Matsuo et al. (6) calculated the X-ray diffraction intensities of cubic form BNN, SNN and SLN on the assumption that the Ba ion (or Sr ion) was located at A site, and one fourth Na ion (or Li ion) and three fourths Nb ion was located at the B sites in a cubic unit cell of perovskite Type ABO_3. The calculated X-ray diffraction intensities were almost the same as the observed values. The above assumption was consequently proved by the experimental facts.

Thus, it seems reasonable to presume the chemical formulae of the cubic form solid solutions as follows: $Ba(Na_{x/4}Nb_{3x/4}Ti_{1-x})O_3$, $Sr(Na_{x/4}Nb_{3x/4}Ti_{1-x})O_3$ and $Sr(Li_{x/4}Nb_{3x/4}Ti_{1-x})O_3$.

During the reaction for the formation of the complex perovskites carried out at 1000-1450°C, there was no weight loss. Therefore, the complex cubic perovskites seem to be produced by the following reactions:

$$8BaO + xNa_2O + 3xNb_2O_5 + 8(1-x)TiO_2 = 8Ba(Na_{x/4}Nb_{3x/4}Ti_{1-x})O_3$$
$$8SrO + xNa_2O + 3xNb_2O_5 + 8(1-x)TiO_2 = 8Sr(Na_{x/4}Nb_{3/x4}Ti_{1-x})O_3$$
$$8SrO + xLi_2O + 3xNb_2O_5 + 8(1-x)TiO_2 = 8Sr(Li_{x/4}Nb_{3x/4}Ti_{1-x})O_3$$

Cubic BNNT, SNNT and SLNT have three cations in the B site for 0 < x < 1. These complex perovskites were annealed at 1000-1450°C for time periods of 1 to 10 hours in an attempt to observe ordering. However, no detectable super-

structure lines due to ordered distribution of B site cation were observed in the powder diffraction patterns.

Galasso et al. (7,8) and Setter et al. (9) reported that ordered distribution of B and C cations in complex perovskite $A(B_{1/2}C_{1/2})O_3$ were most probable when large differences existed in either charge or ionic radius. For example, $Ba(Mg_{1/2}W_{1/2})O_3$ and $Ba(La_{1/2}Ta_{1/2})O_3$ have ordered configurations. In the complex perovskites, there are large differences in either charge or ionic radius between Na (or Li) and Nb (or Ti).

Cubic BNN, SNN and SLN were annealed at 400–1450°C for times ranging from 1.5 to 240 hours, however no superstructure lines were observed in the powder diffraction patterns. Udagawa et al. (10) first prepared the new cubic perovskite $Pb(Li_{1/4}Nb_{3/4})O_3$ (a = 4.069Å, PLN) and also reported that no superstructure lines were observed in the powder X-ray diffraction patterns of cubic PLN.

It seems to be more difficult for cubic ABN compounds and their solid solutions to achieve ordered distributions than for the $A(B_{1/2}C_{1/2})O_3$ ceramics to do so.

In order to clarify the question of order or disorder among the octahedral ions in the cubic $A(B_{1/4}Nb_{3/4})O_3$ and their related solid solutions, it is desirable to prepare and study additional $A(B_{1/4}C_{3/4})O_3$ perovskites. At the present time, it is very difficult to compare the relative distributions among octahedral ions in the cubic perovskite series $A(B_{1/4}Nb_{3/4})O_3$ and related solid solutions because few ABN compounds have been reported.

Dielectric constants and dielectric losses of sintered complex cubic perovskites are shown in Fig. 2 and 3. Measurements were carried out from –80 to +200°C at 10^5 Hz, or at 20°C for frequencies of 10^3 to 10^7 Hz. Dielectric losses of sintered samples were less than 0.007.
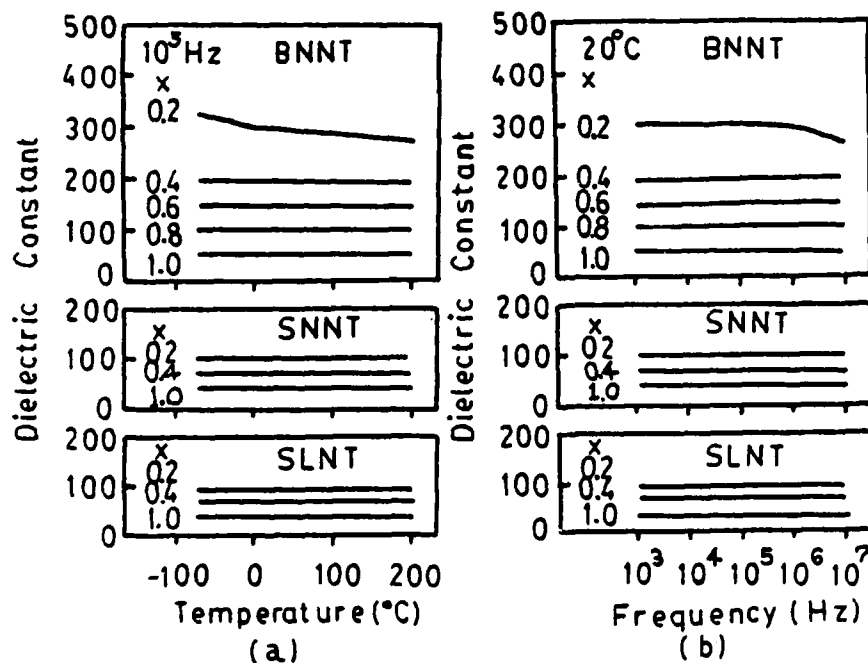

FIG. 2

Dielectric constants of sintered complex cubic perovskites. (a) at –80 to +200°C under 10^5 Hz, (b) at 20°C under 10^3 to 10^7 Hz.
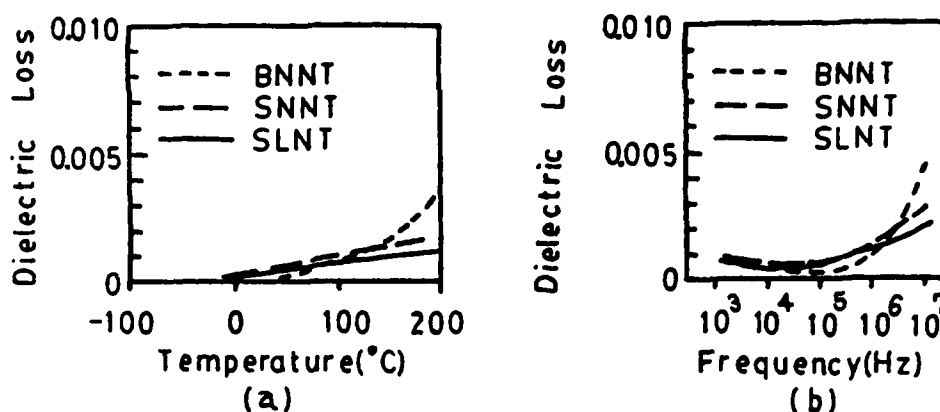
FIG. 3

Dielectric losses of sintered complex cubic perovskite
$(x = 0.6)$.   (a) at -80 to +200°C under 10^5 Hz, (b) at
20°C under 10^3 to 10^7 Hz.

The temperature coefficient (α) of the dielectric constant is normally
defined by the following equation:

$$\alpha = (K_{80} - K_{20}) / (K_{20}(80 - 20))$$

where K_{80} is a dielectric cosntant at 80°C and K_{20} is a dielectric constant at
20°C. The dielectric constant was measured five times for each sample, and
the mean temperature coefficient was calculated. Table 2 lists the temperature
coefficient obtained for each sintered sample.

There is an increasing need for dielectric materials of high dielectric
constant, low dielectric loss and low temperature coefficient (α). High di-
electric constant materials are very important in making small, compact capac-
itors, and low dielectric loss prevents heating. Low temperature coefficient
of dielectric constant permits the dielectric to be used over a wide tempera-
ture range.

$BaTiO_3$ and $SrTiO_3$ are very important materials. $BaTiO_3$ has the ideal
cubic perovskite structure above the Curie point, but on cooling below this
temperature the oxygen and titanium ions shift to form a tetragonal structure
with the c-axis about 1% longer than the other two. At about 0°C, the symmetry
of the crystal becomes orthorhombic, and at -90°C trigonal. Therefore, struc-
ture is very sensitive to the temperature. $SrTiO_3$ has the cubic perovskite
structure, and has a dielectric constant of about 200 at room temperature.

Khodakov (11) attempted to modify the properties of $BaTiO_3$ by using a fine
particle size of $BaTiO_3(1-20\,\mu)$ and found that the peaks in the dielectric
constant versus temperature curves were flatter with decreasing particle size.
This is one of important methods of obtaining materials whose dielectric con-
stants are high and relatively independent of temperature.

$BaTiO_3$ group perovskite have active ions in octahedral sites such as
Ti^{4+}, Nb^{5+} and W^{6+} which tend to promote distortions. If inactive ions such
is Na^+ or Li^+ occupy some of the octahedral sites instead of Ti^{4+}, Nb^{5+} or
W^{6+}, the dielectric properties become relatively insensitive to the change of
temperature and frequency. The Na^+ or Li^+ ions tend to prop open the structure,
and destroy the cooperative motions associated with the phase transition. The
dielectric constants of cubic ABN ceramics are not large, but are relatively

TABLE 2

Dielectric constant (K) and Temperature Coefficient (α) of sintered cubic perovskite at 20°C under 10^5 Hz.

Sample	K	α
BNNT 0.2	300	−1000
0.4	193	−300
0.6	147	−150
0.8	98	<−50
1.0	53	<−50
SNNT 0.2	100	<+50
0.4	73	<+50
0.6	60	<+50
0.8	47	<+50
1.0	40	<+50
SLNT 0.2	96	<+50
0.4	70	<+50
0.6	58	<+50
0.8	45	<+50
1.0	38	<+50

independent of temperature (−80 to +200°C) and frequency (10^3 to 10^7 Hz) because a quarter of the octahedral sites are occupied by inactive Na or Li ions.

Cubic perovskite BNNT, SNNT and SLNT are solid solutions between cubic ABN and $BaTiO_3$ (or $SrTiO_3$). As shown in Fig. 2, 3 and Table 2, several of these complex perovskites have relatively high dielectric constants and low loss over a wide range of temperature (−80 to +200°C) and frequency (10^3 to 10^7 Hz).

Matsuo et al. (1) and Mizutani et al. (2) have described some of these materials in patents. For example, they report that sintered cubic $Ba(Na_{0.125}Nb_{0.375}Ti_{0.5})O_3$ has a dielectric constant of 160 and a temperature coefficient of −210 ppm/°C, and $Sr(Li_{0.225}Nb_{0.675}Ti_{0.1})O_3$ with a dielectric constant of 34 and a temperature coefficient of +1 ppm/°C. These results are consistent with those presented here.

These properties make the cubic perovskites BNNT, SNNT and SLNT attractive as new materials with relatively high dielectric constants which are independent of temperature and frequency.

Acknowledgement

References

1. Y. Matsuo, H. Sasaki, and S. Hayakawa. United States Patent, No. 3,709,704 (1973).

2. T. Mizutani, H. Iwasaki, and H. Egami, Japan Kokai Patent, 76, 84099, 23, July 1976, Appl. 75/8361, 21 Jan. 1975.

3. Y. Hikichi, Zhili Chen, R.E. Newnham, and L.E. Cross, Mat. Res. Bull., 17, 1371 (1982).

4. O. Muller and R. Roy, "The Major Ternary Structural Families", p. 344, Springer-Verlag, New York (1974).

5. F.S. Galasso, "Structure Properties and Preparation of Perovskite-type compounds", p42, Pergamon Press (1969).

6. Y. Matsuo, H. Sasaki, and S. Hayakawa, Patent, Ser. No. 45869.

7. F.S. Galasso and J. Pinto, Inorg. Chem., 4, 255 (1965).

8. F.S. Galasso and W. Darby, S. Phys. Chem., 66, 131 (1962).

9. N. Setter and L.E. Cross, J. Mat. Sci., 15, 2478 (1980).

10. S. Udagawa, S. Shin, and K. Kumata, Mat. Res. Bull., 8, 1165 (1973).

11. A.L. Khodakov. Sov. Phys., Solid State 2, 1904 (1960).

APPENDIX 3

Low-Temperature Dielectric Properties of Ceramic Potassium Tantalate (KTaO₃)

Z. X. CHEN, X. L. ZHANG,* and L. E. CROSS*

Materials Research Laboratory, The Pennsylvania State University, University Park, Pennsylvania 16802

Dielectric properties of KTaO₃ ceramic fabricated by both conventional sintering and sintering followed by isostatic hot pressing (HIP) were measured at T=4.2 to 300 K over a frequency range from 400 Hz to 4 MHz. The weak field response shows a faint peak near 10 K which has a clear relaxation character, as in high-purity single crystals. The general response is well reproduced by the Barrett function, but additional polarizability with relaxation character is also in evidence at higher temperatures. No dielectric hysteresis was observed at high fields for cycling frequencies down to 0.04 Hz anywhere in the temperature range.

I. Introduction

LOW-TEMPERATURE properties of single-crystal KTaO₃ have been extensively investigated by dielectric, thermal conductivity, specific heat, light, and neutron scattering measurements, but the results are not yet in complete agreement. The earlier measurement of the dielectric properties of single-crystal KTaO₃ by Hulm et al.[1] showed a peak in the temperature dependence of permittivity at 13 K. In subsequent measurements made by Demurov and Venevtsev,[2] both hysteresis loops in $P(E)$ and a very high peak in $K(T)$ were observed at 10 K. All of the preceding results suggested that a ferroelectric transition may have occurred. Measurements by Wemple,[4] however, indicated that KTaO₃ remains essentially paraelectric and cubic to at least 4.2 K and no hysteresis loops were observed[3] to 1.6 K. Wemple suggested that impurities were responsible for the ferroelectric transition observed by Hulm et al. Most later measurements of the dielectric properties for single-crystal KTaO₃[5-7] have tended to support Wemple's conclusion that there is no ferroelectric transition above the liquid helium temperature, even though a very weak peak in $K(T)$ was still often observed at 3 K.[8,9] The peak is only about 0.2% higher than the K values at the lowest temperature, and has been attributed to a low-frequency relaxation effect.[8]

In addition to the results of the dielectric measurements, an anomalous behavior was observed by inelastic neutron scattering measurement[10] at 4.3 K, a discontinuity in the thermal conductivity curve at 4.5 K was found,[11] and a large discrepancy between the measured specific heat and the Debye contribution for θ (182 K and 580 K) at low temperature was indicated.[12] A possible explanation for these anomalous behaviors is that a nonferroelectric transition has set in near these temperatures. The interaction of TO and TA modes may be the cause of a "small" phase transition, without dielectric anomaly.[10]

Finally, an earlier study of nonlinear dielectric properties in single-crystal KTaO₃ at 4 K reported that some of the dielectric properties could not be explained if the crystal retained a center of symmetry at this temperature.[13] Both the irreversible electrocaloric effect and the loop openings observed in the dielectric data indicated that KTaO₃ does not retain a center of symmetry at low temperature.[12]

Therefore, low-temperature properties are still not quite clear even in single-crystal KTaO₃.

The available dielectric data on ceramic KTaO₃ are quite limited:

the only report (published by Siegwarth et al.[8]) could not provide any applicable experimental data. It seems that no excellent ceramic samples which can be used for dielectric measurement have been fabricated.

In the present work, ceramic samples of KTaO₃ which can be used for dielectric measurement were fabricated by both conventional sintered and isostatic hot-pressing (HIP) techniques. Although a dopant can also improve the grain growth to obtain improved microstructure, small additions may change the intrinsic properties of KTaO₃. Doping studies will be reported elsewhere and are not included in this paper. The temperature dependence of permittivity and loss tangent were measured at T=4.2 to 300 K and over the frequency range 400 to 10⁶ Hz. Slight peaks in both the permittivity and loss tangent were observed near the liquid helium temperature in every sample for which such measurements were made. A very clear shifting of the measured tan δ peaks toward higher temperature was observed with increasing measuring frequency, and we believe provides the first clear proof of the relaxation character of these low-temperature maxima.

Relaxation effects were also observed in $K(T)$ at T>50 K and make very significant departures from the expected Curie-Weiss behavior. Clearly, from the frequency response and temperature domain of observation, these are relaxations and are *not* associated with quantum effects.

II. Preparation and Samples

The KTaO₃ powders used in these studies were obtained from two sources. Powder I possessed the higher purity (nominal purity 99.9+%).* Powder II was prepared from mixtures of K_2CO_3 and Ta_2O_5 (nominal purity 99.8% and 99.5%, respectively). The components were thoroughly mixed by wet ball-milling for 24 h, the powders were calcined in a closed crucible at 800°C for 16 h, and the reacting mixtures were then ground to pass a 400-mesh screen.

X-ray analysis for both types of powder specimens showed that powder I had second phase $K_3Ta_4O_{11}$; powder II was completely reacted and there was no second phase.

Spectrochemical results for both powder specimens, indicating the amount of contained impurities, are shown in Table I. Ceramic samples of both types of powder were sintered by conventional methods. To avoid excessive loss of volatile potassium, the pressed pellets were covered with calcined powder of the same composition and fired in a close crucible. Samples sintered at 1310°C exhibited very poor microstructure with little grain growth as observed by SEM (Fig. 1(A)) and physical properties were not those of the crystalline phase. By increasing the sintering temperatures to 1330°C for 1 h, some grain growth was observed by SEM (Fig. 1(B)). Although the density of these ceramic samples is still only about 87% of theoretical, properties of the

---

*Alfa Div., Ventron Corp., Danvers, MA.

Table I. Spectrochemical Analysis Data

Powder	Impurity content (wt%)						
	Si	Al	Mg	Zr	Ti	Ca	Nb
I	0.05	0.05	0.05	<0.002	0.005	0.005	<0.005
II	0.05	0.2	0.2	0.002	<0.001	0.005	0.02

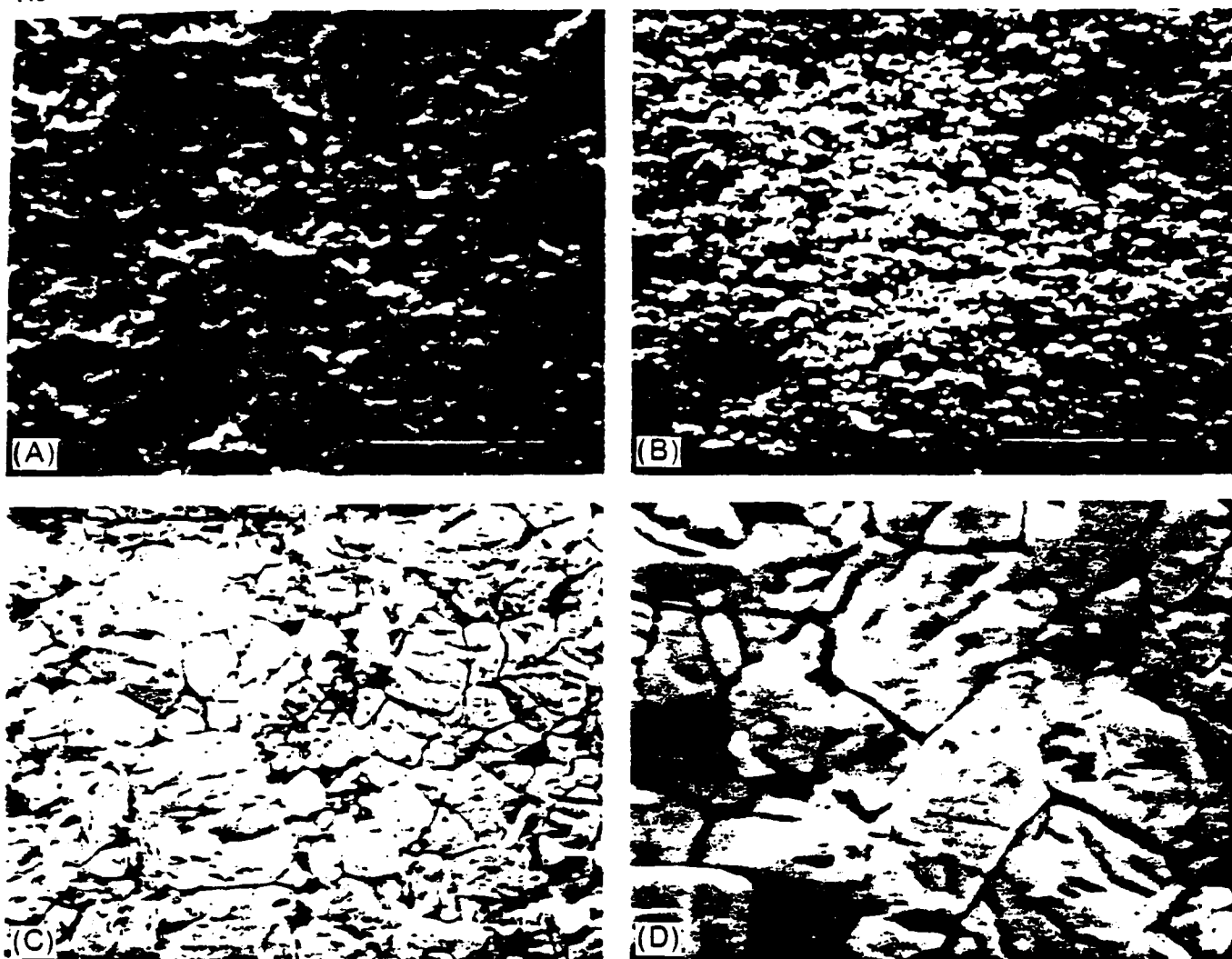**Fig. 1.** Microstructure of ceramic $KTaO_3$ sintered for 1 h at (A) 1310°C (× 1500) and (B) 1330°C (× 1500) and isostatically hot-pressed for 1 h at 1300°C ((C) × 1500 and (D) × 4700).
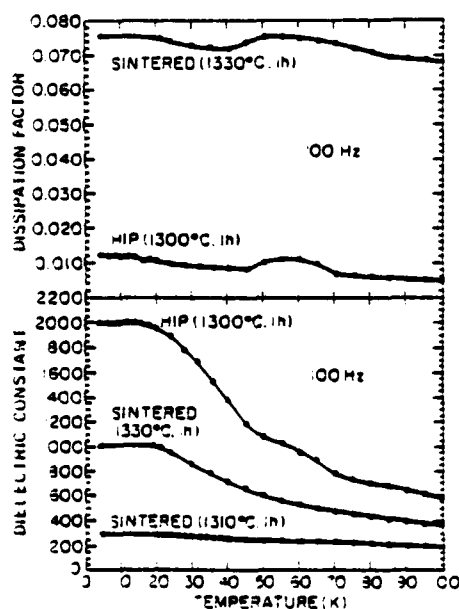

Fig. 2. Dielectric properties of ceramic $KTaO_3$ fabricated by different methods.

crystalline phase have started to appear. Such ceramic samples can be used for dielectric measurements. When the sintering temperature is further increased, the ceramic samples are difficult to extract from the packing powder. Extending the sintering time did not appear to improve the microstructure significantly.

X-ray analysis showed that all second phase disappears in ceramic sample I and there is only $KTaO_3$ phase in both ceramic samples.

To improve the properties of the ceramic samples, they were isostatically hot-pressed. Specimens wrapped in platinum foil were heated to 1300° to 1310°C under 20.7×10^6 Pa argon for 1 h and then cooled at the rate of 20°C/min. Ceramic sample III has a much improved density (92%) and microstructure with grain sizes of 1 to 8 μm (Fig. 1(C),(D)). The dielectric measurements which follow were made largely on ceramic samples of type III.

III. Experimental Techniques

Dielectric measurements were made on three kinds of ceramic samples; at least three samples of each kind were measured. Gold electrodes were sputtered on the surface to form capacitors. The automatic LCR bridges[*] were used to measure the capacitance and loss of the samples. Measuring frequencies ranged from 10^2 to
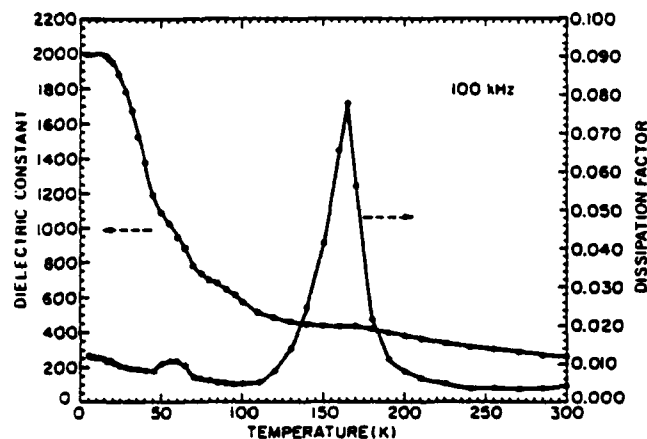
Fig. 3. Dielectric properties of ceramic KTaO₃ sample III.

10' Hz. but we found that reliable results cannot be obtained at frequencies below 400 Hz and above 4 MHz due to the effects of the noise and the inductance of connecting wires. So all of the data which follow are limited to the frequency range of 4×10^2 to 1×10^6 Hz. Capacitance accuracy is about ±0.15%. The small signal measuring electric field is <10 V/cm.

Measurements were made at T-4.2 to 300 K. The accuracy of the temperature was controlled within ±0.5 K. Hysteresis loops were observed by a Sawyer-Tower circuit at a frequency of 0.04 Hz. Measurements were recorded and controlled by a computer through the data bus system.[z]

IV. Experimental Results and Discussion

Figure 2 shows the temperature dependence of the dielectric properties of ceramic KTaO₃ samples which are fabricated by different methods. Ceramic samples conventionally sintered at 1310°C for 1 h did not exhibit the crystalline physical properties which we expected. By increasing the sintering temperature to 1330°C for 1 h, we obtained ceramic samples which can be used for dielectric measurement; the permittivity increases from 180 at room temperature to 1000 and loss tangent 0.08 at liquid helium temperature for a frequency of 100 kHz. High dielectric dissipation of the samples are, we believe, due to the unsatisfactory density. The densification of the samples was much improved by HIP processing. For these ceramics, the permittivity is enhanced to 230 at room temperature and to 2000 at 4.2 K and loss tangent is down to 0.01 at liquid helium temperature.

The temperature dependence of the dielectric properties of the ceramic sample III indicated that here are three anomalous dispersion regions within the measuring temperature range (Fig. 3).

The first dispersion region is near the liquid helium temperature: a very weak $K(T)$ peak was observed at 10 K, similar to that observed in single-crystal KTaO₃.[8,9] The maximum is only about 0.5% higher than the K values at the lowest temperature. but decreases in height in the higher-purity ceramic sample I (0.2%). The $K(T)$ peak appears to be slightly shifted with measuring frequencies (Fig. 4(A)), but it is difficult to observe clearly. The tan $\delta(T)$ peak shifts in a pronounced manner with measuring frequencies shown in Fig. 4(B). No hysteresis loops were observed below 10 K, even at field strengths of 20 kV/cm (Fig. 5).

Our results of the dielectric measurement showed that different nominal-purity ceramic KTaO₃ samples do not exhibit the ferroelectric phase transition near the liquid helium temperature. This result tends further to confirm the conclusion, supported by a number of measuring data, that no ordering transition takes place at low temperature in single-crystal KTaO₃.

Fig. 4. First dispersion region of ceramic KTaO₃ near liquid helium temperature showing (A) $K(T)$ and (B) tan $\delta(T)$.
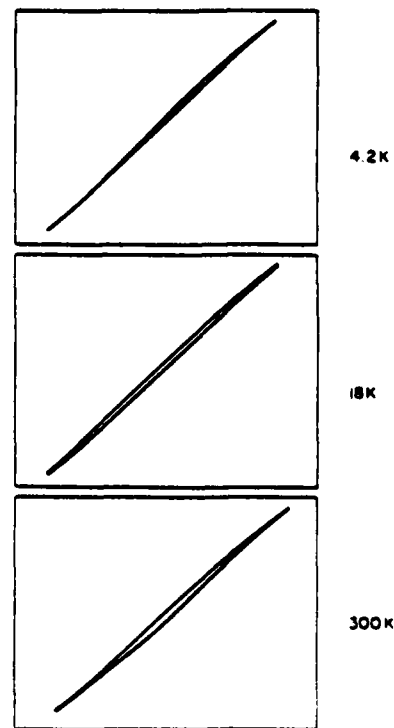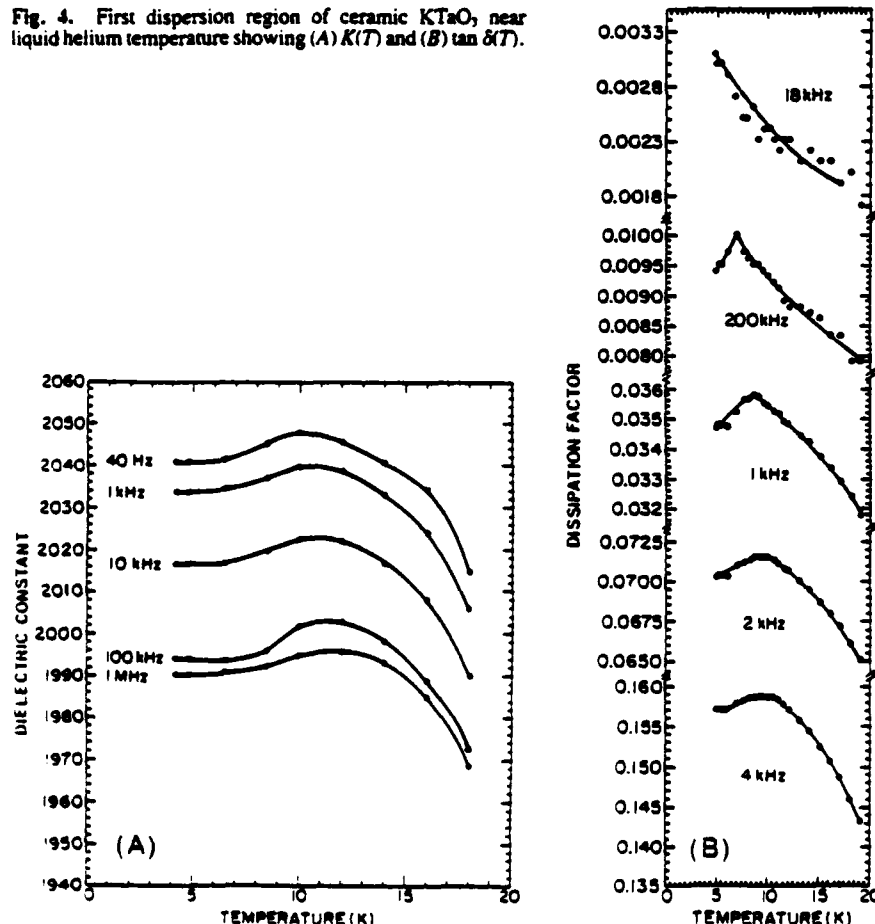

(A)

(B)

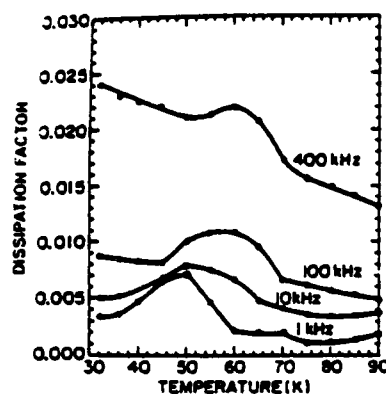Fig. 5. Hysteresis loops in 20-kV/cm field.
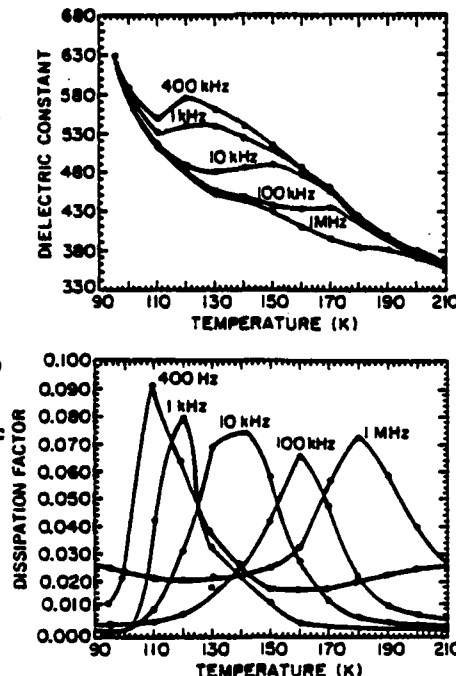
Fig. 6.   Second dispersion region of ceramic KTaO₃.
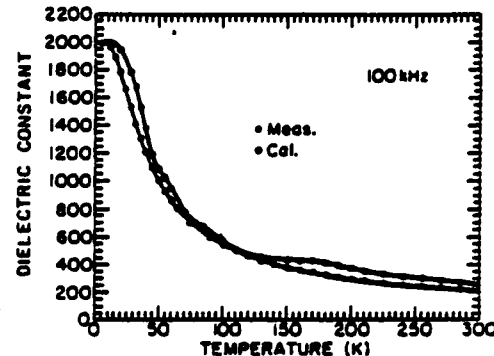
Fig. 8.   Deviation of experimental curve from calculated curve.

Fig. 7.   Third dispersion region of ceramic KTaO₃.

The very weak $K(T)$ peaks are due to the relaxation effect which was explained in detail by Siegwarth and coworkers.[8,14] It suggests that all of the KTaO₃ single-crystal and ceramic samples investigated probably contain impurities in sufficient amounts to alter the intrinsic dielectric properties from those of pure KTaO₃. Our dielectric measurements first revealed that the tan $\delta(T)$ peaks shift markedly with measuring frequencies near the liquid helium temperature and that the $K(T)$ peak does decrease in height in higher-purity ceramic KTaO₃ sample I. These results are in good agreement with Siegwarth and coworkers' explanation.

Activation energy U_1 and intrinsic vibration frequency ν_1 of the relaxor were estimated approximately from the following formula.

$$\omega_m \tau = 1 \tag{1}$$

$$\tau = \frac{1}{2\nu} e^{U/kT} \tag{2}$$

$$U = kT_1 T_2 \cdot (\ln \omega_{m_1} - \ln \omega_{m_2})/(T_1 - T_2) \tag{3}$$

where ω_{m_1} and ω_{m_2} are the angular frequencies corresponding to tan δ maxima at T_1 and $T_{/2}$, respectively, and τ is the relaxation time. From these relations we calculate $U_1 \approx 8 \times 10^{-22}$ J and $\nu_1 \approx 2.5 \times 10^9$ Hz.

The second and third dispersion regions, starting from 50 K and 100 K, respectively, have pronounced relaxation characterization, as seen in Figs. 6 and 7. The corresponding activation energies and intrinsic vibration frequencies are $U_2 \approx 9.6 \times 10^{-21}$ J, $\nu_2 \approx 3.0 \times 10^{10}$ Hz and 3.68×10^{-19} J, $\nu_3 \approx 2.0 \times 10^{13}$ Hz, respectively. Impurities, defects, and space charges at the grain boundary are the possible source of the relaxation. It was not investigated further in this work.

The temperature dependence of the permittivity of single-crystal KTaO₃ obeys the Curie-Weiss law from 50 K to at least 300 K.[15] the temperature range below 50 K being where deviations ascribed to quantum effect dominate. An equation was derived by Barrett[16] using a model based on a quantum-statistical ensemble of oscillators for the permittivity in a temperature region covering the classical and the quantum range.

$$K = A + \frac{B}{T_{1/2} \coth T_{(1/2)} - T_0} \tag{4}$$

where T_1 represents the dividing temperature between the classical and quantum regions.

We found that the temperature dependence of the permittivity of ceramic KTaO₃ deviates from the Curie-Weiss law even above 50 K due to the relaxation effect throughout the measuring temperature range. A set of parameters used in a fitting to the Barrett function was obtained from some selected experimental data which exhibited the least relaxation effect, as shown in Table II. Figure 8 shows a plot of the permittivity vs temperature as calculated from the data in Table II. The deviation of values between the experimental and calculated curves indicates approximately the increasing values of the permittivity due to the relaxation effect.

We summarized the experimental results to indicate that a real and very weak $K(T)$ peak exists at liquid helium temperature in ceramic KTaO₃, similar to recent findings in single-crystal KTaO₃. In the ceramic, it is clearly caused by relaxation effects rather than an ordering transition. Our experimental results revealed further that a real relaxation effect also exists throughout the measuring temperature range in ceramic KTaO₃ and that the measured data of $K(T)$ deviate from the Curie-Weiss law. We can infer that the permittivity of ceramic KTaO₃ may be attributed to the sum of contributions from the transverse optical mode and the relaxation effects.

Table II.   Parameters Used in Fitting
to Barrett Function for KTaO₃

Parameter	Value	
	Single crystal	Ceramic
A	48	49
$B \times 10^{-4}$	6.18	4.86
T_0 (K)	8.02	5.22
T_1 (K)	48.3	60

References

[1] J. K. Hulm, B. T. Matthias, and E. A. Long, "A Ferroelectric Curie Point in KTaO₃ at Very Low Temperatures," *Phys. Rev.*, **79** [5] 885–86 (1950).

[2] D. G. Demurov and Yu. N. Venevtsev, "Character of Phase Transition of Ferroelectric KTaO₃," *Sov. Phys. Solid State*, **13** [3] 553–56 (1971).

[3] S. H. Wemple, "Some Transport Properties of Oxygen-Deficient Single-Crystal Potassium Tantalate (KTaO₃)," *Phys. Rev. A*, **137** [5] 1575–82 (1965).

[4] W. R. Abel, "Effect of Pressure on the Static Dielectric Constant of KTaO₃," *Phys. Rev. B*, **4** [8] 2696–2701 (1971).

[5] G. A. Samara and B. Morosin, "Anharmonic Effects in KTaO₃: Ferroelectric Mode, Thermal Expansion and Compressibility," *Phys. Rev. B*, **8** [3] 1256–63 (1973).

[6] R. P. Lowndes and A. Rastogi, "Stabilization of the Paraelectric Phase of KTaO₃ and SrTiO₃ by Strong Quartic Anharmonicity," *J. Phys. C: Solid State Phys.*, **6**, 932–44 (1973).

[7] I. M. Buzin, I. V. Ivanov, N. N. Moiseev, and V. F. Chuprakov, "Nonlinearity and Dielectric Losses in Potassium Tantalate," *Sov. Phys.-Solid State*, **22** [7] 1200–1202 (1980).

[8] J. D. Siegwarth, J. C. Hölste, and A. J. Morrow, "Polarization and Dielectric Constant of Potassium Tantalate," *J. Appl. Phys.*, **47** [11] 4791–93 (1976).

[9] W. N. Lawless, "Recent Topics in Ferroelectric Properties at Low Temperatures," *Ferroelectrics*, **24**, 327–35 (1980).

[10] G. Shirane, R. Nathans, and V. J. Minkiewicz, "Temperature Dependence of the Soft Ferroelectric Mode in KTaO₃," *Phys. Rev.*, **157** [2] 396–99 (1967).

[11] E. F. Steigmeier, "Field Effect on the Cochran Modes in SrTiO₃ and KTaO₃," *Phys. Rev.*, **168** [2] 523–30 (1968).

[12] W. N. Lawless, "Specific Heat and Electrocalorie Properties of KTaO₃ at Low Temperatures," *Phys. Rev. B*, **16** [1] 433–39 (1977).

[13] J. E. Geusic, S. K. Kurtz, T. J. Nelson, and S. H. Wemple, "Nonlinear Dielectric Properties of KTaO₃ Near Its Curie Point," *Appl. Phys. Lett.*, **2** [10] 185–87 (1963).

[14] J. D. Siegwarth and A. J. Morrow, "Low-Temperature Polarization in Impure SrTiO₃ Ceramics," *J. Appl. Phys.*, **47** [11] 4784–90 (1976).

[15] D. Rytz, J. L. Servoin, and F. Gervais, "Deviation from the Curie-Weiss Law in KTa₁₋ₓNbₓO₃ at High Temperature," *Ferroelectrics*, **38**, 817–20 (1981).

[16] J. H. Barrett, "Dielectric Constant in Perovskite Type Crystals," *Phys. Rev.*, **86** [1] 118–20 (1952).

APPENDIX 4

POLARIZATION MECHANISMS IN HIGH K DIELECTRICS

L. E. Cross
Associate Director of Materials Research Laboratory
Professor of Electrical Engineering
Materials Research Laboratory
The Pennsylvania State University
University Park, PA 16802

ABSTRACT

The polarization mechanisms which contribute to the high weak field dielectric permittivity in the current generation of BaTiO$_3$ based high K dielectrics used in multilayers are considered for both paraelectric and ferroelectric phase regions. In the ferroelectrics with diffuse phase transitions, new information from the compositions in the Pb(Sc$_{1/2}$Ta$_{1/2}$)O$_3$ and Pb(Sc$_{1/2}$Nb$_{1/2}$)O$_3$ families will be considered, and the behavior compared and contrasted with that of the (Bi$_{(2/3)}$)$_x$Sr$_{1-x}$)TiO$_3$ and more recent 'Skanavi' type' relaxation materials. Evidence for a very strong 'domain' contribution to the permittivity in the soft PZTs will be briefly discussed.

2

(1) INTRODUCTION

In this paper, attention will be focused upon high permittivity ceramic dielectric materials of types which are of interest or potential future interest for multilayer capacitor application. For the present discussion 'high' is taken to mean a relative dielectric permittivity K$_R$ significantly greater than 100. To stay within a well-defined family of materials it will also be required that this K$_R$ be due to true bulk dielectric polarizability and not an artifact of a highly inhomogeneous electric field distribution as in the Maxwell:Wagner phenomenon in barrier layer dielectrics. For high permittivity defined in the above manner, it is essential that one or more of the crystalline phases of the dielectric be of a ferroelectric or an antiferroelectric material.

Before examining possible new dielectric systems, the polarization mechanisms which contribute to the dielectric response in the present generation of high K materials will be briefly reviewed. The discussion will illustrate the basic need for a complex phase assemblage to flatten the very peaked temperature dependence in the BaTiO$_3$ based systems and perhaps explain why most presently useful compositions have been achieved by almost pure "cut and try" empiricism.

For materials like the perovskite structure ferroelectrics, where the response is dominated by the intrinsic weak field permittivity of the paraelectric and single domain ferroelectric states Devonshire theory[1,2] indicates that the Curie Weiss constant C is an effective scaling parameter for the dielectric response in both para and ferroelectric states, so that the larger is C, the higher and less 'peaky' is the response, with the consequence that useful practical materials may be engineered without complex phase mixing or composition gradient manipulation. For this reason, data for the relaxor ferroelectric perovskites are discussed, where C is some five times larger than in

BaTiO₃. Interesting materials in these relaxor families are already in wide-spread use for multilayers in China, and are under intensive study in Japan.

(2) POLARIZATION MECHANISMS IN BaTiO₃ CERAMICS

Since almost all presently used high K_R dielectric formulations are based on the ferroelectric barium titanate, it is useful to start by examining the polarizability mechanisms in high purity stoichiometric BaTiO₃ crystals and ceramics.

2.1 Paraelectric Phase

BaTiO₃ belongs to the perovskite structure family. Above the ferroelectric Curie temperature near 135°C in the pure material, the symmetry is cubic (m3m) and the weak field permittivity K_R is isotropic, following in its temperature dependence a Curie Weiss law of the form

$$K_R = \frac{C}{T-\theta}$$

where C the Curie Weiss constant is of order 1.5×10^5 °K

3 the Curie Weiss temperature is some 10°C below the ferroelectric Curie point

i.e., the phase change at T_c is first order. Following the pioneer work of Fröhlich[4], Anderson[5] and Cochran[6] it is believed that the major contribution to the dielectric response comes from the 'softening' of one of the normal transverse optical modes of vibration of the ions at the Brillouin zone center. From the Lydanne-Sachs-Teller[7] relation

$$\epsilon_w = \pi_j [\frac{v_{LO}}{v_{TO}}]^2 \qquad (1)$$

where v_{LO} and v_{TO} are longitudinal and transverse modes respectively and the sum π_j is taken over all active modes. If one of the frequencies v_{TO} decreases

markedly, this term will soon dominate the sum π_j, and thus to account for Curie Weiss behavior we must have

$$v_{TO}^2 \, \alpha(T-\theta) \text{ or } v_{TO}^2 = A(T-\theta).$$

In crystals for which data is available for the constants A and C (Table 1), it is evident that for widely different ferroelectric perovskites C x A is a constant of order $(16 \pm 2) \cdot 10^{-5}$ cm^{-2}. The constancy of the C x A product suggests a general relation between mode frequency and permittivity so that in Figure 1 only the scaling of the T axis need change to describe all perovskites. In caution, however, it must be stated that there is mounting evidence that simple soft mode theory does not account for the total dielectric polarizability in the paraelectric phase of the oxygen octahedron ferroelectrics, particularly for temperatures close to T_c where the highest K_R values are obtained. Raman Brillouin scattering[9] and recent mm wave spectroscopy[10] show evidence for much lower lying excitations with relaxation character, and these appear also to be reflected in the strong 'glass-like' character of the low temperature specific heat[11,12]. Fortunately for practical purposes, the frequencies are in the

high GHz region and do not significantly perturb the broad largely frequency independent response to RF and microwave frequencies. In pure ceramic BaTiO₃ above T_c, great care must be exercised in judging what is true material response, since processing modifications can exert a profound influence upon the effective impedance of the grain boundary region[13]. The excellent data from Kinoshita and Yamaji[14] does appear to show as expected a K_R above T_c which is largely independent of grain size over a very wide range of sizes (Fig. 2, Table 2) and thus no detectable contribution to the impedance from grain boundar

2.2 Polarization Mechanisms in the Ferroelectric Phases

Below 125°C pure BaTiO₃ passes successively into the tetragonal ferro-electric phase, then at 0°C to an orthorhombic modification, and finally at -90°C to a rhombohedral symmetry which is stable to the limit of temperature measurement. Early experimental work on Remeika type crystals[15] has been well summarized by Jona and Shirane[16] and new data is up dated in the Landolt Bornstein new series volumes 3, 9 and 16[17].

Listing only major possible contributors to the polarizability there are:

(1) Intrinsic single domain responses. In each ferroelectric phase there is a family of anisotropic single domain permittivities $[K_{ij}]_R(w)$ for weak fields which characterize the response to alternating E fields for the isolated single domain state. Since the single domain is in a polar symmetry it is necessarily piezoelectric so that the permittivities measured at constant and zero mechanical stress $X_{ij} = 0$ are not the same as those measured at constant spontaneous strain $x_{ij} = x_{ij}(s)$. In BaTiO₃ at 25°C the single domain intrinsic permittivity is markedly anisotropic with $K_{33}^{X=0} = 179$ and $K_{11}^{X=0} = 4,500$, thus in a single crystal or crystallite R_{ij} is markedly dependent on the ferroelectric domain arrangement which is itself a strong function of thermal, electrical and elastic pre-treatment. For a high purity ceramic, the situation is even further compli-cated by elastic boundary conditions. Particularly for K_{11}, because of the close approach of the orthorhombic 'Curie point' at 0°C, $K_{11}^{X=0} \neq K_{11}^{X=0}$ thus R_{ij} can be further modified by internal stresses set up due to the onset of spontaneous strain at T_c, and these internal stresses can themselves be much modified by the influence of the grain size upon the relative stabilities of different domain structures. In particular it is believed that the strong grain size dependence exhibited in the data of Fig. 2 below T_c is due to this internal stress phenom-enon[13].

(2) Polarization due to domain re-arrangement. All ferroelectric phases of BaTiO₃ and of other perovskite ferroelectrics contain both ferroelectric; ferroelastic (shape changing) and pure ferroelectric (non-shape changing) domains. Characteristics and switching processes for the pure ferroelectric 180° domains have been extensively studied[19,20]. For the ferroelastic 90° domains in BaTiO₃ at 25°C, domain statics have been explored in both single crystal and ceramic materials[21,22] but the kinetics of wall motion are still uncertain. The wall region which separates domains is exceedingly narrow (less than 100 Å) and it would appear that true sideways motion of 180° walls is unlikely[23]. Evidence from single crystals suggest that these walls do not contribute to K_{ij}, but may contribute more strongly to the out of phase K_{ij}'' [24]. Definitive measurements have not been carried out for ferroelastic type walls, but there is some evidence from optical studies that quasi reversible motion may be possible[25].

In donor doped PZTs and in PLZT which are in the rhombohedral ferroelectric phase there is much clearer evidence that wall motion contributes to K_R. Cal-culations suggest that K_v is some 2 to 3 times larger than $[K_{ij}]_{WR}^{X=0}$ the intrin-sic average, and recent measurements[25] show that this enhanced permittivity freezes out at temperatures below 30°K where wall motion would be expected to become difficult. An uncomfortable ancilliary consequence of the ferroelectric domain structure is the aging phenomenon evident in all the dielectric properties of high K materials which contain one or more ferroelectric components. A complete explanation for aging even in a simple 'pure' BaTiO₃ has not been given. Current thinking appears to favor a mechanism which gives slowly increasing volume stabilization of P_s through a slow re-arrangement of polar defects with-in the domain in accommodation to the ferroelectric order parameter[26]. Clearly, however, this is not a complete explanation as antiferroelectric perovskite cc

positions also exhibit aging[27]. In this case it is believed that slow re-arrangement of the shape changing ferroelastic:antiferroelectric twin-domains may better accommodate mechanical internal stresses generated by the spontaneous strain arising at T_c[28].

2.3 Piezoelectric Effects

As was indicated in 2.1 above, the individual domains of a ferroelectric phase are necessarily piezoelectric and in BaTiO$_3$, for example, the coupling coefficients k_{33}, k_{31} and h_{15} are large. Thus, there is a large difference between K^x and K^X the constant stress and constant strain values of the domain permittivity. It has long been suspected that the dispersion which appears for most ferroelectric ceramics in the range of 10^7 to 10^8 Hz may be associated with piezoelectric resonance of the partially mechanically clamped domains pumping energy into acoustic modes of vibration. Very recently Yao Xi[29] has proven beyond doubt that such grain resonance contributes the dominant dispersion in LiNbO$_3$ model ceramics.

At lower frequencies (below 10^7 Hz) the random arrangement of crystallites in a ferroelectric ceramic averages the piezo-effect to zero. However under bias field, the electrostriction can develop a polarization biased bulk piezo-electricity which may be a troublesome converter of acoustic noise. More information about these induced piezoelectric effects in practical materials would certainly be advantageous for circuit designers.

2.4 Interactions with the Defect Structure

For any polar defect, symmetry dictates that there must be an interaction with the developing polarization of the ferroelectric domain. If the relaxation time for reorientation of the defect dipole is very long, the phenomenon will contribute to the stabilization of the domain structure and be measurable

In the aging response. If however the relaxation time is short, the defect dipoles will respond to the modulation of the P_s by external fields and thus contribute a defect dipole component to the dielectric polarizability. Such effects have been demonstrated in the simplest form in the paraelectric phase for bismuth[30], lanthanum[31], and rare earth-substituted strontium titanate[32].

Overt demonstration and separation is more difficult in the ferroelectric phases due to the plethora of other mechanisms which may intervene, but recently there is good evidence of a defect dominated mechanism enhancing the low temperature polarizability in the acceptor doped hard PZT compositions[33].

2.5 Discussion

Even in this very brief discussion it becomes clear

(a) That the simple intrinsic response of pure BaTiO$_3$ in the paraelectric phase above T_c is too sharply peaked to be of interest in practical capacitors.

(b) Introducing a ferroelectric phase necessarily brings a complex panoply of polarization mechanisms which even in a simple high purity BaTiO$_3$ ceramic are difficult to separate and impossible to control separately.

Unfortunately since the single phase composition is much too sharply peaked in its response, there is a need to introduce heterogeneity either by mixing phases on a grain-by-grain basis, between grain and boundary phases or by composition gradients within the grain structure. To a significant extent it is this need for controllable heterogeneity which makes the electronic capacitor ceramics difficult to process reproducibly. The necessity to "mix in" the complex polarization mechanisms of the ferroelectric phase frustrates simple control and separation of mechanisms and it is perhaps not surprising that the development of the useful BaTiO$_3$ based compositions has been largely empirical.

disorder of the cations can be eliminated by thermal annealing to give a normal sharp first order ferroelectric phase change[36,37,38].

$Pb(Sc_{1/2}Ta_{1/2})O_3$ is the easier compound to study, since the x-ray scattering factors for Sc and Ta are sufficiently different that the evolution of the ordered form can be followed from the development of the x-ra super-lattice lines associated with the effective doubling of the unit cell edge length in the ordered form.

A summary of the argument is given in Fig. 5, which shows the evolution of the superlattice intensities with annealing. The marked change between the dielectric properties of disordered and ordered states is shown for the weak field permittivity is shown in Fig. 6, and on the high field hysteret properties in Fig. 7. These data are for single crystals; however, analysis of the x-ray superlattice line widths show that in the single crystal the order domains are less than 1,000 Å in dimensions, and in fact crystals and ceramics do not exhibit major differences, another clear indication that the scale of inhomogeneity responsible for 'diffusing' the phase transition is much below that of normal grain sizes.

It is perhaps interesting to compare and contrast the ferroelectric relaxors, these diffuse transition materials, with the Stenavi type materials in the $(Bi_{(2/3)x}Sr_{1-x})TiO_3$[30], $(La_{(2/3)x}Sr_{1-x})TiO_3$[31] and $(Re_{(2/3)x}Sr_{1-x})TiO_3$ compositions. In these crystals the suggestion as indicated previously is of a defect polarization which interacts strongly with the soft mode in $SrTiO_3$. For these materials the dielectric properties only show smaller departures from linearity even though permittivities up to 5,000 (c_R) are accessible.

It may be suggested that perhaps a complete spectrum exists from isolated defect dipoles, through to coupled ferroelectric regions. Certainly in the system $PbNi_{1/3}Nb_{2/3}O_3 : PbMg_{1/3}Nb_{2/3}O_3$ complete solid solution occurs

(3) RELAXOR FERROELECTRICS

From the discussion in 2.1 above, it is evident that a desirable direction to move in the response function is towards perovskite type compositions with large C and thus correspondingly small A values. In the ferroelectric relaxors like $Pb(Mg_{1/3}Nb_{2/3})O_3$ (PMN) the Curie constant is more than three times larger than in $BaTiO_3$ and the dielectric response is correspondingly smoother and less peaked. It is perhaps not surprising to find that the PMN relaxor has been used as a dielectric formulation in multilayer technology in China for more than 10 years[34], and that other relaxor compositions are under intensive study in Japan[35].

Basically, the relaxor ferroelectrics are characterized by a weak field permittivity which exhibits a broad frequency dependent maximum often termed in Soviet literature a diffuse phase transition (Fig. 3) with obvious Debye type relaxation in the lower temperature domain, as evidenced by the plot of K and K'' at -25°C shown in Fig. 3b.

Until recently, the speculation has been that the behavior which occurs most typically in compositions such as $PbMg_{1/3}Nb_{2/3}O_3$ and $PbZn_{1/3}Nb_{2/3}O_3$ is associated with statistical fluctuations in the random distribution of the Mg and Nb, or Zn and Nb cations on the B sites of the ABO_3 perovskite. It has been suggested that such short range fluctuations may give rise to strong local fluctuations in the ferroelectric Curie temperature. Thus through any cross-section in the crystal at a temperature within this Curie range, the material is an intimate mixture of ferroelectric and paraelectric regions (Fig. 4). With the scale of 100 ~ 1,000 A° and the volume fraction of ferroelectric increasing continuously as the temperature decreases. Recently, this model has been largely conformed by studies on the compounds $PbSc_{1/2}Nb_{1/2}O_3$, $PbSc_{1/2}Ta_{1/2}O_3$ where the

between two end members which have classical Skanavi and authentic diffuse transition behavior, with no sudden breaks in dielectric response functions.

One suspects that similar ranges could be developed by lead addition to the SrTiO$_3$ based Skanavi systems.

TABLE 1

MAGNITUDES OF THE PARAMETERS A AND C

SUBSTANCE	C(x10^5 K)	A(cm^{-2}K^{-1})
BaTiO$_3$	1.5	9.5
PbTiO$_3$	1.7	8.2
KTaO$_3$	0.5	29.1
SrTiO$_3$	0.77	28.6
Pb(Mg$_{1/3}$Nb$_{2/3}$)O$_3$	4.7	3.4
Pb(Zn$_{1/3}$Nb$_{2/3}$)O$_3$	4.7	3.8

$$C \times A = (16 \pm 2) \times 10^5 \text{ cm}^{-2}$$
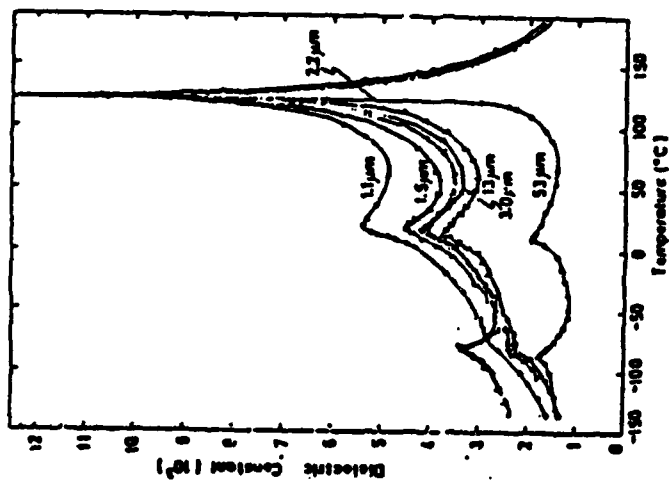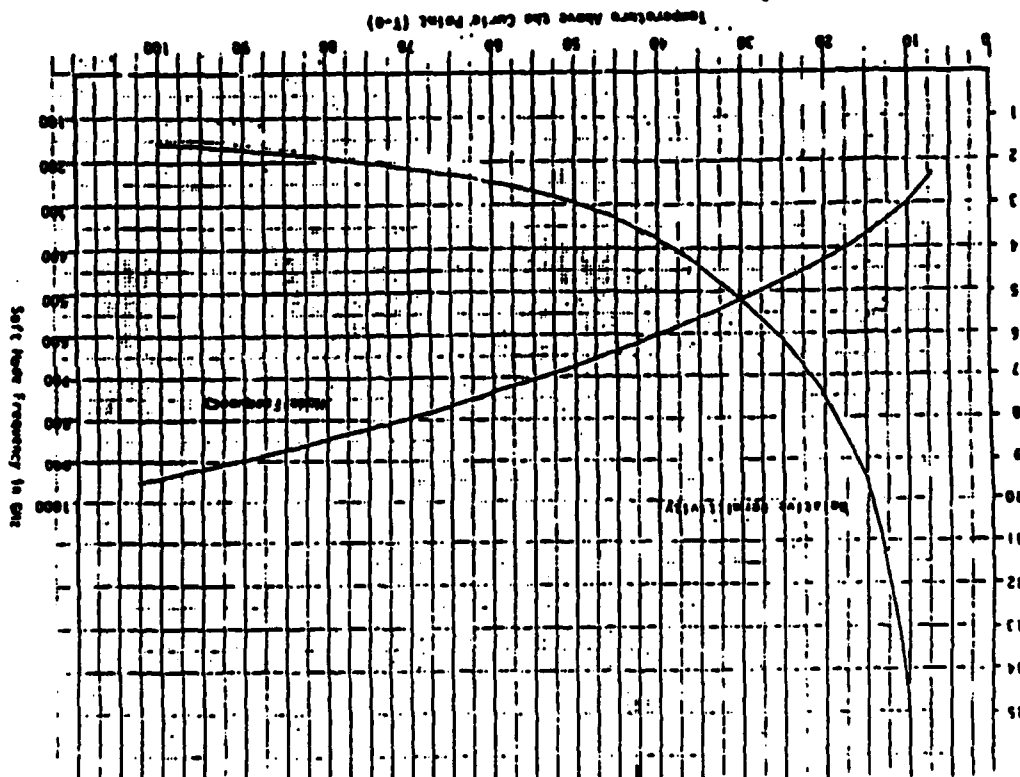
Fig. 2. Temperature Dependence of Dielectric Constant in Various Grain-Size High-Purity $BaTiO_3$ Ceramics

Table 2. Grain-Size Dependence of C, T_1, T_c, κ_{max}, T_2 and T_3 in High-Purity $BaTiO_3$ Ceramics
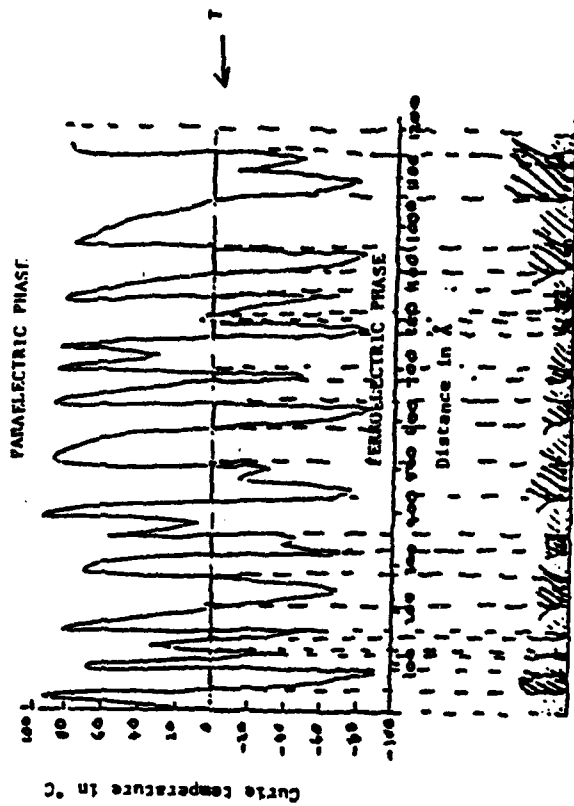

Fig. 1. Scaled for $BaTiO_3$

T-7

Fig. 4. Close Mixture of Ferroelectric and Paraelectric Micro-Regions With Linear Dimension in the Range 100 to 1,000 Å

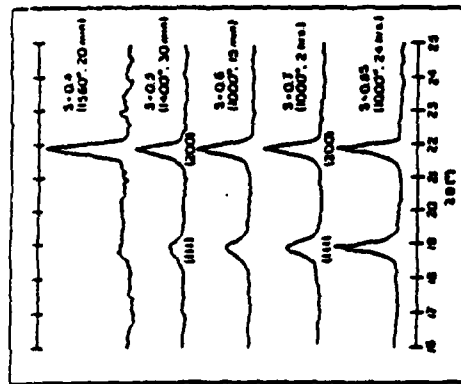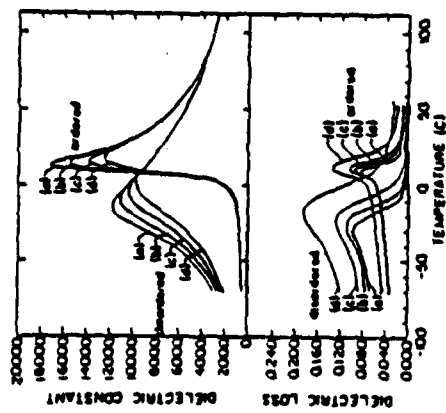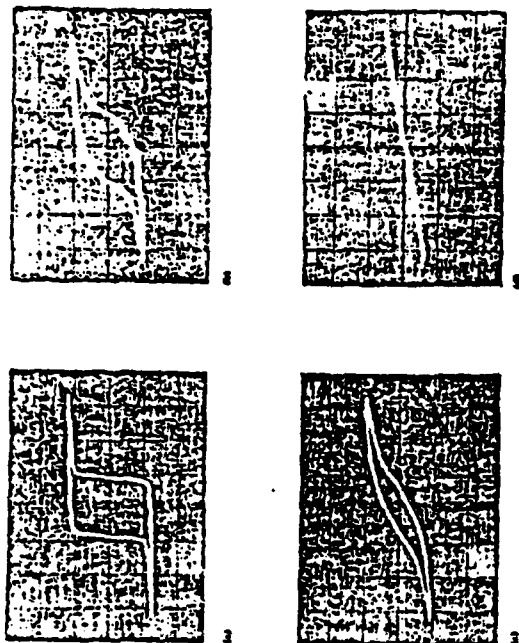Fig. 3a. Dielectric Constant as a Function of Temperature and Frequency in $Pb(Mg_{1/3}Nb_{2/3})O_3$

Fig. 3b. Relative Permittivity as a Function of Frequency in PMN at -25°C

Fig. 7. High Field Dielectric Response

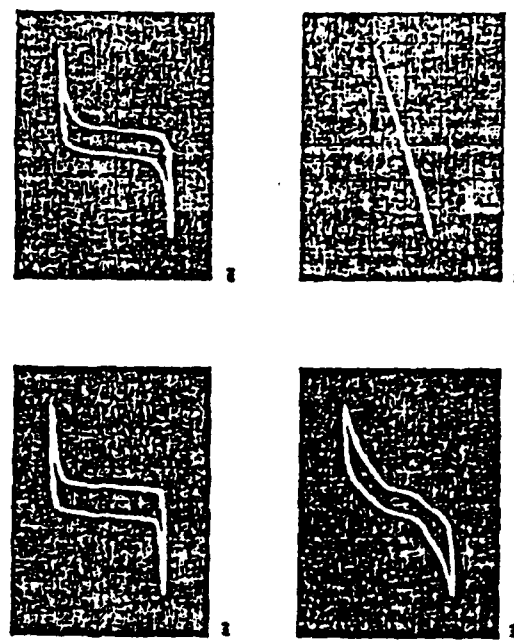Fig. 5. X-Ray Diffraction Data

Fig. 6. Weak Field Dielectric Properties

T-7

References

1. A.F. Devonshire, Theory of Barium Titanate Part 1., Phil. Mag. 40, 1040 (1949).

2. A.F. Devonshire, Theory of Barium Titanate Part 2., Phil. Mag. 42, 1065 (1951).

3. C. Kittel, Theory of Antiferroelectric Crystals, Phys. Rev. 82, 729 (1951).

4. H. Fröhlich, Theory of Dielectrics, 18, 155, Clarendon Press, Oxford (1958).

5. P.W. Anderson, Fizika Dielektrikov, 290 Acad. Nauk SSSR, Moscow (1960).

6. W. Cochran, Crystal Stability and the Theory of Ferroelectrics, Adv. in Phys. 9, 387 (1960).

7. R.H. Lyddane, R.G. Sachs, E. Teller, On the Polar Vibrations of Alkali Halides, Phys. Rev. 59, 673 (1941).

8. S.M. Shapiro, J.D. Axe, G. Shirane, Critical Neutron Scattering in SrTiO$_3$ and KMnF$_3$, Phys. Rev. B 6, 4332 (1972).

9. K.B. Lyons, Light Scattering Studies of Ferroelectric Transitions: Mode Coupling Phenomena, Ferroelectrics 35, 37-42 (1981).

10. W. Hall, W. Ho (Private Communication).

11. W. Lawless, J.C. Wolste, G.A. Samara, Dielectric Properties of KH$_2$PO$_4$; BaTiO$_3$; PbZr$_{65}$ Ti$_{0.35}$O$_3$ and TlCl between 0.015 and 10°K, Ferroelectrics 11, 337 (1976).

12. D.A. Acherman, D. Moy, R.C. Potter, A.C. Anderson and W. Lawless, Glassy Behavior of Crystalline Solids at Low Temperature. Phys. Rev. B 23, 3886 (1981).

13. D. Payne, The Role of Internal Boundaries on the Dielectric Properties of Polycrystal Ferroelectric Materials, Ph.D. Thesis, Solid State Science, The Pennsylvania State University (1973).

14. K. Kinoshita, A. Yamaji, Grain Size Effects on the Dielectric Properties in Barium Titanate Ceramics, J. Appl. Phys. 47, 371 (1976).

15. J.P. Remeika, A Method for Growing Barium Titanate Single Crystals, J. Am. Chem. Soc. 76, 940 (1954).

16. F. Jona, G. Shirane, Ferroelectricity in Crystals, Pergamon Press, NY (1962).

17. K. Hellwege, Landolt Bornstein, Group 3. Crystals and Solid State Physics, Vol. 3, Ferroelectric and Antiferroelectric Crystals; Vol. 9, Ferroelectric and Antiferroelectric Crystals; Vol. 16a, Oxide Ferroelectrics.

18. W.R. Buessem, L.E. Cross and A.K. Goswami, A Phenomenological Theory of the High Permittivity in Fine Grain BaTiO$_3$, J. Am. Ceram. Soc. 49, 33-35 (1966); Effects of Two Dimensional Pressure on the Permittivity of Fine Grain BaTiO$_3$, J. Am. Ceram. Soc. 49, 36-39 (1966).

19. E. Fatuzzo, W.J. Merz, Ferroelectricity, North Holland, Amsterdam (1967).

20. W.J. Merz, Double Hysteresis Loops of BaTiO$_3$ Near the Curie Point, Phys. Rev. 91, 513 (1953).

21. G. Remaut, R. Gevers, A. Lagasse and S. Amelinckx, Dynamical Theory of the Images of Micro Twins as Observed in the Electron Microscope III Observation and Results of Numerical Calculation, Phys. Stat. Sol. 13,

22. M.D. Denis, R.C. Bradt, Thickness of 90° Domain Walls in (BaPb)TiO$_3$ Single Crystals, J. Appl. Phys. 45, 1931 (1974).

23. R.C. Miller and G. Weinreich, Mechanism of Sideways Motion of 180° Domain Walls in BaTiO$_3$. Phys. Rev. 117, 1460 (1960).

24. J. Fousek, Contribution of Domain Walls to the Small Signal Complex Permittivity of BaTiO$_3$, Czech. J. Appl. Phys. 815, 412 (1965).

25. J. Fousek and B. Brezina, Relaxation of 90° Domain Walls of BaTiO$_3$ and Their Equation of Motion, J. Phys. Soc. Japan 19, 830-838 (1964).

26. X.L. Zhang, Z.X. Chen, L.E. Cross and W.A. Schulze, Dielectric and Piezoelectric properties of Lead Zirconate Titanate Ceramics at 4.2 to 300°K Bull. Am. Ceram. Soc. 61, 358 (1982).

27. J. Jonker, Aging in Ferroelectric Ceramics, International Summer School on Applications of Ferroelectrics, Erice, Sicily (July 1980).

28. W. Schulze, Dielectric Properties of PbZrO$_3$:PbTiO$_3$, La$_2$O$_3$ Ceramics, Ph.D. Thesis in Solid State Science, The Pennsylvania State University, June (1973).

29. Yao Xi and L.E. Cross, Piezoelectric Grain Resonance in Ceramic LiNbO$_3$, Bull. Am. Ceram. Soc. 61, 362 (1982).

30. G.I. Skanavi, Yu Ksendzov and V.A. Trigubenko, Relaxation Polarization and Losses in Non-Ferroelectric Dielectrics of High Dielectric Constant. Zh. Eks. Teor. Fiz. 30, 1047 (1956).

31. T.Y. Tien, X-ray and Dielectric Studies of SrTiO$_3$ Solid Solutions, Ph.D. Thesis in Ceramics, The Pennsylvania State University, December (1965).

32. D. Johnson, L.E. Cross and F.A. Hummel, Dielectric Relaxation in Strontium Titanates Containing Rare-Earth Ions, J. Appl. Phys. 41, 2828-2833 (1970)

33. X.L. Zhang, Z.X. Chen and L.E. Cross, Dielectric and Piezoelectric Properties of PbZrO$_3$:PbTiO$_3$ to 4.2°K, Bull. Am. Ceram. Soc. 61, 358 (1982).

34. Yao Xi (Private Communication).

35. M. Yonezawa, K. Utsumi and T. Ohno, Properties of Multilayer Ceramics in the $Pb(Zn_{1/3}Nb_{2/3})O_3$:$PB(Fe_{1/2}Nb_{1/2})O_3$:$PB(Fe_{2/3}W_{1/3})O_3$ Ternary System, Proc. 2nd Mtg. on Ferroelectric Appl., Kyoto, 215 (1979).

36. N. Setter and L.E. Cross, The Role of B Site Cation Disorder in Diffuse Phase Transition Behavior of Perovskite Oxides, J. Appl. Phys. 51, 4356 (1980).

37. N. Setter and L.E. Cross, Pressure Dependence of the Dielectric Properties of $Pb(Sc_{1/2}Ta_{1/2})_3$, Phys. Stat. Sol (a) 61, K71 (1980).

38. N. Setter and L.E. Cross, An Optical Study of the Ferroelectric Relaxors $PbMg_{1/3}Nb_{2/3}O_3$, $PbSc_{1/2}Ta_{1/2}O_3$, $PbSc_{1/2}Nb_{1/2}O_3$, Ferroelectrics 37, 551 (1981).

APPENDIX 5

POSSIBLE SPACE CHARGE EFFECTS IN MULTILAYER CAPACITORS

W.A. Schulze

Introduction

Studies of the current-voltage characteristics of TiO_2 based dielectric ceramics have since the 1950's shown that ionic or vacancy migration under field could cause space charge formation and eventually a degradation of resistivity. In modern dielectrics with valency compensating dopants, electrodes sealed from the atmosphere, and with improved density, there is some question as to whether the earlier degradation mechanisms are still active. The much lower, but still finite incident of failure in modern dielectrics, indicates that either the traditional degradation mechanisms must be still operating at orders of magnitude reduced rates or totally different mechanisms, too weak to be detected in earlier studies, now plague reliability. Another possibility is that in modern multilayer capacitors, the complex internal structure and thin dielectric layers combined with possible physical defects may concentrate mechanical and electrical stress to a level that allows a very local degradation to occur in a material that would otherwise be resistant to failure.

The work we wish to present in this paper covers the current versus time temperature and voltage characteristics of a limited number of commercial multilayer 8X capacitors. The voltage-current relation was also studied in the form of polarization-field hysteresis loops to observe the ferroelectric nature of these dielectrics.

Procedure

All experiments were performed by applying a fixed voltage from a battery pack and observing the current flow with an electrometer-multimeter operating in the current feedback mode which has an effective series resistance of about 10^6 ohm. This is about 10^4 to 10^5 times smaller than the "resistance" of the multilayer samples. All leads, battery pack and room-temperature sampleholder were constructed using low-thermal solder and shielded with the electrometer guard to minimize spurious voltages. The basic experiment consisted of applying voltage and recording current from 1 to 64 minutes. The voltages used were 1.5, 3, 6, 12, 24, 48, 100 and 200 volts. The voltage was applied in three patterns:

1) Increasing voltage from 0 to 200 volts, then returning to zero with only one 64-minute period spent at 200 volts.

2) Increasing voltage from 0 to 200 volts, then repeating the run with reversed polarity.

3) At a fixed level of 48 volts, the time dependence of current was repeated every 25°C to 175°C.

Polarization-field experiments were recorded from 0.001 Hz to 100 Hz (triangular wave form with rates from 0.2 to 2 x 10^4 v/sec) at 50 volts or about 20 KV/cm peak. Because of the very low frequency it was necessary to use an electrometer buffer with the integrating capacitor, giving a system tim

constant > 10^{12} seconds. The measurements were made in silicon oil for uniform heat dissipation at room temperature and 80°C. The loops displayed are after many cycles and recorded in order of decreasing frequency.

Results and Discussion

The time dependence of current for increasing voltage in all cases was a decreasing function with time. The most striking feature is that in log-log form the functions are near parallel with slopes of approximately 1 and there is a near doubling of current with doubling of voltage.

The linear relation broke down for approximately 50% of the samples tested in both lots of BX parts. Since all parts had received "burn-in testing" many months earlier it can be suggested that the current is affected by the chance influence of the voltage prehistory. The long time constant and two other features of the I-V plots suggest an ionic phenomenon: (1) at any given time the current is "ohmic," that is, when the voltage is doubled the current is doubled, (2) the current reduction is linear with time, suggesting a back voltage that is a sum of the current.

The summation of current to produce a back emf is demonstrated after an increasing voltage sequence. A reduction in voltage to 100 V results in a current reversal for a portion of the 64-minute period and further reduction in voltage is characterized by current flowing opposite to the polarity of the battery. If the voltage is set to 0 and polarity reversed after the increasing sequence, a large current flows independent of applied voltage. If it is assumed that all the current flowing is stored in a space charge, the summation of the current measured over all the 1- to 64-minute periods is 3 to 4 micro coulomb. Estimations of currents down to time zero can probably double this value.

A few thermally stimulated current curves were run to determine if the current from a 1.5 to 200 V sequence could be recovered. Summation of the charge liberated during a 4°C/min heating indicated that most of the charge was removed in the first cycle and that this was of a similar level to the total current from the earlier experiment. Samples undergoing a prolonged voltage at elevated temperatures had maximum in thermally stimulated current at slightly higher temperature. A typical sample liberated about 2.2 uc of charge which is about half that estimated from the integration of the applied current. This indicated that the charge storage mechanism can be reasonably efficient. The mechanism also seemed to be long lived. As-received parts which had been stored many months exhibited large currents when heated to their maximum rated temperature of 125°C. It is possible that such a discharge could damage high impedance circuitry if the multilayer has not been discharged by a heat treatment.
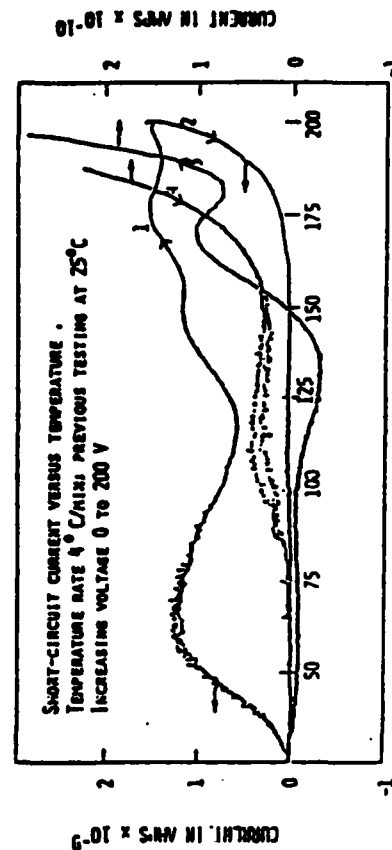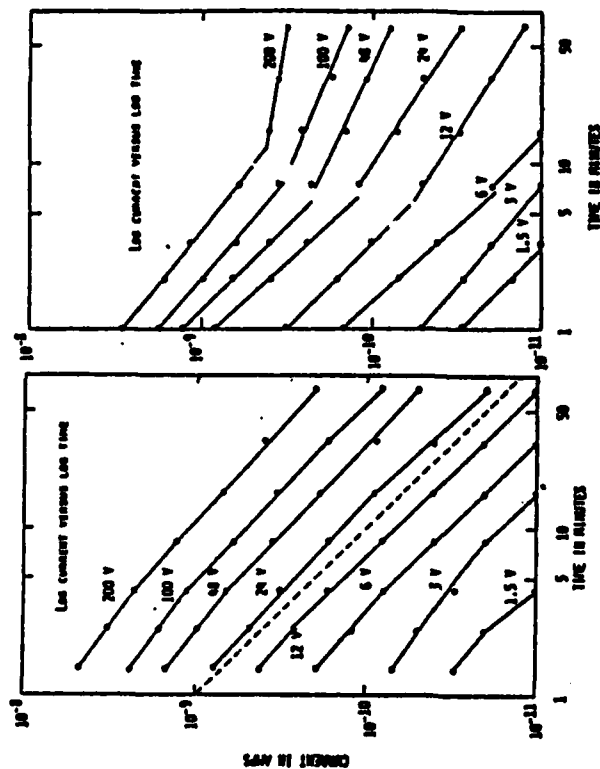
All compositions including an NPO material had similar activation energies of about 1.2 eV at temperatures about 100°C. The time necessary for the current to stabilize decreased rapidly with increasing temperature; steady state levels were usually reached in a few minutes above 100°C.
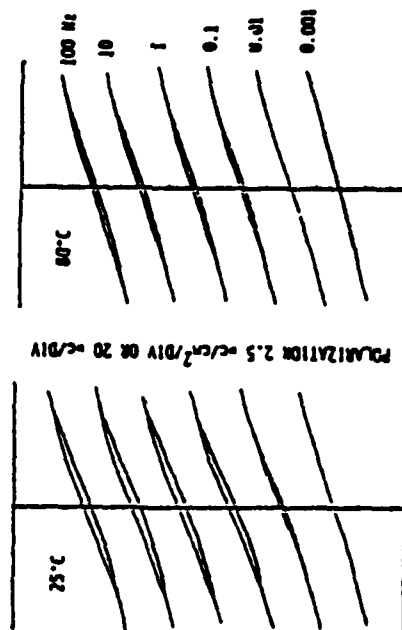
The question of the amount of ferroelectric activity was explored using a low frequency Sayner-Tower bridge. Loops made at 25° and 80°C were similar for all of the BX lots examined. At the higher frequencies there is a measurable hysteresis which appears to relax at lower frequencies. At 80°C the frequency of zero hysteresis increases and conduction hysteresis becomes evident at the lowest frequencies. The hysteresis represents currents that relax in the order of 10 seconds, or at rates too rapid to be measured on the electrometer circuit of the I-V plots. This does show, however, that under bias these BX compositions should exhibit a moderate amount of piezoelectricity.

SHORT-CIRCUIT CURRENT VERSUS TEMPERATURE.
TEMPERATURE RATE 4°C/MIN. PREVIOUS TESTING AT 25°C.
INCREASING VOLTAGE 0 TO 200 V

Log Current versus Log Time

It is obvious that when dealing with small numbers of commercial ceramic dielectrics that definite conclusions are impossible. What we would like to do is suggest the following to explain the time dependence of current.

Ferroelectricity although present in these materials is believed to operate at time constants much lower than those observed in the I-V plots. Electronic conduction is probably dominant at high temperature where the current stabilizes rapidly for any voltage. At room temperature, the conduction is characterized by long time constants and a time dependent current reduction that scales approximately with the sum of the current or at least a major fraction of the current.

Thus we wish to suggest that the current reduction is the result of a back emf resulting from the formation of a space charge. At room temperature the speculation is that the migrating species are probably oxygen vacancies although there is no direct evidence to separate ionic and electronic processes. In older studies with dielectrics two orders of magnitude thicker the induced space charge formed as virtural anode near the cathode. These space charge regions were reported to be thicker than the total dielectric in this study. A more recent study has indicated that grain boundaries limit the transport of oxygen vacancies. Without potential probe studies there is no way to distinguish between a space charge appearing at the cathode or at the cathode side of each grain. Either way the density of charges necessary to achieve the level measured is relatively low. If all the oxygen vacancies to achieve 3 uC charge transport were stored in a single atomic layer, there would only be one vacancy in every 500 unit cells.

5

P-7

LEAKAGE CURRENT VERSUS INVERSE TEMPERATURE

0.29 eV

(0.4) eV

175 150 125 100 75 50 25

CURRENT IN AMPS

10^{-6} 10^{-7} 10^{-8} 10^{-9} 10^{-10} 10^{-11}

2.0 2.5 3.0

INVERSE TEMPERATURE $\times 10^{-3}$ °C^{-1}

Group 14 006
Group 32 007 (NPO)
Group 23 004
Group 30 003
Group 21 002
Group 22 001
Group 7 001

100 Hz
10
1
0.1
0.01
0.001

80°C

25°C

POLARIZATION 2.5 µc/cm²/DIV OR 20 µc/DIV
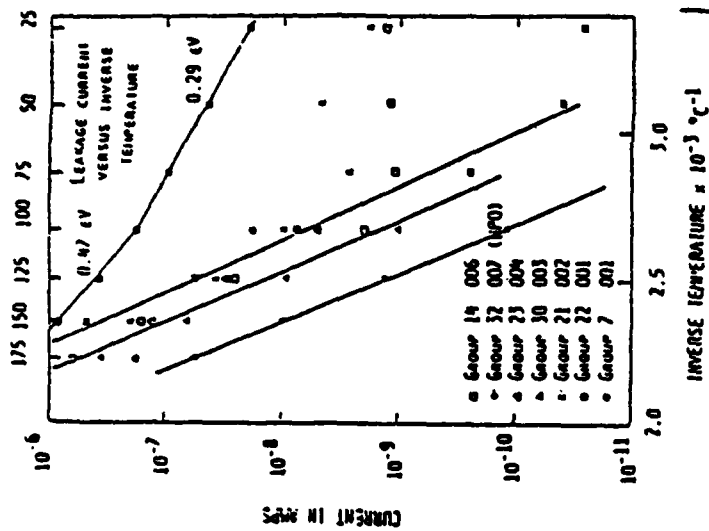
FIELD AT 4 kV/DIV OR 50 VOLTS PEAK

APPENDIX 6

NEW DIELECTRICS

L. E. Cross
The Pennsylvania State University
University Park

ABSTRACT

The polarization mechanisms that are exploited in the current generation of
$BaTiO_3$ based high K dielectrics used in multilayers are briefly summarized
for both paraelectric and ferroelectric based compositions to determine
intrinsic limitations. The possibility of using relaxor ferroelectric base
compositions in the perovskite and tungsten bronze structure field are
discussed, the mechanisms of polarization in these systems are considered, and
possible advantages of the relaxors are delineated. The possible advantage of
anitferroelectric systems is illustrated theoretically. Some alternative
technologies for fabricating multiple dielectric-electrode layers structures
are very briefly outlined, and a number of the lower symmetry ferroelectric
structures that could exhibit high K under these conditions are discussed.

INTRODUCTION

In this paper, attention will be focused upon high permittivity ceramic
dielectric materials of types that are of interest or potential future interest
for multilayer capacitor application. For the present discussion, "high" is
taken to mean a relative dielectric permittivity K_R significantly greater
than 100. To stay within a well-defined family of materials it will also be
required that the K_R be due to true bulk dielectric polarizability and not
an artifact of a highly inhomogeneous electric field distribution as in the
Maxwell-Wagner phenomenon in barrier layer dielectrics. For high permittivity
defined in the above manner, it is essential that one or more of the
crystalline phases of the dielectric be of a ferroelectric or an
antiferroelectric material.

Before examining possible new dielectric systems, the polarization
mechanisms that contribute to the dielectric response in the present
generation of high K materials will be briefly reviewed. The discussion will
illustrate the basic need for a complex phase assemblage to flatten the very
peaked temperature dependence in the $BaTiO_3$ based systems and perhaps
explain why most presently useful compositions have been achieved by almost
pure "cut and try" empiricism.

293

For materials like the perovskite structure ferroelectrics, in which the response is dominated by the intrinsic weak field permittivity of the paraelectric and single domain ferroelectric states, Devonshire theory (Devonshire 1949 and 1951) indicates that the Curie-Weiss constant C is an effective scaling parameter for the dielectric response in both paraelectric and ferroelectric states so that the larger is C, the higher and less "peaky" is the response, with the consequence that useful practical materials may be engineered without complex phase mixing or composition gradient manipulation. For this reason, data are discussed for the relaxor ferroelectric perovskites in which C is some five times larger than in $BaTiO_3$. Interesting materials in these relaxor families are already in wide-spread use for multilayers in China and are under intensive study in Japan.

Theoretically, it is demonstrated by an elementary extension of Kittel theory (1951) that an almost temperature-independent, single-phase, high-K_R material is theoretically possible in a crystal that goes directly from paraelectric to antiferroelectric phase by a second order phase change. Possible material systems that might be engineered to effect this type of change are briefly considered.

Finally, some alternative technologies that may be used to fabricate multiple layered dielectric-electrode structures are considered with a view to exploring methods that may relieve or modify the high symmetry constraint imposed by conventional ceramic processing and, thus, open up a much wider range of lower symmetry families of high K_R ferroelectric and antiferroelectric crystals for capacitor application.

Polarization Mechanisms in $BaTiO_3$ Ceramics

Since almost all presently used high K_R dielectric formulations are based on the ferroelectric barium titanate, it is useful to start by examining the polarizability mechanisms in high purity stoichiometric $BaTiO_3$ crystals and ceramics.

Para-electric Phase

$BaTiO_3$ belongs to the perovskite structure family. Above the ferroelectric Curie temperature near 135°C in the pure material, the symmetry is cubic (m3m) and the weak field permittivity K_R is isotropic, following in its temperature dependence a Curie-Weiss law of the form:

$$K_R = \frac{C}{T-\theta}$$

where C, the Curie-Weiss constant, is of order $1.5 \cdot 10^5$°K and θ, the Curie Weiss temperature, is some 10°C below the ferroelectric Curie point (i.e., the phase change at T_c is first order). Following the pioneer work of Forhlich (1958), Anderson (1960), and Cochran (1960), it is believed that the

major contribution to the dielectric response comes from the "softening" of one of the normal transverse optical modes of vibration of the ions at the Brillouin zone center. From the Lydane-Sachs-Teller (1941) relation:

$$\varepsilon_w = \Pi_j \frac{\nu_{LO}}{\nu_{TO}}^2 \qquad (1)$$

where ν_{LO} and ν_{TO} are longitudinal and travsverse modes, respectively, and the sum Π_j is taken over all active modes. If one of the frequencies $_{TO}$ decreases markedly, this term soon will dominate the sum ν_j and, thus, to account for Curie Weiss behavior we must have:

$$\nu_{TO}^2 \, \alpha(T-\theta) \text{ or } \nu_{TO}^2 = A(T-\theta).$$

In crystals for which data are available for the constants A and C (Table 1), it is evident that for widely different ferroelectric perovskites C $\cdot$ A is a constant of order $(16 \pm 2) \cdot 10^{-5}$ cm^{-2}. The constancy of the C $\cdot$ A product suggests a general relation between mode frequency and permittivity, so that in Figure 1 only the scaling of the T axis need change to describe all perovskites. In caution, however, it must be stated that there is mounting evidence that simple soft mode theory does not account for the total dielectric polarizability in the paraelectric phase of the oxygen octahedron ferroelectrics, particularly for temperatures close to T_c where the highest K_R values are obtained. Raman (Shapiro et. al., 1972), Brillouin scattering (Lyons 1981), and recent mm wave spectroscopy (private communication from H. Hall, W. Ho) show evidence for much lower lying excitations with relaxation character, and these appear also to be reflected in the strong "glass-like" character of the low temperature specific heat (Acherman et al. 1981, Lawless et. al., 1975). Fortunately for practical purposes, the frequencies are in the high GHz region and do not significantly perturb the broad largely frequency independent response to RF and microwave frequencies. In pure ceramic BaTiO$_3$ above T_c, great care must be exercised in judging what is true material response since processing modifications can exert a profound influence on the effective impedance of the grain boundary region (Payne 1973). The excellent data from Kinoshita and Yamaji (1976) do appear to show as expected a K_R above T_c that is largely independent of grain size over a very wide range of sizes (Figure 2, Table 2) and, thus, no detectable contribution to the impedance from grain boundaries.

TABLE 1 Magnitudes of the Parameters A and C[a]

SUBSTANCE	C(x10^5 K)	A(cm^{-2}K^{-1})
BaTiO$_3$	1.5	9.5
PbTiO$_3$	1.7	8.2
KTaO$_3$	0.5	29.1
SrTiO$_3$	0.77	28.6
Pb(Mg$_{1/3}$Nb$_{2/3}$)O$_3$	4.7	3.4
Pb(Zn$_{1/3}$Nb$_{2/3}$)O$_3$	4.7	3.8

[a] C $\cdot$ A = $(16 \pm 2) \cdot 10^5$ cm^{-2}

TABLE 2 Grain size dependence of C, T_1, T_c, K_{mass}, T_2 and T_3 in high-purity $BaTiO_3$ ceramics.

Mean Grain size (μm)	C (×10⁵°C)	T_1 (°C)	T_c (°C)	K_{max} (×10⁵)	T_2 (°C)	T_3 (°C)
53	1.14	115	122	1.075	10	−86
13	1.23	113	122	1.091	14	−82
3.0	1.23	111	121	1.058	17	−80
2.2	1.67	108	121	1.283	16	−81
1.5	1.43	112	121	1.315	17	−78
1.1	1.45	112	120	1.078	19	−76

SOURCE: Kinoshita and Yamaji 1976.

TEMPERATURE ABOVE THE CURIE POINT (T-θ)
Scaled for $BaTiO_3$
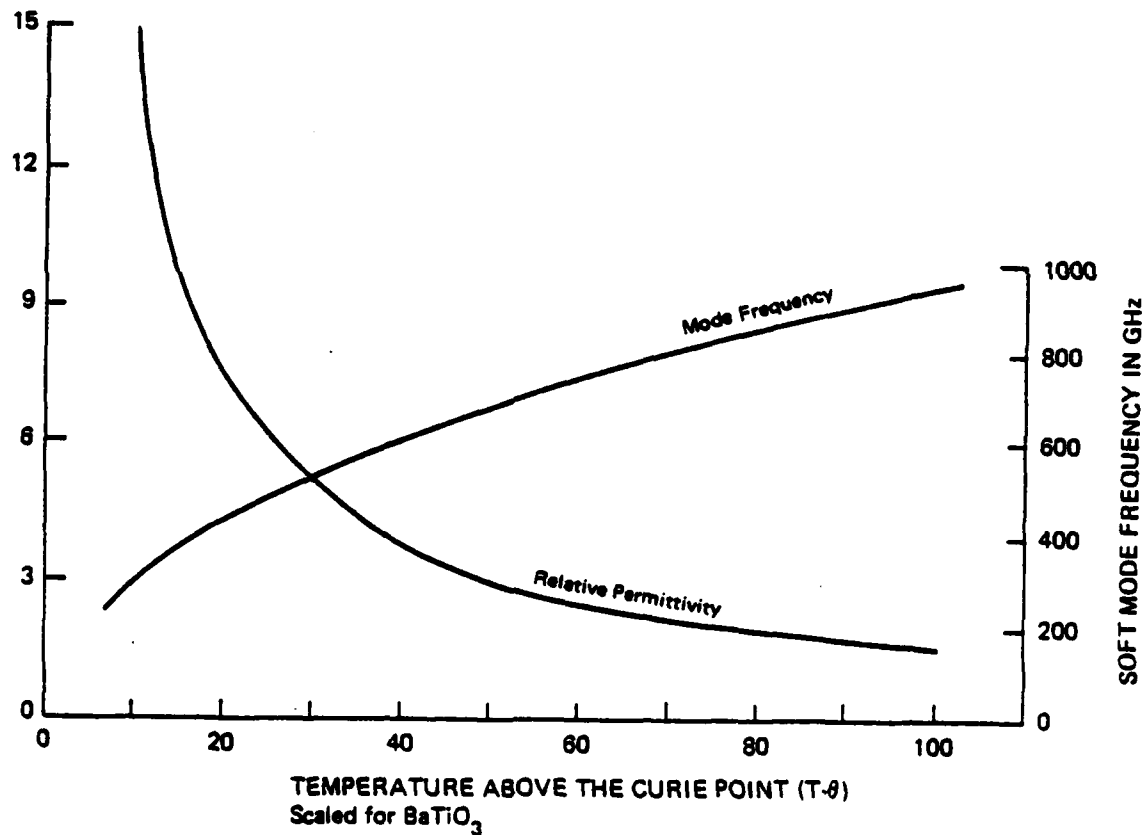
FIGURE 1 Temperature dependence of relative permittivity and mode frequency.
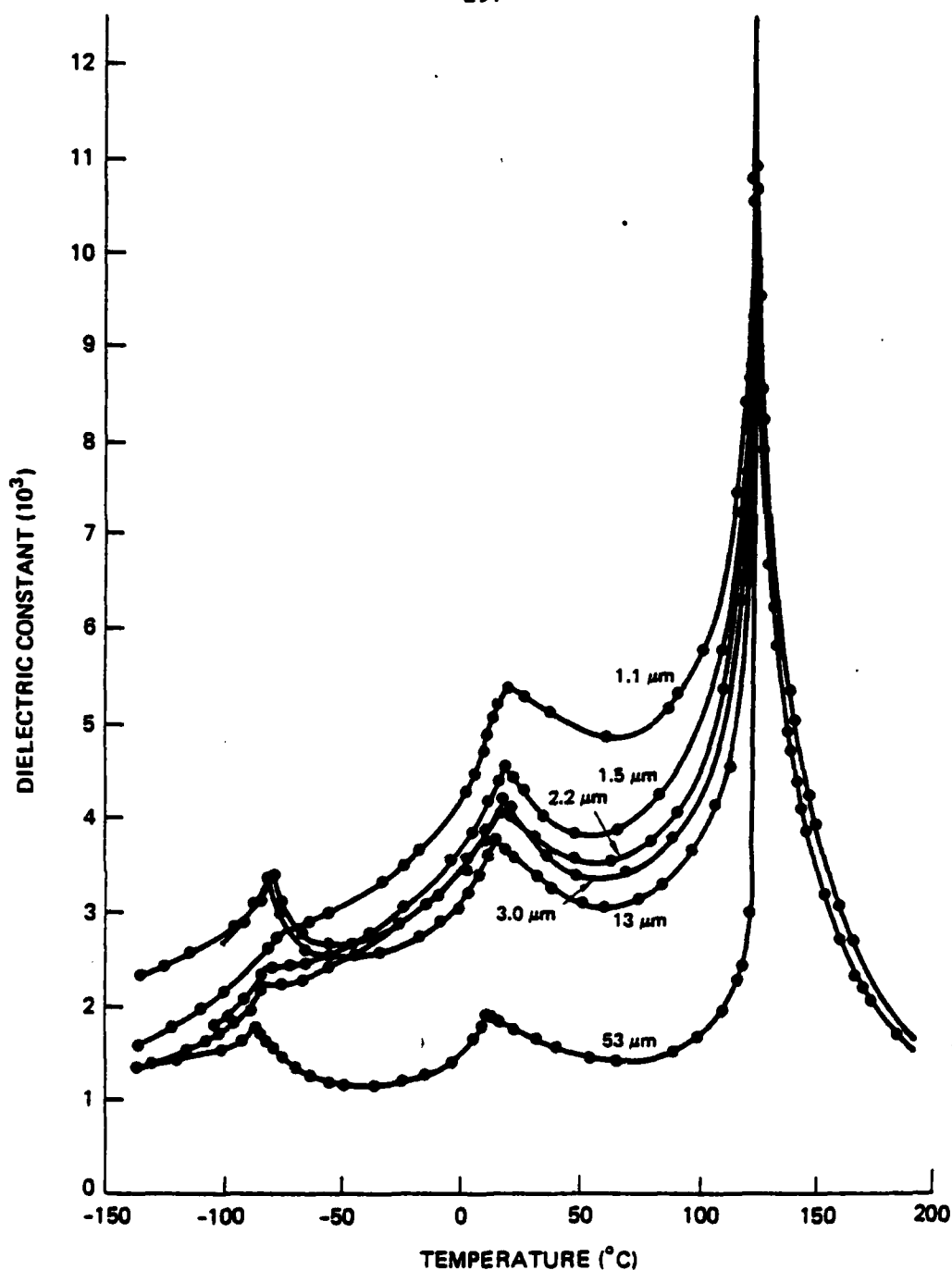
FIGURE 2 Temperature dependence of dielectric constant in various grain-size
high-purity BaTiO$_3$ ceramics (Kinoshita and Yamaji 1976).

Polarization Mechanisms in the Ferroelectric Phases

Pure BaTiO$_3$ passes successively into the tetragonal ferroelectric phase
below 125°C to an orthorhombic modification at 0°C and finally, at -90°C, to a
rhombohedral symmetry that is stable to the limit of temperature measurement.
Early experimental work on Remeika type crystals (Remeika 1954) has been well
summarized by Jona and Shirane (1962) and new data are presented in the Landolt
Bornstein new series volumes 3, (1969), 9 (1974), 16a (1981).

Listing only major possible contributors to the polarizability there are:

1. Intrinsic single domain responses. In each ferroelectric phase there is a family of anisotropic single domain permittivities $[K_{ij}]_{R(W)}$ for weak fields that characterizes the response to alternating $\vec{E}$ fields for the isolated single domain state. Since the single domain is in a polar symmetry, it is necessarily piezoelectric so that the permittivities measured at constant and zero mechanical stress $X_{ij} = 0$, are not the same as those measured at constant spontaneous strain, $x_{ij} = x_{ij}(s)$. In $BaTiO_3$ at $25°C$ the single domain intrinsic permittivity is markedly anisotropic with $K_{33}^{X=0} = 179$ and $K_{11}^{X=0} = 4500$ and, thus, in a single crystal or crystallite $\bar{K}_{ij}$ is markedly dependent on the ferroelectric domain arrangement that is itself a strong function of thermal, electrical, and elastic pretreatment. For a high purity ceramic, the situation is even further complicated by elastic boundary conditions. Particularly for K_{11}, because of the close approach of the orthorhombic Curie point at $0°C$, $K_{11}^{X=0} \neq K_{11}^{X=\sigma}$ and, thus, $\bar{K}_{ij}$ can be further modified by internal stresses set up due to the onset of spontaneous stratin at T_c, and these internal stresses can themselves be much modified by the influence of the grain size on the relative stabilities of different domain structures. In particular it is believed that the strong grain size dependence exhibited in the data of Figure 2 T_c is due to this internal stress phenomenon (Buessem et. al., 1966a and 1966b).

2. Polarization due to domain re-arrangement. All ferroelectric phases of $BaTiO_3$ and of other perovskite ferroelectrics contain both ferroelectric-ferroelastic (shape changing) and pure ferroelectric (non-shape changing) domains. Characteristics and switching processes for the pure ferroelectric 180 degree domains have been extensively studied (Fatuzzo and Merz 1967, Merz 1953). For the ferroelastic 90 degree domains in $BaTiO_3$ at $25°C$, domain statics have been explored in both single crystal and ceramic materials (Denis and Bradt 1974, Remaut et al. 1966), but the kinetics of wall motion are still uncertain. The wall region that separates domains is exceedingly narrow (less than $100Å$) and it would appear that true sideways motion of the 180 degree walls is unlikely (Miller and Weinreich 1960). Evidence from single crystals suggests that these walls do not contribute to K_{ij}' but may contribute more strongly to the out of phase K_{ij}'' (Fousek 1965). Definitive measurements have not been carried out for ferroelectric type walls, but there is some evidence fom optical studies that quasi-reversible motion may be possible (Fousek and Brezina 1964).

In donor doped PZTs and in PLZT that are in the rhombohedral ferroelectric phase, there is much clearer evidence that wall motion contributes to K_R. Calculations suggest that K_w is some 2 to 3 times larger than $[\bar{K}_{ij}]_{WR}^{X=0}$, the intrinsic average, and recent measurements (Fousek and Brezina 1964) show that this ennanced permittivity freezes out at temperatures below $30°K$ where wall motion would be expected to become difficult. An uncomfortable ancilliary consequence of the ferroelectric domain structure is the

aging phenomenon evident in all the dielectric properties of high K materials that contain one or more ferroelectric components. A complete explanation for aging even in a simple "pure" BaTiO3 has not been given. Current thinking appears to favor a mechanism that gives slowly increasing volume stabilization of P_s through a slow re-arrangement of polar defects within the domain in accommodation to the ferroelectric order parameter (Zhang et al. 1982b). Clearly, however, this is not a complete explanation as antiferroelectric perovskite compositions also exhibit aging (Jonker 1980). In this case it is believed that slow rearrangement of the shape changing ferroelastic-antiferroelectric twin-domains may better accommodate mechanical internal stresses generated by the spontaneous strain arising at T_c (Schulze 1973).

Piezoelectric Effects

As was indicated above, the individual domains of a ferroelectric phase are necessarily piezoelectric and in BaTiO3, for example, the coupling coefficients k_{33}, k_{31} and k_{15} are large. Thus, there is a large difference between $\bar{K}^X$ and $\bar{K}^x$, the constant stress and constant strain values of the domain permittivity. It has long been suspected that the dispersion which appears for most ferroelectric ceramics in the range of 10^7 to 10^8 Hz may be associated with piezoelectric resonance of the partially mechanically clamped domains pumping energy into acoustic modes of vibration. Very recently Xi (Xi and Cross 1982) has proven beyond doubt that such grain resonance contributes the dominant dispersion in LiNbO3 model ceramics.

At lower frequencies (below 10^7 Hz) the random arrangement of crystallites in a ferroelectric ceramic averages the piezo-effect to zero. However, under bias field, the electrostriction can develop a polarization biased bulk piezoelectricity that may be a troublesome converter of acoustic noise. More information about these induced piezoelectric effects in practical materials would certainly be advantageous for circuit designers.

Interactions with the Defect Structure

For any polar defect, symmetry dictates that there must be an interaction with the developing polarization of the ferroelectric domain. If the relaxation time for reorientation of the defect dipole is very long, the phenomenon will contribute to the stabilization of the domain structure and be measurable in the aging response. If, however, the relaxation time is short, the defect dipoles will respond to the modulation of the P_s by external fields and, thus, contribute a defect dipole component to the dielectric polarizability. Such effects have been demonstrated in the simplest form in the paraelectric phase for bismuth (Skanavi et al. 1956), lanthanum (Tien 1965), and rare earth substituted strontium titanate (Johnson et al. 1970). Overt demonstration and separation are more difficult in the ferroelectric phases due to the plethora of other mechanisms that may intervene, but recently there is good evidence of a defect dominated mechanism enhancing the low temperature polarizability in the acceptor doped hard PZT compositions (Zhang et al. 1982a)

DISCUSSION

Even in this very brief discussion it becomes clear that:

1. The simple intrinsic response of pure $BaTiO_3$ in the paraelectric phase above T_c is too sharply peaked to be of interest in practical capacitors.

2. Introducing a ferroelectric phase necessarily brings a complex panoply of polarization mechanisms that even in a simple high purity $BaTiO_3$ ceramic are difficult to separate and impossible to control separately.

Unfortunately, since the single phase composition is much too sharply peaked in its response, there is a need to introduce heterogeneity either by mixing phases on a grain-by-grain basis, between grain and boundary phases, or by composition gradients within the grain structure. To a significant extent it is this need for controllable heterogeneity that makes the electronic capacitor ceramics difficult to process reproducibly. The necessity to "mix in" the complex polarization mechanisms of the ferroelectric phase frustrates simple control and separation of mechansims, and it is perhaps not surprising that the development of the useful $BaTiO_3$ based compositions has been largely empirical.

Relaxor Ferroelectrics

From the discussion above, it is evident that a desirable direction to move in the response function is towards perovskite type compositions with large C and, thus, correspondingly small A values. In the ferroelectric relaxors like $Pb(Mg_{1/3}Nb_{2/3})O_3$ (PMN), the Curie constant is more than three time larger than in $BaTiO_3$ and the dielectric response is correspondingly smoother and less peaked. It is perhaps not surprising to find that the PMN relaxor has been used as a dielectric formulation in multilayer technology in China for more than 10 years (private communication, Ydo Xi) and that other relaxor compositions are under intensive study in Japan (Yonezawa et al. 1979).

Basically, the relaxor ferroelectrics are characterized by a weak field permittivity that exhibits a broad frequency dependent maximum often termed in Soviet literature a diffuse phase transition (Figure 3) with obvious Debye type relaxation in the lower temperature domain, as evidenced by the plot of K' and K'' at $-25°C$ shown in Figure 4.
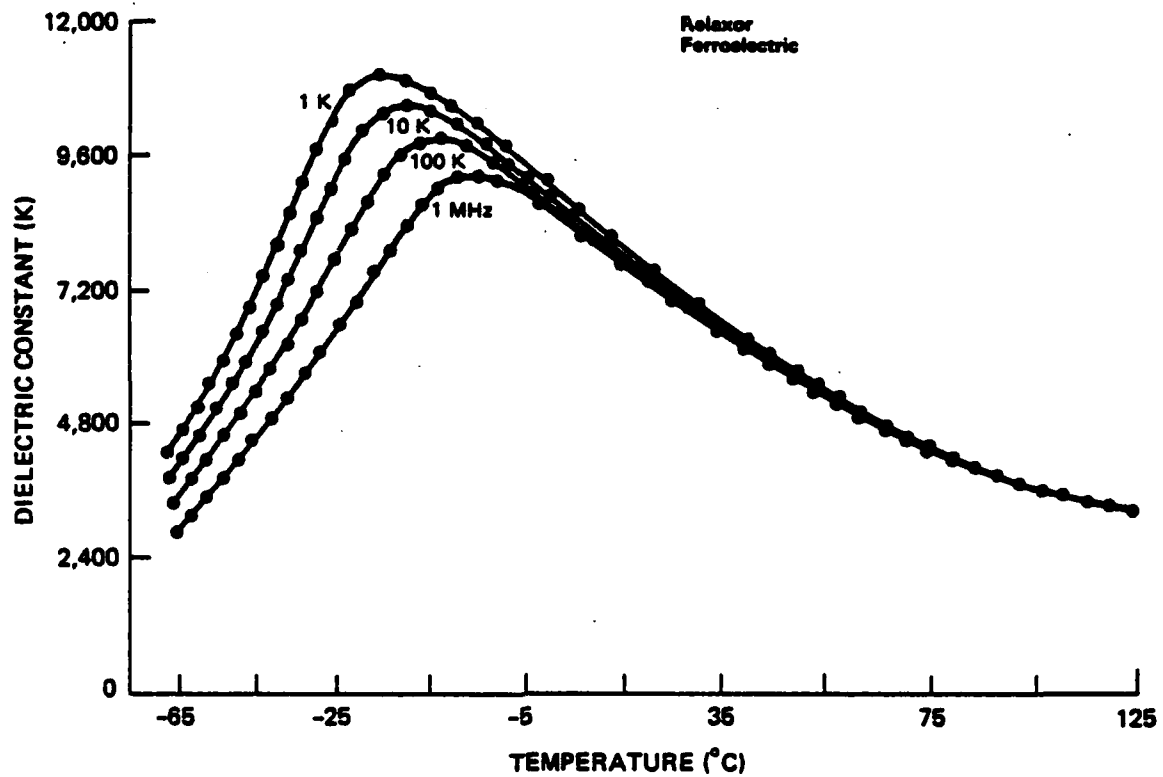
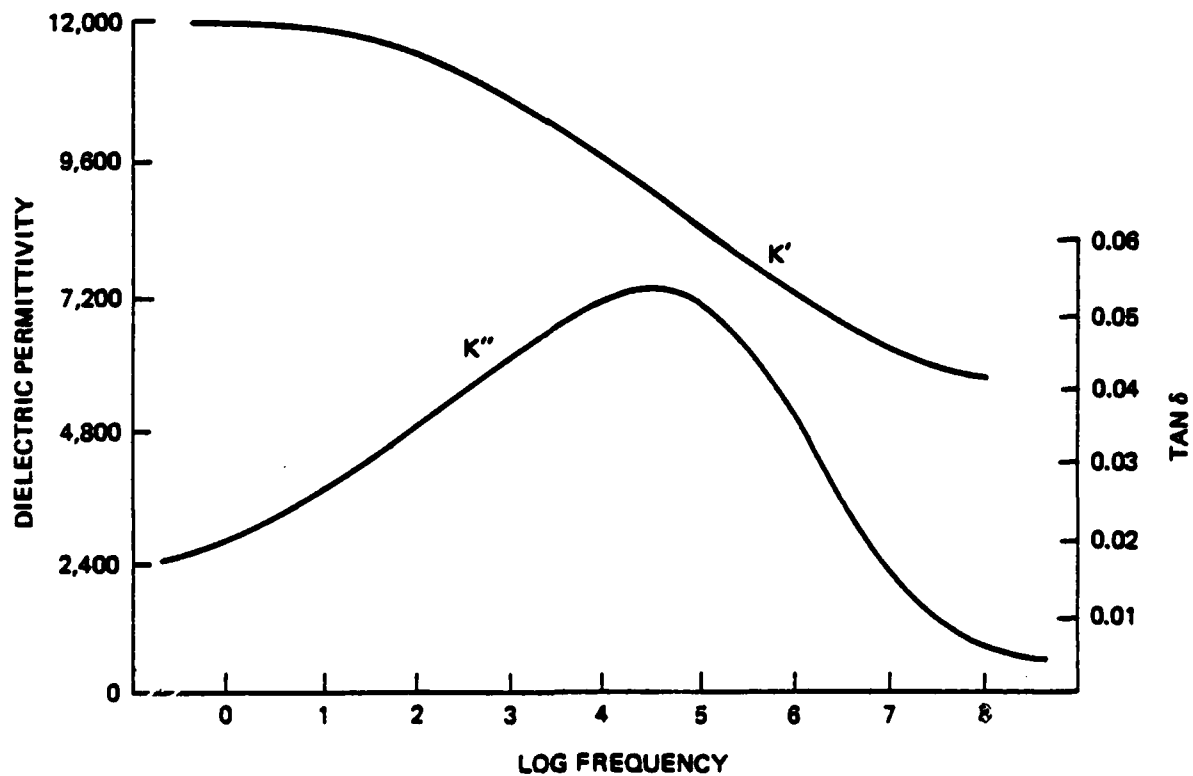FIGURE 3   Dielectric constant as a function of temperature and frequency in $Pb(Mg_{1/3}Nb_{2/3})O_3$.

FIGURE 4   Relative permittivity as a function of frequency in PMN at -25°C.

Until recently, the speculation has been that the behavior that occurs most typically in compositions such as $Pb(Mg_{1/3}Nb_{2/3})O_3$ and $PbZn_{1/3}Nb_{2/3}O_3$ is associated with statistical fluctuations in the random distribution of the Mg and Nb or the Zn and Nb cations on the B sites of ABO_3 perovskites. It has been suggested that such short range fluctuations may give raise to strong local fluctuations in the ferroelectric Curie temperature. Thus, through any cross section in the crystal at a temperature within this Curie range, the material is an intimate mixture of ferroelectric and paraelectric regions (Figure 5) with the scale of 100 ∿ 1,000 A and the volume fraction of ferroelectric increasing continuously as the temperature decreases. Recently this model has been largely confirmed by studies on the compounds $PbSc_{1/2}Nb_{1/2}O_3$, $PbSc_{1/2}Ta_{1/2}O_3$ where the disorder of the cations can be eliminated by thermal annealing to give a normal sharp first order ferroelectric phase change (Setter and Cross 1980a, 1980b, and 1981).

Advantages that may be claimed for the lead based relaxor compositions are:

1. Low firing temperatures (800-900°C in many systems).

2. Direct compatibility with inexpensive silver electrodes.

3. No spontaneous strain at temperatures below T_c so that there are no internal stress effects.

4. Larger values of Curie constant C.

5. The possibility of processing to preserve separate relaxation regions in complex compositions with correspondingly flattened temperature response (Cross 1956).

6. Lower electrostriction constants so that the induced mechanical strain for any change of polarization ΔP is five times smaller than $BaTiO_3$.

7. Much lower thermal expansion.

8. Micro heterogeneity leading to flatter temperature dependence, but being on a scale much smaller than the ceramic grain size so that single crystals and ceramics have closely comparable properties.

9. No stable domain structure and thus no aging at temperatures above the dielectric maximum.

For these reasons it would appear that further study of a number of the relaxor compositions would merit strong consideration.
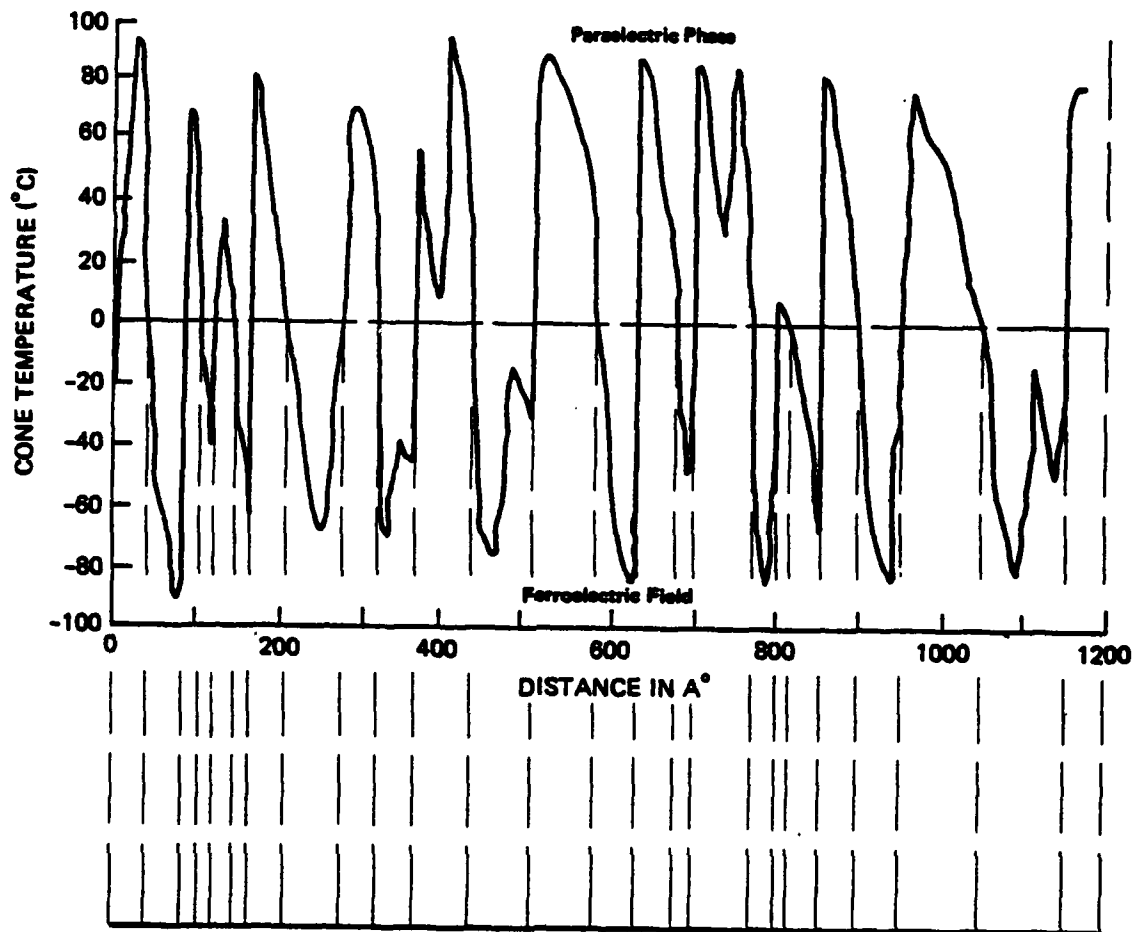
FIGURE 5 Close mixture of ferroelectric and paraelectric micro-regions with linear dimensions in the range 100 to 1,000 A°.

Antiferroelectric Systems

Kittel (1951) has given an elementary phenomenological theory that may be used to characterize the elastic Gibbs free energy in a simple uniaxial two-sublattice antiferroelectric in the form:

$$\Delta G = A(P_a^2 + P_b^2) + B P_a P_b + C(P_a^4 + P_b^4), \qquad (2)$$

where P_a and P_b are the two sublattice polarizations and A, B, and C are temperature dependent constants characteristic of the system.

Equation (2) may be rewritten more conveniently for our purpose in the form:

$$\Delta G = \frac{1}{2} \alpha_F P_F^2 + \frac{1}{4} \gamma_F P_F^4 + \frac{1}{2} \alpha_A P_A^2 + \frac{1}{4} \gamma_A P_A^4 + \frac{1}{2} \beta P_A^2 P_F^2 , \qquad (3)$$

where $P_A = P_a - P_b$ a measure of the antiferroelectric polarization ($P_a = -P_b$) and $P_F = P_a + P_b$ a measure of the ferroelectric polarization ($P_a = +P_b$).

If α_A has the form $\alpha_{Ao}(T-\theta_A)$ and α_F is of the form $\alpha_{Fo}(T-\theta_F)$, γ_A and γ_F must be positive for stability. For $\theta_A > \theta_F$, the system will go directly from a nonpolar paraelectric state at $T > \theta_A$ to an antiferroelectric state given by:

$$\theta = \alpha_{Ao}(T-\theta_A)P_A + \gamma_A P_A^3$$

and

$$P_A^2 = \frac{\alpha_{Ao}(\theta_A - T)}{\gamma_A}$$

for $T < \theta_A$. The dielectric stiffness will be given by $\dfrac{\partial^2 \Delta G}{\partial P_F^2}$, which takes the form:

$$\chi = \gamma_{Fo}(T-\theta_F) + 3\gamma_F P_F^2 + \beta P_A^2 .$$

Above θ_A, $P_F = 0$ and $P_A = 0$ so that:

$$\chi = \alpha_{Fo}(T-\theta_F) \text{ or } K = \frac{1/\alpha_{Fo}}{T-\theta_F}$$

(i.e., Curie-Weiss Law).

At the Neel temperature, θ_A:

$$K = \frac{1/\alpha_{Fo}}{\theta_A - \theta_F} ,$$

So that if θ_F is close to θ_A, K can be very large.

Below θ_A, $P_F = 0$ and $P_A^2 = \dfrac{\alpha_{Ao}(\theta_A - T)}{\gamma_A}$:

$$\chi = \alpha_{Fo}(T - \theta_F) + \frac{\beta\alpha_{Ao}}{\gamma_A}(\theta_A - T).$$

If $\dfrac{\beta\alpha_{Ao}}{\gamma_A}$ can be adjusted to be equal to α_F, then:

$$\chi = \alpha_F(\theta_A - \theta_F) \text{ or } K = \frac{1/\alpha_{Fo}}{\theta_A - \theta_F}$$

(i.e., the system could have a very high _temperature_ _independent_ permittivity).

Clearly the situation will be more complex in a multiaxial perovskite type antiferroelectric where the tensor nature of α, β, and γ must be considered. However, as has been demonstrated for $NaNbO_3$ single crystals (Cross 1956), the antiferroelectric phase change at 450°C comes close to the required form.

A much more versatile system of antiferroelectrics is in the $PbZrO_3$, $PbSnO_3$, $PbTiO_3$, La_2O_3, $SrTiO_3$, solid solution family. Although these materials have been quite widely studied for piezoelectric and depolarization fusing applications, they have not been well explored as dielectrics, and interesting property combinations of the type suggested may be possible.

Alternative Processing Methods

Ceramic processing using tape casting and spray application techniques has been the mainstay of the multilayer ceramic capacitor industry. A necessary consequence of processing designed to achieve a fine grained, closely densified, randomly axed, polycrystal assemblage in the dielectric is that one must work with very high symmetry multiaxial ferroelectric phases that dictate using only the limited family of perovskite or tungsten bronze structure oxides.

It is interesting to inquire whether there are other alternative processing methods that might be better adapted to producing more strongly anisotropic microstructures in which a very strong orientation texture could be preserved. If so, there are many families of lower symmetry uniaxial ferroelectrics and antiferroelectrics that could contribute fascinating combinations of dielectric parameters is suitable strong texturing were developed.

Thermal Evaporation-Recrystallization

Many efforts to product thin films of high K_R oxide ceramic dielectrics by thermal evaporation have been made over the years with, unfortunately, a singular lack of success. A major problem with the vacuum deposition onto cold substrates is the amorphous nature of the deposited film and the reduced oxidation state of the deposited material. Post deposition thermal treatment and deposition upon heated substrates destroys much of the advantage of the method and little advantage remains. For non-oxide ferroelectrics with much lower processing temperatures, however, the method may offer intriguing possibility. An interesting candidate material for such study is antimony sulphur iodide, SbSI (Figure 6 and Table 3).

SbSI is a uniaxial ferroelectric with profoundly anisotropic character. At room temperature the orthorhombic structure (Figure 6a which is based on parallel stacking of strong covalently bonded chains held together by weak Van der Waals forces is paraelectric with a $K_R > 10,000$ (Figure 6b). The crystal has the highest know piezoelectric, d_{33}, at temperatures just below T_c, and the Curie temperature can be manipulated by doping or by mechanical stress effects.

Recent studies have shown that stoichiometric SbSI can be vacuum deposited onto cold substrates to form an amorphous coherent film and then, by low temperature (T <250°C) annealing in a strong temperature gradient, recrystallized into a strongly textured microstructure. These ordered films have high permittivity that can be well controlled by the "ceramic" process.

SbSI family materials look interesting as candidates for evaporative film systems.

Sputter-Deposited Films

A major problem in the application of sputtering techniques to conventional oxide films is the high annealing temperatures required to reconstitute the crystalline ferroelectric phases. Equilibrium thermal processing of film and substrate lead to undesirable chemical interaction except with noble metal substrates. An area that clearly would repay much additional study is the exploration of nonequilibrium thermal techniques for annealing without raising substrate temperature. Laser surface treatment is now very widely used in semiconductor processing and permits both annealing and surface melting and epitaxial recrystallization in silicon.

Laser annealing has been studied for $PbTiO_3$ films with encouraging results. Fortunately, not only the capacitor but also transducer pyroelectric and surface acoustic wave devices would be ready markets for thin, high quality ferroelectric film structures. Thus, there are many potential markets that would help to support basic studies aimed towards the development of single-layer and multilayer film structures. For capacitors, the fact that such techniques might permit direct deposition on the rear surface of the silicon chip, with correspondingly shortened lead paths, could be of major importance as charge transfer times decrease with large scale integration.
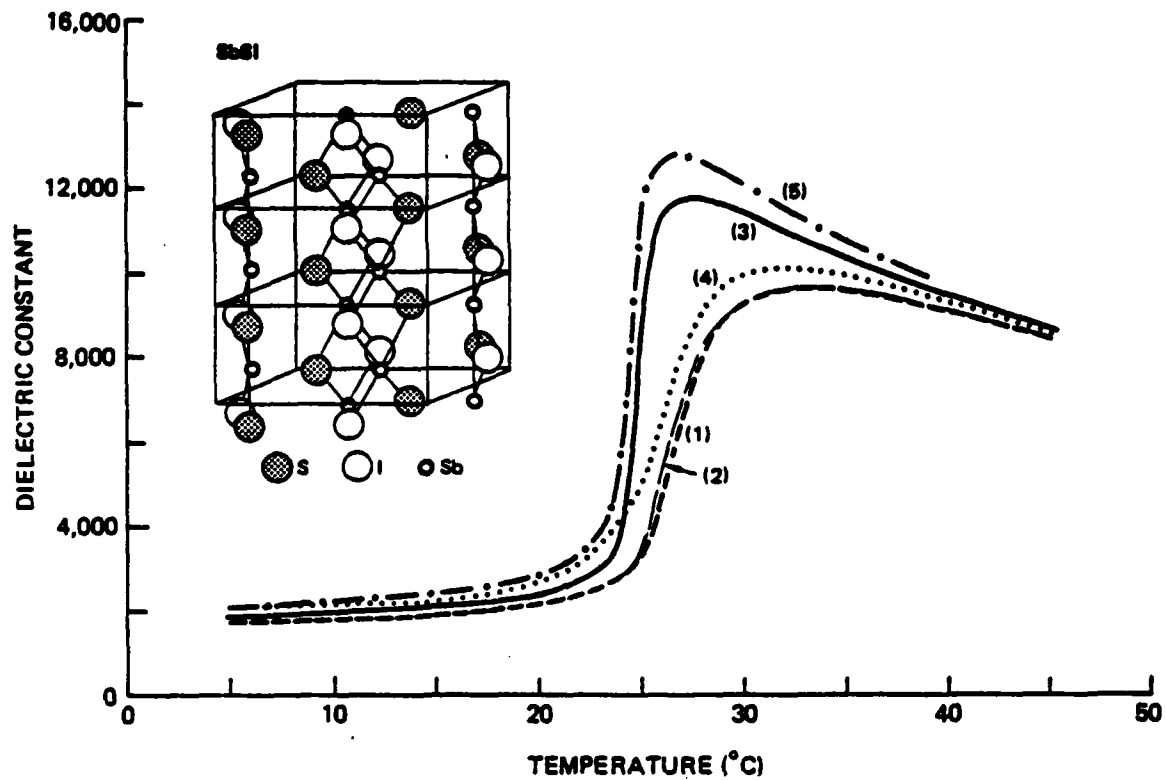
FIGURE 6 Temperature dependence of the dielectric constant of vapor grown SbSI at 1 MHz, (1) and (2) with bias-800 V/cm, (3) no bias, (4) bias + 800 V/cm, and (5) no bias.

TABLE 3   Some Characteristic Properties of SbSI

Property	Value
Resistivity	10^9 ohm-cm
Sp. heat (C)	0.29 $Jg^{-1}{}^{\circ}K^{-1}$
Density (ρ)	5.2 g/cm^3
$c' = C\rho$	1.5 J $cm^{-3}{}^{\circ}K^{-1}$
d_{33}	$4 \cdot 10^{-9}$ C/N at $\sim 20^{\circ}C$
α_{11}	$-5.83 \cdot 10^{-5}/^{\circ}C$ $(10^{\circ}C)$
α_{22}	$12.08 \cdot 10^{-5}/^{\circ}C$ $(10^{\circ}C)$
α_{33}	$-37.5 \cdot 10^{-5}/^{\circ}C$ $(10^{\circ}C)$
s_{33}^{D}	$40 \cdot 10^{-12}m^2/N$ $(10^{\circ}C)$
s_{33}^{E}	$12.5 \cdot 10^{-11}m^2/N$ $(10^{\circ}C)$
$\epsilon||C$	$\begin{cases} 7.5 \cdot 10^3 & (1K)\ (10^{\circ}C) \\ 6 \cdot 10^4 & (1K)\ (at\ T_c \approx 20^{\circ}C) \end{cases}$
$\epsilon\perp C$	25
P_s	25 $\mu c/cm^2$ $(0^{\circ}C)$
T_c	$20^{\circ}C$
E_C	670 V/cm
E_S	$\sim 4 \cdot 10^3 V/cm$

Crystal data: Orthorhombic space group.

$a = 8.527$ $\overset{\circ}{A}$ $b = 10.13 \overset{\circ}{A}$ $c = 4.08 \overset{\circ}{A}$ @ $35^{\circ}C$

CONCLUSIONS

Exploration of the polarization mechanisms in current $BaTiO_3$ based dielectrics leads to the conclusion that, because of the strong temperature variation in the intrinsic response, heterogeneity in some form is a mandatory requirement. This conclusion carries with it the unfortunate consequence that mixing in the complex ferroelectric polarization mechanisms makes systematic development and control most difficult. In newer relaxor ferroelectric compositions, the heterogeneity is introduced on a much finer subgrain scale and the possibility exists for better control and reproducibility. Theoretically, antiferroelectric compositions could be highly advantageous, but much work needs to be done to explore such systems. Alternative processing methods offer the possibility of extending the useful family of ferroic materials for dielectric applications and for lowering process temperature requirements from those necessary in the oxygen octahedron based compositions.

REFERENCES

Acherman, D. A., D. Moy, R. C. Potter, A. C. Anderson and W. Lawless. 1981. Glassy behavior of crystalline solids at low temperature. Phys. Rev. B 23:3886.

Anderson, P. W. 1960. Fizika Dielektrikov, 290 Acad. Nauk SSSR, Moscow.

Buessem, W. R., L. E. Cross, and A. K. Goswami. 1966a. A phenomenological theory of the high permittivity in fine grain $BaTiO_3$. J. Am. Ceram. Soc. 49: 33-35. 1966b. Effects of two dimensional pressure on the permittivity of fine grain $BaTiO_3$. J. Am. Ceram. Soc. 49:36-39.

Cochran, W. 1960. Crystal stability and the theory of ferroelectrics. Adv. in Phys. 9:387.

Cross, L. E. 1956. A thermodynamic treatment of ferroelectricity and antiferroelectricity in pseudo cubic dielectrics. Phil. Mag. 81:76.

Denis, M. D., and R. C. Bradt. 1974. Thickness of 90° domain walls in $(BaPd)TiO_3$ single crystals. J. Appl. Phys. 45:1931.

Devonshire, A. F. 1949. Theory of Barium Titanate, Part 1. Phil. Mag. 40:1040.

Devonshire, A. F. 1951. Theory of Barium Titanate, Part 2. Phil. Mag. 42:1065.

Fatuzzo, E. and W. J. Merz. 1967. Ferroelectricity. North Holland, Amsterdam.

Fousek, J. 1965. Contribution of domain walls to the small signal complex permittivity of $BaTiO_3$. Czech. J. Appl. Phys. 815:412.

Fousek, J., and B. Brezina. 1964. Relaxation of 90° domain walls of $BaTiO_3$ and their equation of motion. J. Phys. Soc. Japan 19:8380-838.

Frohlich, H. 1958. Theory of Dielectrics. Oxford, Clarendon Press. 18:155.

Hellwege, K., Landolt Bornstein, Group 3. Crystals and Solid State Physics, Vol. 3 (1969), Fe-roelectric and Antiferroelectric Crystals; Vol. 9 (1974) Ferroelectric and Antiferroelectric Crystals; Vol. 16a (1981), Oxide Ferroelectrics.

Johnson, D., L. E. Cross, and F. A. Hummel. 1970. Dielectric relaxation in strontium titanates containing rare-earth ions. J. Appl. Phys. 41:2828-2833.

Jona, F., and G. Shirane. 1962. Ferroelectricity in crystals. New York: Pergamon Press.

Jonker, J. 1980. Aging in ferroelectric ceramics. Paper prepared for the International Summer School on Applications of Ferroelectrics, Erice, Sicily, July.

Kinoshita, K., and A. Yamaji. 1976. Grain size effects on the dielectric properties in barium titanate ceramics. J. Appl. Phys. 47:371.

Kittel, C. 1951. Theory of Antiferroelectric Crystals. Phys. Rev. 82:729.

Lawless, W., J. C. Holste, and G. A. Samara. 1976. Dielectric Properties of KH_2PO_4, $BaTiO_3$, $PbZr_{.65}Ti_{0.35}O_3$ and TICl between 0.015 and 10^8K. Ferroelectrics 11:337.

Lyddane, R. H., R. G. Sachs, and E. Teller. 1941. On the polar vibrations of alkali halides. Phys. Rev. 59:673.

Lyons, K. B. 1981. Light scattering studies of ferroelectric transitions: Mode coupling phenomena. Ferroelectric 35:37-42.

Merz, W. J. 1953. Double hysteresis loops of $BaTiO_3$ near the Curie point. Phys. Rev. 91:513.

Miller, R. C. and G. Weinreich. 1960. Mechanism of sideways motion of 180° domain walls in $BaTiO_3$. Phys. Rev. 117:1460.

Payne, D. 1973. The role of internal boundaries on the dielectric properties of polycrystal ferroelectric materials. Ph.D. Thesis in solid state science, The Pennsylvania State University.

Remeika, J. P. 1954. A method for growing barium titanate single crystals. J. Am. Chem. Soc. 76:940.

Remaut, G., R. Gevers, A. Lagasse, and S. Amelinckx. 1966. Dynamical theory of the images of micro twins as observed in the electron microscope III observation and results of numerical calculation. Phys. Stat. Sol. 13:125.

Schulze, W. 1973. Dielectric properties of $PbZrO_3:PbTiO_3$, La_2O_3 ceramics. Ph.D. Thesis in Solid State Science. The Pennsylvania State University.

Setter, N., L. E. Cross. 1980a. The role of B site cation disorder in diffuse phase transition behavior of perovskite oxides. J. Appl. Phys. 51:4356.

Setter, N., L. E. Cross. 1980b. Pressure dependence of the dielectric properties of $Pb(Sc_{1/2}Ta_{1/2})_3$. Phys. Stat. Sol. (a) 61:K71.

Setter, N., L. E. Cross. 1981. An optical study of the ferroelectric relaxors $PbMg_{1/3}Nb_{2/3}O_3$, $PbSc_{1/2}Ta_{1/2}O_3$, $PbSc_{1/2}Nb_{1/2}O_3$. Ferroelectrics. 37:551.

Shapiro, S. M., J. D. Axe, and G. Shirnae. 1972. Critical neutron scattering in $SrTiO_3$ and $KMnF_3$, Phys. Rev. B 6:4332.

Skanavi, G. I., Yu Ksendzov, and V. A. Trigubenko. 1956. Relaxation polarization and losses in non-ferroelectric dielectrics of high dielectric constant. Zh. Eks. Teor. Fiz. 30:1047.

Tien, T. Y. 1965. X-ray and dielectric studies of $SrTiO_3$ solid solutions. Ph.D. Thesis in ceramics, The Pennsylvania State University.

Xi, Yao, and L. E. Cross. 1982. Piezoelectric grain resonance in ceramic $LiNbO_3$. Bull. Am. Ceram. Soc. 61:362.

Yonezawa, M., K. Utsumi, and T. Ohno. 1979. Properties of multilayer ceramics in the $Pb(Zn_{1/3}Nb_{2/3})O_3:PB(Fe_{1/2}Nb_{1/2})O_3:PB(Fe_{2/3}W_{1/3})O_3$ ternary system. In the proceedings of the 2nd meeting of Ferroelectric Application. Kyoto, Japan.

Zhang, X. L., Z. X. Chen, and L. E. Cross. 1982a. Dielectric and piezoelectric properties of $PbZrO_3:PbTiO_3$ to 42°K. Bull. Am. Ceram. Soc. 61:358.

Zhang, X. L., Z. X. Chen, L. E. Cross, and W. A. Schulze. 1982b. Dielectric and piezoelectric properties of lead zirconate titanate ceramics at 4.2 to 300°K. Bull. Am. Ceram. Soc. 61:358.

APPENDIX 7

STRUCTURE-PROPERTY RELATIONS IN MULTILAYER CERAMICS

R. E. Newnham
Materials Research Laboratory
The Pennsylvania State University
University Park

ABSTRACT

The structures of the crystalline phases found in multilayer capacitors are related to the reliability problems facing the manufactures of these devices. Several sources of mechanical strain are examined including thermal expansion, electrostriction, and elastic compliance mismatch. Possible reaction products and interface structures between ceramic dielectric, flux, and electrode are considered.

INTRODUCTION

Gross defects and processing accidents probably are responsible for most reliability problems in multilayer capacitors, but it is worthwhile examining some of the underlying material properties that aggravate these problems. In this paper the atomic structures of the dielectric phases, the metallic electrodes, flux components, and their possible reaction products are reviewed. The relationships between these structures and strain-producing properties are then examined.

CERAMIC DIELECTRICS

Many capacitor formulations are based on $BaTiO_3$, one of a number of ferroelectric substances crystallizing with the perovskite structure (Figure 1). Barium atoms are located at the corners of the unit cell and oxygen atoms at the face-centers. Both barium and oxygen ions have radii of about 1.4 Å and together they make up a face-centered cubic array having a lattice parameter near 4 Å. As discussed later, the perovskite unit cell matches that of the face-centered cubic electrode metals very well.

Octahedrally coordinated titanium ions located at the center of the cubic perovskite cell are the active ions in promoting ferroelectricity. The low-lying d-orbitals of titanium lead to acentric atomic arrangements and large electric polarizability.

An enormous number of compositional modifications have been developed to alter the dielectric properties of $BaTiO_3$. Some of the additives are Curie point shifters (usually downward) whereas others broaden and suppress the dielectric constant peak. A typical additive is Zr^{4+} that substitutes for Ti^{4+} in the octahedral sites causing all three $BaTiO_3$ transitions to "pinch" together with increasing Zr content (Figure 2), merging the dielectric peaks. Further broadening (Figure 3) occurs because of relaxor behavior caused by localized compositional fluctuations. Room temperature lattice parameters of $BaTiO_3$-$BaZrO_3$ solid solutions are shown in Figure 4. Any substantial inhomogeneity in composition could lead to strains of 1 percent or larger.

THERMAL STRAIN

X-ray diffraction measurements on ferroelectric ceramics demonstrate the magnitude and anisotropy of thermal strains in $BaTiO_3$. Lattice parameters are plotted as a function of temperature in Figure 5. In the tetragonal phase the c lattice parameter is about 1 percent longer than a.

As in most materials, the thermal expansion coefficient of $BaTiO_3$ increases with temperature. For ceramic specimens, α is about $5 \cdot 10^{-6}$ near room temperature and it increases to $12 \cdot 10^{-6}$ at 200°C and to $16 \cdot 10^{-6}$ at 1300°C.

Sizeable strains develop during the firing of ceramic capacitors. Shrinkage as great as 2 percent has been observed in $BaTiO_3$ ceramics cooled from 1000°C to room temperature (Figure 6). Down to 120°C the strains are isotropic, but anisotropy develops at the cubic-tetragonal transformation. If the grain size is sufficiently large, most of the anisotropic strain is relieved by 90°C domains.
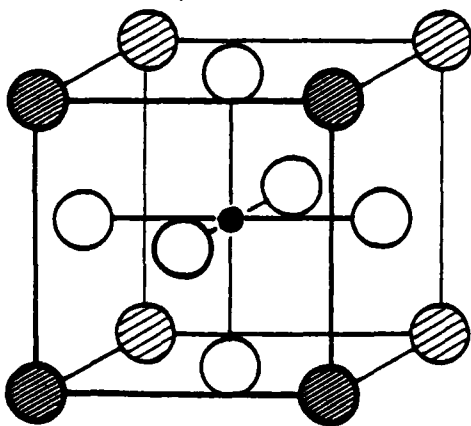
FIGURE 1 The perovskite structure
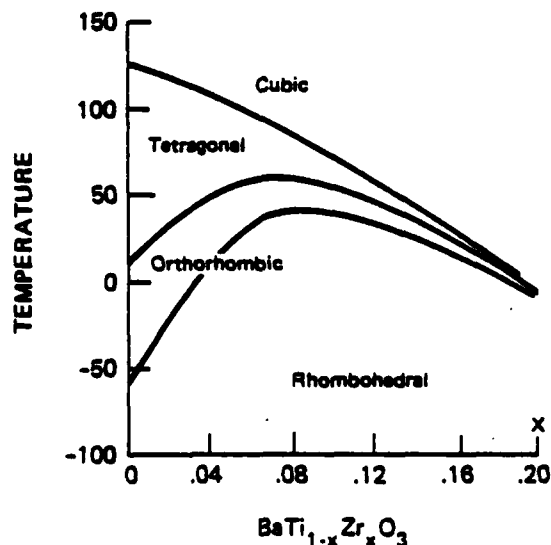
FIGURE 2 The $BaTiO_3$ phase diagram.
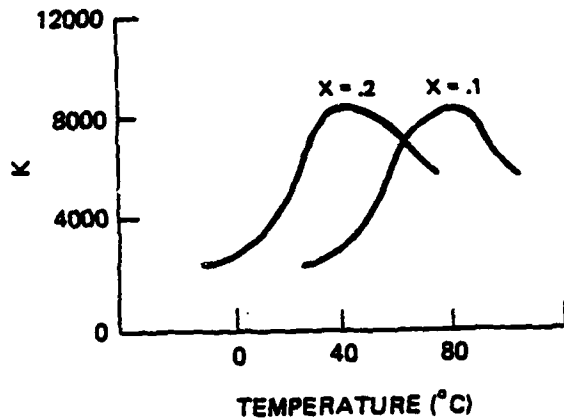
FIGURE 3   Dielectric constant of two
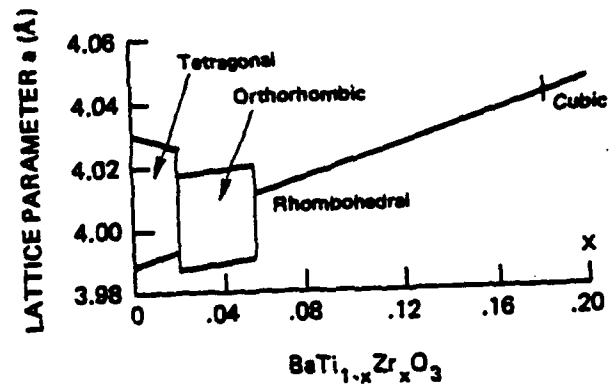$BaTi_{1-x}Zr_xO_3$ compositions
showing broadened peaks

FIGURE 4   Unit cell parameters of
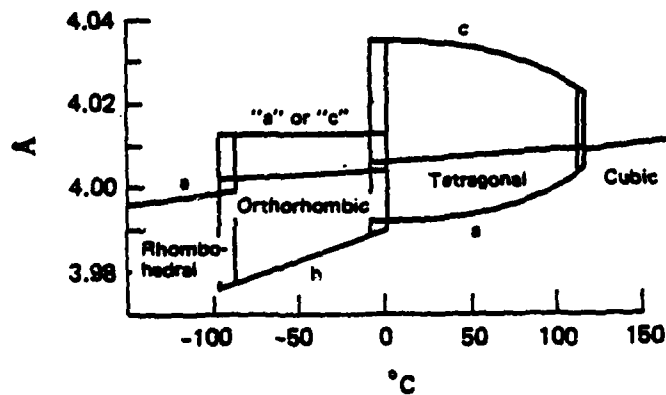$BaTiO_3-BaZrO_3$ ceramics
measured at room temperature.

FIGURE 5   Unit cell dimensions of barium titanate showing the large changes in
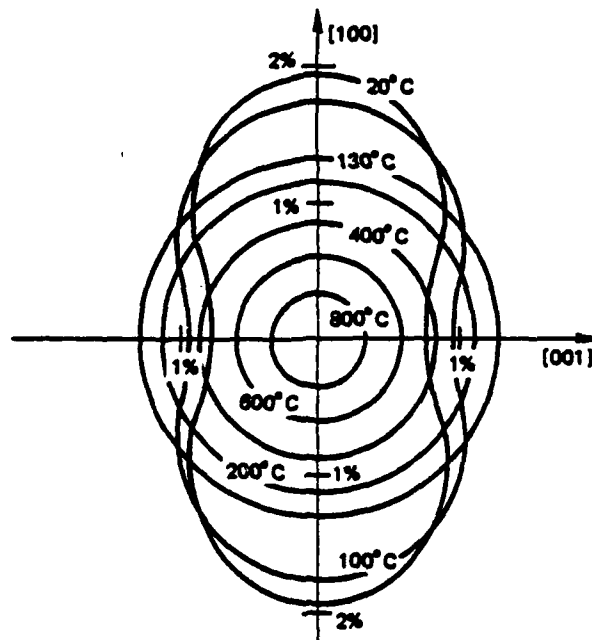thermal strain near room temperature.

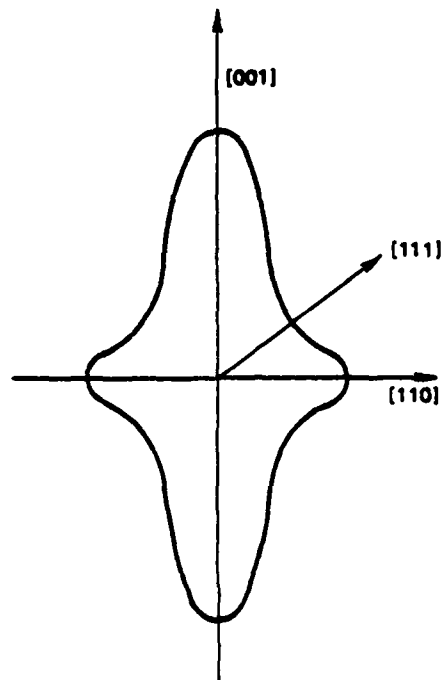FIGURE 6   Thermal shrinkage in BaTiO$_3$ cooled from 1000 to 20°C.

FIGURE 7   Longitudinal electrostrictive strain coefficients plotted as a
function of direction for cubic BaTiO$_3$.

ELECTRTOMECHANICAL STRAIN

All capacitor materials are electrostrictive and some are piezoelectric as well. Electrostriction coefficients Q_{ijkl} couple mechanical strain components ϵ_{ij} to electric polarization components P_k and P_ℓ through a quadratic relationship:

$$\epsilon_{ij} = Q_{ijkl}\, P_k P_\ell \quad .$$

Directional subscripts, i, j, k, ℓ = 1,2,3 refer to the cubic axes x_1=[100], x_2=[010], x_3=[001] of the perovskite unit cell.

In cubic $BaTiO_3$ there are three independent electrostriction coefficients Q_{1111}=0.11m^4/C^2, Q_{1122}=-0.045, and Q_{1212}=0.0145. The longitudinal electrostrictive surface (Figure 7) is highly anisotropic despite the cubic symmetry. Large electromechanical strain lobes occur along <100> directions, the same directions in which spontaneous strain occurs at lower temperatures. Electrostrictive strains are four times smaller in <111> directions corresponding to the close-packed directions in the perovskite structure.

Electrostrictive strains are quite large for sizeable electric fields found in multilayer capacitors. Fields of 10^7 V/m produce polarizations of about 0.1 C/m^2 and mechanical strains of about 10^{-3}. Anisotropic strains of this magnitude are large enough to cause intergranular microfractures. Similar anisotropic strains occur in tetragonal $BaTiO_3$ where the grains are piezoelectric.

Electrostriction also may be important in the ac degradation of $BaTiO_3$ dielectrics. The mechanism involves the electromechanical pumping of oxygen vacancies from partially reduced grain centers to the most insulating grain boundaries, thereby increasing the electrical conductivity and eventually causing thermal breakdown.

ELECTRODE METALS

All the metals used as electrodes in multilayer capacitors are face-centered cubic with lattice parameters (a) between 3.5 and 5.0 Å (see Figure 8):

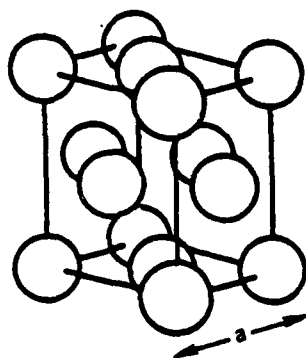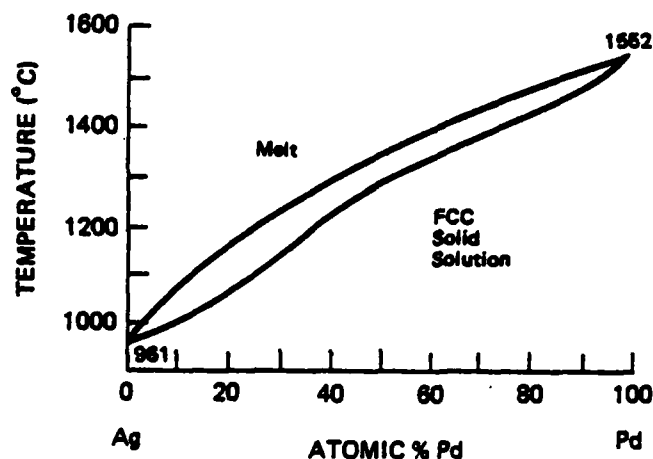|	Lattice Parameter (a)	Specific Gravity	Melting Point (°C)
Platinum	3.92	21.5	1769
Palladium	3.89	12.0	1552
Nickel	3.52	8.9	1453
Copper	3.62	8.9	1083
Gold	4.08	19.3	1063
Silver	4.09	10.5	961
Lead	4.95	11.3	327

FIGURE 8   FCC structure.

FIGURE 9   Silver-palladium phase diagram.

Palladium is used widely because of its high melting point. Silver is a better conductor and less expensive but its melting point is rather low. Low-firing multilayer capacitors are made using Ag-Pd electrodes. The two metals form a complete solid solution series (Figure 9). Similar phase diagrams are found for the alloy systems Pd-Cu, Pd-Au, Pd-Pt, and Pd-Ni with FCC solid solutions for all compositions. According to the 15 percent rule, substitutional solid solutions form only when the atomic radii differ by less than 15 percent. The rule is obeyed for these intermetallic electrode compositions where the radius of Pd differs by less than 10 percent from those of Au, Ag, Cu, Ni, and Pt. As is discussed later, Pd and Pb differ by 25 percent and do not form appreciable solid solution. Extensive compound formation takes place between palladium and lead.

Up to several percent carbon and hydrogen can dissolve in palladium at room temperature. These are interstitial solid solutions with the smaller H or C atoms occupying octahedral interstitial sites at the center of the face-centered cubic unit cell (Figure 10). The lattice parameter of Pd increases from 3.891 to 3.902 Å when it is saturated with hydrogen. The solubility of H in Pd decreases sharply when heated. Hydrogen evolved from a metal electrode in this way could play a role in electrical breakdown.

Thermal expansion coefficients of the electrode metals range from $8 \cdot 10^{-6}/°C$ for Pt to $30 \cdot 10^{-6}$ for Pb. As shown in Figure 11 thermal expansion coefficients are inversely proportional to melting points. The more strongly bonded metals have high melting points and small coefficients of thermal expansion. This is consistent with the observation that many materials expand about 15 percent before melting.
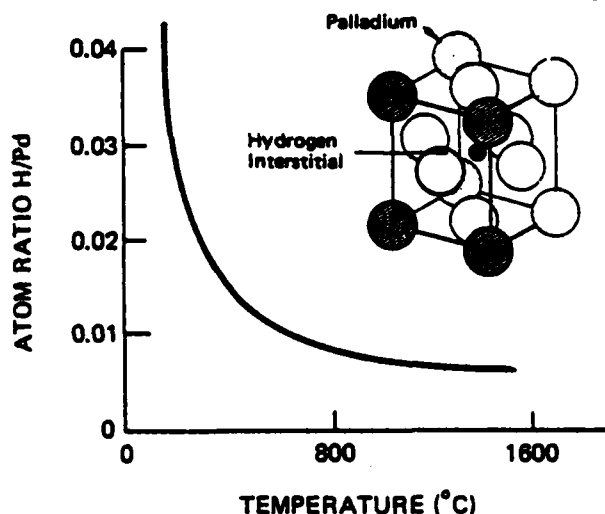
FIGURE 10 Appreciable amounts of hydrogen
can dissolve in palladium by occupying
interstitial sites that normally are
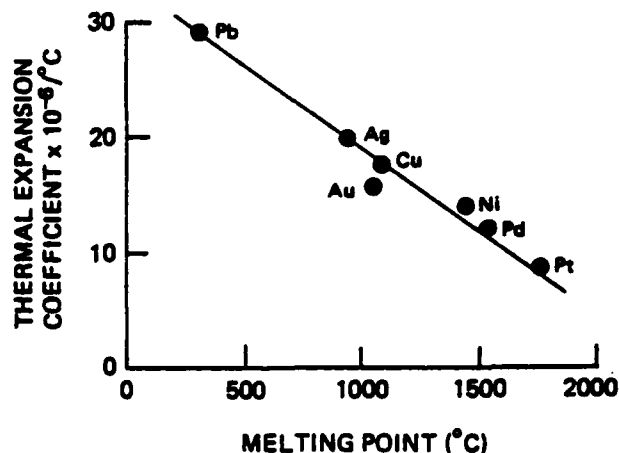empty. Solubilities were measured at
one atmosphere.

FIGURE 11 Relationship between α
and melting temperature
for electrode metals.

ELECTRODE-CERAMIC INTERFACE

The lattice parameters and thermal expansion coefficients of the electrode
metals match those of barium titanate reasonably well. Ag_7Pd_3, a commonly
used composition, has a face-centered-cubic unit cell 4.03 Å on edge. Its
thermal expansion coefficient is $17 \cdot 10^{-6}/$ C. Both values are close to
those of $BaTiO_3$ with less than 1 percent mismatch (Figures 12 and 13).
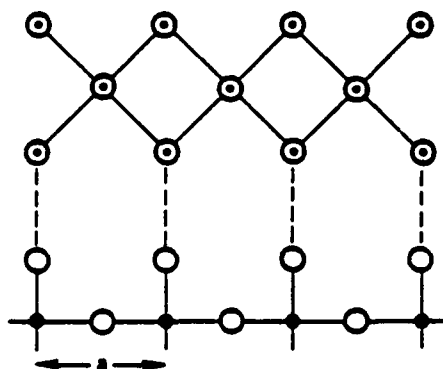
FIGURE 12 Schematic diagram
illustrating the excellent match in
lattice parameters between cubic unit
cells of the electrode metal and the
perovskite dielectric. Shaded circles
represent Ag or Pd, open circles oxygen,
and black circles titanium.
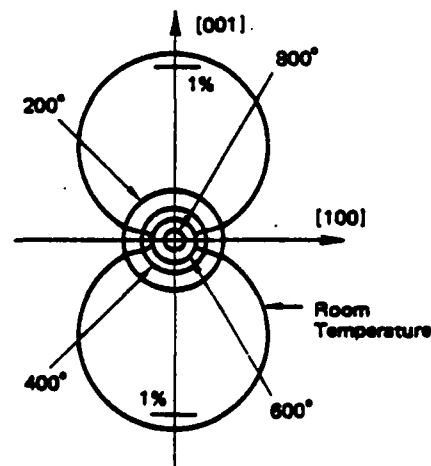
FIGURE 13 Thermal strain between
the silver-palladium electrode and
barium titanate dielectric caused
by thermal expansion mismatch.
When cooled from 1000°C, most of
the strain occurs below T_c, and
this probably is compensated by
90°C domains in the dielectric.

ELASTIC PROPERTIES

Internal stresses sometimes are caused by mismatch in elastic compliance coefficients. Mismatch can occur between two phases or because of elastic anisotropy in a single phase. Young's modulus for polyrrystalline $BaTiO_3$ is compared with various electrode metals in Figure 14. Platinum and nickel are similar in stiffness to the ceramic, the silver and palladium are somewhat more compliant. Melting point is a reasonably good predictor of stiffness; the more compliant materials generally have weaker chemical bonds and lower melting points.

Compliance is fourth rank tensor like electrostriction; therefore, it varies with direction even in cubic crystals. The longitudinal compliance surfaces for several electrode metals and for barium titanate are shown in Figures 15 and 16. The <100> directions are the most compliant in all cases. For face-centered-cubic metals, the <100> directions corresppnd to movements toward the empty interstitial sites, explaining the large compliance. In $BaTiO_3$, movements in the <100> directions correspond to motions associated with the soft optic mode responsible for the ferroelectric properties. Note how the compliance increases along [100] on passing through the Curie temperature as spontaneous polarization develops in this direction.
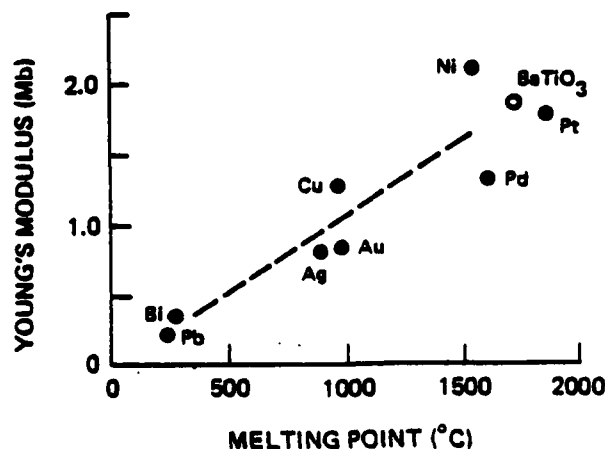

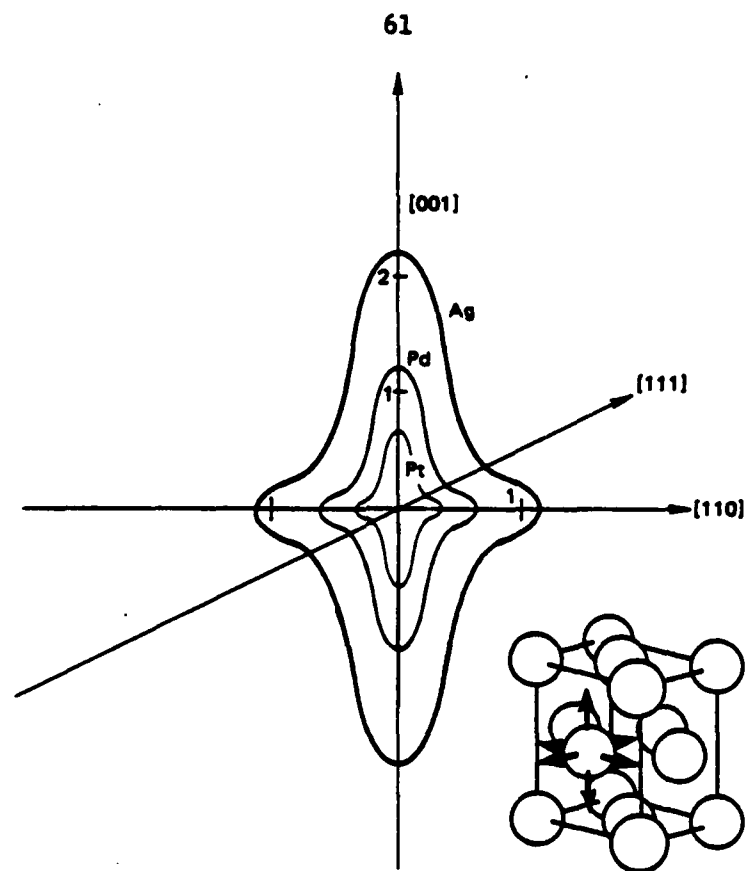FIGURE 14   Elastic stiffnesses can be correlated with melting point.

FIGURE 15   Variation of compliance with direction in several FCC metals.
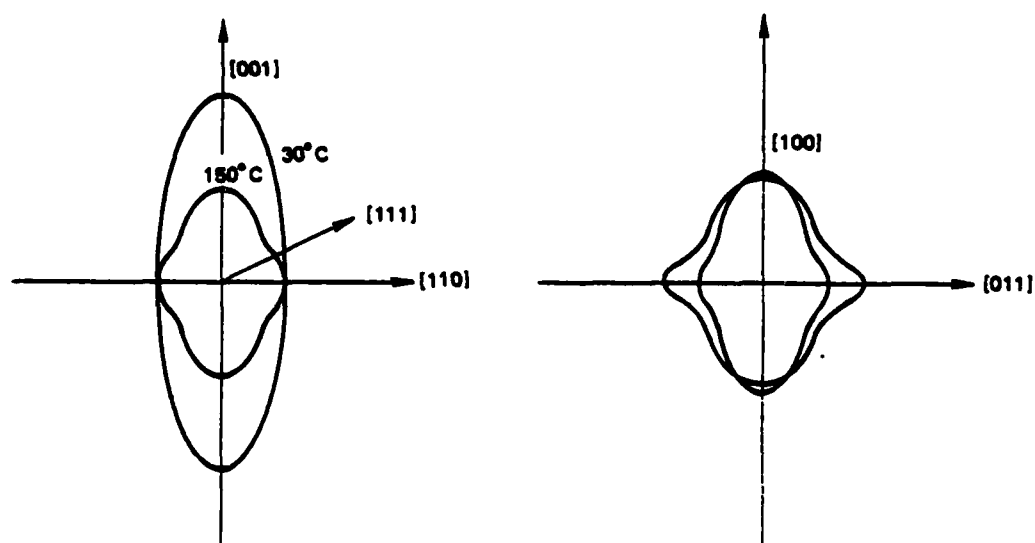Atomic motion is easiest in <100> directions.

FIGURE 16   Compliance surfaces BaTiO$_3$ in the cubic and tetragonal states.

THERMAL CONDUCTIVITY

Thermal breakdown is an important degradation mechanism for multilayer capacitors. Since most dielectrics are wide-band-gap semiconductors, the electrical conductivity increases with increasing temperature, and thermal runaway becomes a hazard. One way to prevent hot spots from developing is to increase thermal conductivity.

Thermal conductivity coefficients for barium titanate and silver-palladium are shown in Figure 17. Rather surprisingly, the metal is only about an order of magnitude better conductor than the ceramic at room temperature, and at low temperatures the two are almost equal. This means that the electrodes are not very effective in withdrawing heat from the capacitor, but the coefficients are sufficiently different to introduce thermal anisotropy into a multilayer system. For directions parallel to the electrodes, the metal and ceramic are connected in parallel, whereas perpendicular to the electrodes the two are in series. Using the appropriate mixing rules and assuming that the electrodes occupy about 10 percent of the volume, thermal conductivity coefficients of 0.11 and 0.06 W.cm K are calculated for directions parallel and perpendicular to the electrodes, respectively. Temperature gradients near thermal breakdown sites will therefore be about twice as large for directions parallel to the electrode. To withdraw heat at a much faster rate without changing the geometry, it would be necessary to use a larger volume fraction of metal electrode.
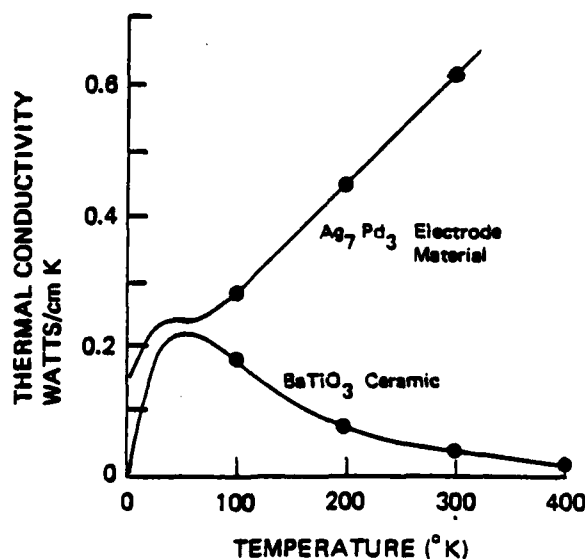

FIGURE 17 Thermal conductivity coefficients of the dielectric and electrode materials plotted as a function of absolute temperature.

OXIDE FLUXES AND FLUX REACTIONS

Bismuth oxide and lead oxide sometimes are used as fluxes in barium titanate capacitors to eliminate the need for precious metal electrodes. The low melting points (800 to 900°C) of Bi_2O_3 and PbO make liquid phase sintering possible near 1000°C. The crystal structures of the two fluxing agents are shown in Figure 18. Both adopt rather open structures because of the peculiar pyramidal bonding characteristic of Bi^{3+}, Pb^{2+}, and other "lone-pair" ions. The $6s^2$ electrons outside a closed d-shell are responsible.
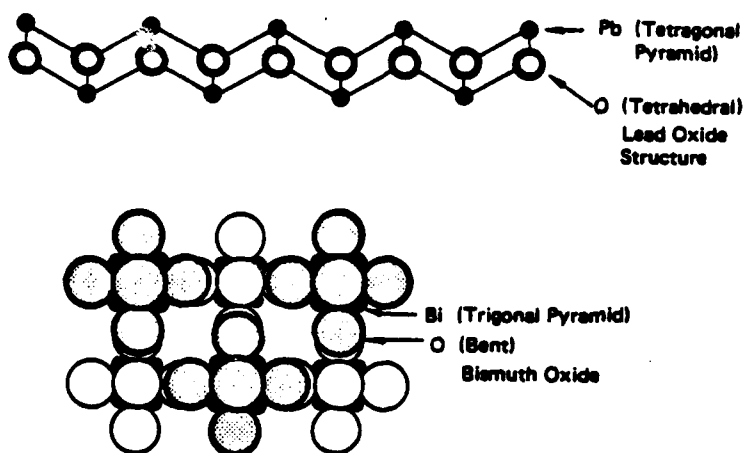
FIGURE 18 Crystal structures of PbO and Bi_2O_3 fluxes.
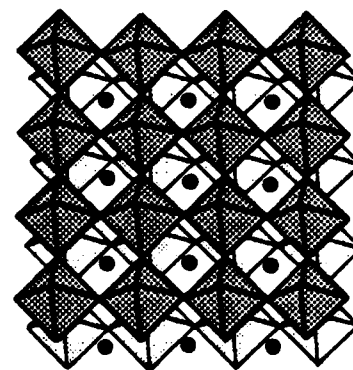
FIGURE 19 $Bi_4BaTi_4O_{15}$ structure consists of a perovskite layer having a thickness of four octahedra separated by pyramidal bismuth oxide sheets.
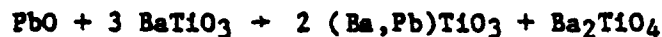
A number of chemical reactions are possible between flux and dielectric and between flux and electrode. There are, for example, several bismuth barium titanate layer structures typified by $Bi_4Ba_2Ti_5O_{18}$ and $Bi_4BaTi_4O_{15}$. These layer structures consist of perovskite-like layers interleaved with pyramidal bismuth oxide layers (Figure 19). $Bi_4Ba_2Ti_5O_{18}$ has five perovskite layers between each pair of bismuth oxide layers, and $Bi_4BaTi_4O_{15}$ four. Both compounds are ferroelectric with room temperature dielectric constants of 200-300 and T_c of 330 to 400°C. The higher values refer to the five-layer structure.

If reactions take place between Bi_2O_3 flux and $BaTiO_3$ ceramic, the layer structures might well appear in grain boundary regions. The interface between $Bi_4Ba_2Ti_5O_{18}$ and $BaTiO_3$ is pictured in Figure 20. The mismatch in lattice parameters is less than 2 percent, and there is also a good match in thermal expansion coefficient. The average linear expansion coefficient in $Bi_4Ba_2Ti_5O_{18}$ which is $11 \cdot 10^{-6}/°C$ over the 0 to 400°C range.

As part of the liquid phase sintering mechanism, reactions such as:

$$2\ Bi_2O_3 + 8\ BaTiO_3 \rightarrow Bi_4Ba_2Ti_5O_{18} + 3\ Ba_2TiO_4$$

or

$$PbO + 3\ BaTiO_3 \rightarrow 2\ (Ba,Pb)TiO_3 + Ba_2TiO_4$$

might occur between the oxide flux and the dielectric. In either reaction, the titania-poor phase Ba_2TiO_4 will form unless precautions are taken. The crystal structure of Ba_2TiO_4 (Figure 21) is very different from the perovskite structures. It consists of isolated TiO_4 tetrahedra rather than a continuously connected TiO_6 octahedral network as in $BaTiO_3$. As a consequence of its poor bonding, Ba_2TiO_4 is notoriously hygroscopic.
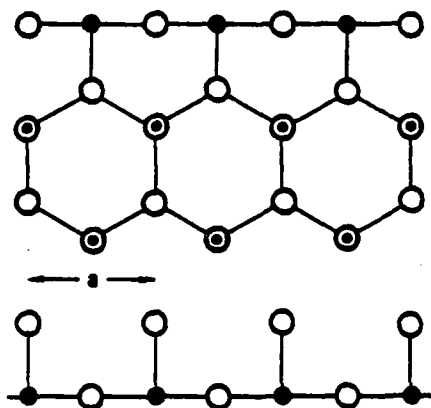

FIGURE 20 Interface between the crystal structures of $Bi_4Ba_2Ti_5O_{18}$ and $BaTiO_3$ (below) showing the excellent match in unit cell dimension a.
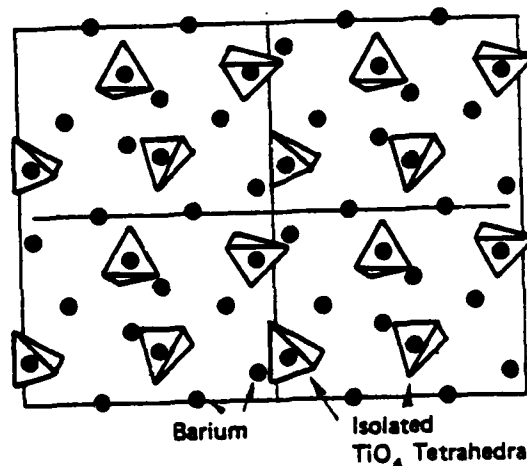
FIGURE 21 Crystal sturcture of hygroscopic Ba_2TiO_4 consists of isolated TiO_4 tetrahedra held together by barium ions.

FLUX-ELECTRODE INTERACTIONS

Palladium oxidizes rather easily forming PdO, a surprisingly dense structure (Figure 22) with Pd bonded to four oxygens in square planar configuration and O tetrahedrally bonded to four palladiums. PdO is stable up to 800°C and in the presence of other oxides forms compounds stable to more than 1000°C.

Several oxidation-reduction reactions between flux and electrode are possible because of the stability of the palladium oxides. Two such reactions are:

$$PbO + 4\ Pd \rightarrow PbPd_3 + PdO$$

and

$$Bi_2O_3 + 9Pd \rightarrow 2BiPd_3 + 3PdO.$$
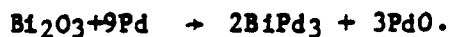
PbPd$_3$ is one of a number of intermetallic compounds found in the palladium-lead phase diagrams (Figure 23). the palladium-bismuth diagram is similar with the following intermediate phases: BiPd$_3$, BiPd$_2$, Bi$_3$Pd$_5$, BiPd, and Bi$_2$Pd.

The intermetallic compounds PbPd$_3$ and BiPd$_3$ crystallize in the Cu$_3$Au structure (Figure 24), which is an ordered derivative of the FCC structure with Pb (or Bi) at the corners of the unit cell and Pd at the face-centers. The lattice parameter is about 4.02 Å, remarkably close to the cell dimensions of the metal electrode and the perovskite dielectric.

Both the PdO and PbPd$_3$ are very dense structures, resulting in a sizeable 9 percent shrinkage in volume for reaction between PbO and Pd. A similar shrinkage of 6 percent occurs for the Bi$_2$O$_3$-Pd reaction. These reductions in volume would occur at the interface between the dielectric and the electrode and may be partly responsible for delamination problems in fluxed multilayer capacitors.
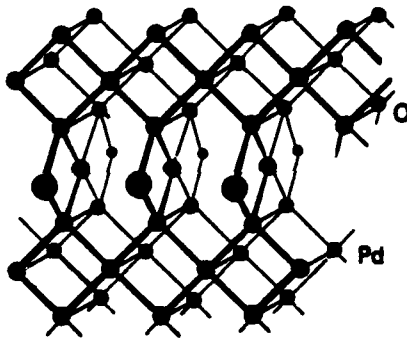

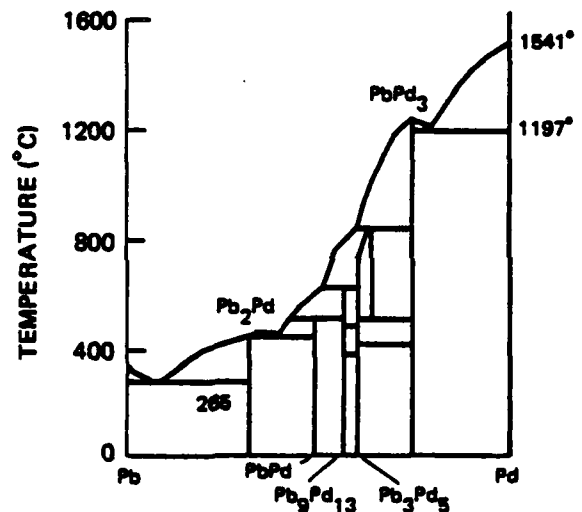
FIGURE 22 Crystal structure of PdO
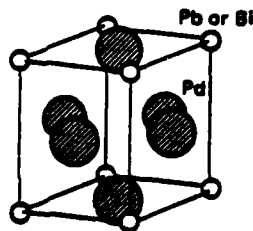

FIGURE 23 Palladium-lead phase diagram.

Figure 24 Unit cell of BiPd$_3$ and PbPd$_3$.

SUMMARY

When examined in detail, the multilayer capacitor poses a very complex problem with many chemical, electrical, and mechanical interactions between its constituent phases. Interactions between ceramic dielectric, metal electrode, and oxide fluxes were examined in this paper. Other interactions arise from the organic binders and vehicles used in tape-casting, from the solder and other materials used in terminations and encapsulation; and from the environment, especially moisture and salts. It is amazing that multilayer capacitors work as well as they do.